SOLAR-DRIVEN VAPOR TRANSPORT IN LIGHTWEIGHT WALLS IN A HOT AND HUMID CLIMATE

Jason Edelstein

A Thesis

in

The Department

of

Building, Civil and Environmental Engineering

Presented in Partial Fulfillment of the Requirements

for the degree of Master in Applied Science at

Concordia University

Montreal, Quebec, Canada

May 2007

Your file Votre référence
ISBN: 978-0-494-34690-7
Our file Notre référence
ISBN: 978-0-494-34690-7

ABSTRACT

SOLAR-DRIVEN VAPOR TRANSPORT IN LIGHTWEIGHT WALLS IN A HOT AND HUMID CLIMATE

Jason Edelstein

Over the last few decades, more and more attention has been given to moisture control in building envelopes. This includes better control of rain, moist-laden air leakage and water vapor diffusion. One aspect of moisture control that is still not quite mastered is the so called solar-driven vapor transport. When rain is absorbed by porous materials such as brick cladding, rapid drying due to solar radiation can lead to vapor pressure driven inward flows. These flows are magnified when the interior space is air-conditioned. Such flows can be important and lead to moisture accumulation in the wall assembly. However, the parameters that impact such flow and the role of thermal loading conditions have not been linked to the hygrothermal performance and durability of wall systems.

The overall goal of this study was to develop a greater understanding of the significance of solar-driven vapor flow, also known as summer condensation, specifically under what conditions it occurs and the negative effects it poses on the building envelope. This research presents the testing performed on a set of small-scale wall specimens under constant loading conditions and the development of an experimental approach to determine the effects of the simulated loading conditions on large-scale wall specimens. Both experimental procedures are successful in reproducing thermal and vapor pressure gradients across test specimens under summer conditions in hot and humid climates similar to those simulated by a heat, air and moisture modeling tool.

The results of these experiments indicate that the effects of solar-driven vapor diffusion are observed in cases where large thermal gradients act on wall assemblies with absorptive cladding repeatedly wetted by rain. The methods implemented in the design of the experimental procedure can be used to simulate these effects for further research.

ACKNOWLEDGMENTS

It was never my intention to further my engineering studies beyond my bachelor's degree until the final year of my undergraduate engineering program when I was approached by Dr. Dominique Derome who planted the idea in my head. I never saw myself as a researcher and would like to thank Dr. Derome for guiding me with her knowledge of building science, offering me the chance to conduct research in Belgium and overall, for giving me the opportunity to be her student.

The work I completed at Concordia could not have been possible without the support of the faculty, staff and my fellow colleagues. The time and help of Joe Hrib, Luc Demers and Rocco Lombardo does not go unnoticed. Thanks to Professor Jan Carmeliet for allowing me access to the lab at KULeuven and the valuable help of Wolfgang Zillig, Paul Verbeek and Wim Bertels. I would also like to thank Guylaine Desmarais for her input and all the stagiaires who helped in the lab with the construction of my experimental setup. In addition, eating lunch on the top floor of the EV building with my colleagues was the only way to keep sane when spending countless hours in a windowless laboratory.

The support of ASHRAE, NSERC and the Faculty of Engineering and Computer Science was gratefully acknowledged.

Throughout this character building journey, much was gained. Although some times were more challenging than others, I acquired first hand experience on the design and construction of a large experimental setup which seemed near impossible at the start of my research. A lot has happened and many emotions were expressed during my two years enrolled as a graduate student. From stress to happiness, and to a sense of satisfaction, I am glad that I had this opportunity.

The encouragement received by my friends was greatly appreciated - You know who you are and what you did for me. And without the loving support and patience of my girlfriend and best friend, I would not be where I am today. My parents and family

deserve special thanks, who were understanding of my absence on several family occasions. They backed me through it right to the end. I would also like to thank my father, in particular, who was constantly willing to drive me between RONA and the lab, and who was always ready to lend a hand.

And now, I can finally say "I did it".

Table of Contents

List of Figures

List of Tables

Nomenclature

Roman Symbols		Units
d	thickness	m
p_v	vapor pressure	Pa
p_c	capillary pressure	Pa
RH	relative humidity	%
R_v	gas constant	J/(kg.K)
T	temperature	K
w	moisture content	kg/m^3
w_g	gravimetric moisture content	kg/kg
x	distance	m

Greek Symbols		
ρ	density	kg/m^3
ϕ	relative humidity	-
μ	permeability	$ng/(Pa.s.m^2)$

Chapter 1: Research Problem and Objectives

1.1 Introduction

The role of the building envelope is to separate the interior environment from the outdoor. The enclosure of a comfortable indoor space is subjected to structural and hygrothermal loadings resulting from the exterior and interior environments and the enclosure itself. Such loads must be resisted to maintain the structural integrity, energy efficiency and durability of the envelope. Moisture is a major factor affecting the durability and performance of building enclosures. Of all environmental conditions, moisture poses the biggest threat to integrity and durability, accounting for up to 80% of damage in building envelopes (Bomberg and Brown, 1993). Failure to accommodate moisture loads can result in building degradation with the occurrence of mold and rot, rusting of metal fasteners and ties, erosion of masonry as well as deterioration of organic compounds.

In studying the different types of moisture flows, it is known that water vapor diffusion, in certain cases, can lead to a significant amount of moisture within assemblies. In cold climates, where the interior is heated for the greater part of the year, the interior vapor pressure is greater than the exterior, leading to vapor flows towards the outside. To accommodate the moisture drive towards the exterior and prevent the occurrence of condensation, a vapor barrier is integrated on the warm side of a wall enclosure. It is also well-known that, in an air-conditioned building, a significant reversed inward vapor drive exists during the warmer summer months, even in cold climates.

1.2 Current State of Knowledge

The research presented here investigates one type of loading on wall assemblies, i.e. solar radiation on a wet porous cladding and the resulting induced moisture flows. As solar radiation increases the temperature of the wet cladding, moisture will exit it. Some of this moisture will move towards the inside, through the sheathing, insulating cavity and

interior finish of the wall due to thermal and partial vapor pressure gradients. Such flows are larger when the interior air is air-conditioned. The resultant flows have been named summer or reversed vapor flow and may lead to "summer condensation".

Summer condensation in walls with vapor barriers have been documented (Wilson 1965; Sandin 1991; Straube 2001) which demonstrate the condensation that may arise from solar-driven vapor transport. Some of these works are presented in the following chapter. Nevertheless, a systematic study of the phenomenon still remains to be performed.

This project, as part of a larger project funded by ASHRAE in moisture flow driven by high temperature gradients, takes the summer conditions found in a hot, humid climate as the loading conditions for a wood-frame wall assembly with wetted cladding and investigates the risks associated with solar-driven vapor flow. The present thesis included the development of a method in recreating and monitoring this vapor flow across large-scale wall specimens. The investigation also included a small-scale study with varying parameters of the weather resistive barrier and permeance of the interior finishing.

1.3 Research Objectives and Overall Methodology

This research project aims to better understand the occurrence of solar-driven vapor transport and its possible consequence, interstitial condensation, through experimental procedures.

The specific objectives of this project are to:

1. Run a series of small-scale experiments using test specimens of various different constructions in a controlled environment
2. Analyze the resulting data from the experiments to establish if condensation and mold growth occur
3. Perform a parametric analysis of the water vapor permeance of the weather resistive barrier and of the interior finishing
4. Develop a large-scale experimental procedure to simulate and monitor solar-driven moisture flow during summer conditions in a hot-humid climate

5. Run an experiment using a large-scale test specimen of same construction as the small-scale specimen in a controlled environment
6. Analyze the resulting data from the experiment to verify the adequacy of the experimental procedure

Solar-driven vapor flow occurs under specific conditions. This flow through light-weight wood-framed North American constructions is the main study of this project while air movement in the air space between the cladding and sheathing is not taken into account. To accurately simulate these conditions, an experimental setup was designed. The setup reproduces solar radiation on the brick cladding of a wood-framed specimen in the days following wetting events. The response of the specimen is monitored and recorded while observations on moisture in the form of moisture content, condensation and relative humidity are monitored.

1.4 Structure of Thesis

The following chapter, Chapter 2, presents a review of past research works concerning summer condensation and suggested moisture control strategies.

Chapter 3 presents the work done to better understand the phenomena at play, where an existing small-scale setup was used to provide some data under constant loading conditions. The setup of the small-scale experiment is explained and the results are analyzed and discussed.

The design and construction of a large-scale test under cyclic loading conditions is discussed in detail in Chapter 4.

The last chapter, Chapter 5, of the project summarizes and concludes the results of the two sets of experiments. Suggestions for optimizing the experiments and possible future works are presented.

The experimental procedures and data are fully documented in the appendices.

Chapter 2: Literature review

2.1 Introduction

This chapter presents a brief overview of the literature on solar-driven vapor flow. Wood-frame buildings are widely used in North American residential constructions. The methods of control of heat, air and moisture flow across the assembly depend somewhat on the type of climatic loads. Based on these differences, the composition of wood-frame wall assemblies for residential buildings may vary substantially.

Walls designed in cold climates typically control the movement of moisture from the inside out during cold weather periods, inferring that walls are often built and designed to withstand winter conditions. In the winter, the indoor air generally contains more moisture than the outdoor air, driving moisture towards the outside. During the summer season, when wall claddings are wet and then heated by solar radiation, a large vapor pressure difference between the interior and exterior often occurs and moisture can be driven inwards. As the vapor flows towards the cool interior, condensation may occur. This condensation can accumulate within the assembly eventually leading to problems such as wood deterioration and mold growth on the gypsum board. The mode of moisture flow involved is diffusion.

Diffusion of water through a material is generally assumed to follow Fick's first law:

$$w = -\mu(\frac{dp}{dx}) \tag{2.1}$$

Where w is the rate of diffusion [ng/s.m^2], $(\frac{dp}{dx})$ is the vapor pressure gradient, p is the

vapor pressure [Pa], x is the distance along the flow path [m] and $-\mu$ is the permeability [ng/ Pa.s.m] which is a function of relative humidity.

The National Building Code of Canada (2005) defines a vapor barrier to have a permeance not greater than 60 ng/Pa.s.m^2.

Since moisture can be driven inwards, as well as outwards, designers of walls located in mixed or hot climates have a difficult time placing vapor retarders to minimize the potential for water vapor condensation while allowing for some drying.

As stated earlier, moisture transport through the building envelope can lead to the accumulation of condensation within assemblies. Condensation occurs when the temperature of air is lowered to its dewpoint temperature. Many building failures are related to exposure to excessive moisture. Mold and mildew are increasingly recognized as a source of indoor air pollution and of respiratory illness of building occupants.

2.2 Observing Summer Condensation

It was Hutcheon (1953) who first reported observed summer condensation in assemblies with a vapor barrier, saying "When a vapor barrier is used, the wall can lose moisture only to the outside. In summer, hot sun following a rain drives moisture as vapor to the inside of the wall, and condensation behind the vapor barrier can occur."

Wilson (1965) studied insulated masonry panels which were heated and humidified. A vapor barrier membrane was provided on the inside of the insulation to control winter condensation. No moisture problems were observed during the winter; however summer condensation was encountered. Wilson suggests that a ventilated air cavity behind the cladding can avoid the deterioration of inner wall components due to condensation.

Anderson (1987) measured moisture content over 20% in the wood materials of a wood frame wall in June, accompanied with elevated moisture contents from May until early September. The moisture content began to decrease slowly in January. Anderson concludes that the construction of a brick clad wall where a vapor barrier is used on the inside of mineral wool insulation and the absence of an air cavity is not recommended.

Sandin (1993) found that relative humidity in the stud wall cavity during the summer depends on the vapor transport from the absorptive cladding to the inner side. Reducing the humidity can be achieved in three ways:

1. Keeping the masonry dry
2. Reducing moisture transport towards the inside
3. Allowing moisture transport to pass through the wall without any obstruction

Between May and September in Texas, Tobiasson (1989) witnessed the accumulation of outside moisture within the building envelope. He states that moisture accumulation is a function of the vapor gradient and duration of wetting period. Lowering the indoor temperature increases the wetting potential.

2.3 Controlling Solar-Driven Moisture

Pressnail (2003) believes there are several ways to control sun-driven moisture flows: using external insulating sheathing materials having a relatively low vapor permeance and implementing thick exterior insulation which can increase a wall's resistance to solar-driven moisture.

Based on measurements and simple calculations performed by Straube and Burnett (1997), the maximum permeance of the layers behind the brickwork and outside the framing of a wall should be of the order of 50 ng/Pa.s.m^2 to prevent vapor from condensing and damaging assembly materials.

2.3.1 Field, Lab Work and Modeling

Field and lab work was performed to evaluate the performance of walls to study the impact of these parameters:

1. low vapor permeance membrane
2. vented air cavities
3. non-absorptive cladding

2.3.1.1 Low Vapor Permeance Membrane

Lawton and Brown (2003) conducted a study using the simulation software hygIRC to understand the impact of removing the polyethylene membrane from a wall system in the

Vancouver climate. The tests performed varied between six different types of paint, and combinations of paint/no paint and/or vapor barrier/no vapor barrier.

Table 2.1 Barrier properties used by Lawton and Brown (2003)

Name	Modeled finish	Properties	
		Vapor Diffusion Thickness	Permeance (ng/Pa.s.m^2)
Poly	Polyethylene vapor barrier	-	15
No poly	Unpainted gypsum board	-	3000
Latex 1	Primer & two coats of latex paint	0.17	1140
Acrylic	Primer & two coats of acrylic paint	0.46	422
Oil	Primer & two coats of oil based paint	0.76	255
Tight	Based on properties of a waterproof coating		5

Each wall assembly was modeled under the following three cases: 1) no direct moisture source into the wall (no construction defect); 2) with a section of the OSB sheathing (1.8 m above the base of the wall) initially wetted to a condition of 34% moisture content; 3) wall assembled with a defect that would allow moisture to enter the assembly every time the wall was subjected to wind-driven rain.

The first two cases modeled had similar results at the end of the year. The walls, which assumed that the OSB sheathing was initially wetted, had similar moisture contents, to the wall assemblies that had no initial wetting at all. This means that during the summer months sufficient drying took place which allowed most of the moisture to escape the assembly. The third wall section, modeled with a defect, had different results. The moisture content of the OSB was observed to significantly increase due to periodic rain loads and the system did not have enough time to dry leading to elevated moisture content levels at the end of the tested year. The simulation also showed that the moisture content in the unfinished gypsum did not vary with the inclusion or absence of a polyethylene vapor barrier. In all other cases, the amount of moisture found in the gypsum was inversely proportional to the permeance of the paint finish that was applied.

Levin (2000) performed moisture measurements in three similar houses without traditional vapor barriers during a two-year period. The moisture supply to the houses ranged from 0.8 g/m^3 to 1.5 g/m^3 per day. It was concluded that wall constructions with

polypropylene fabric might inhibit condensation and high levels of relative humidity when the moisture loads are low. Conversely, Levin claims that indoor moisture production exceeding 2 g/m^3 per day will cause condensation on the external sheathing and high relative humidity in the insulation.

TenWolde *et al.* (1986) studied nine instrumented wall panels of various constructions in Beaumont, TX. It was concluded that walls with an outside vapor retarder or no vapor retarder remained equally dry throughout the study period. However, it is mentioned that more moisture was transferred through the wall without a vapor retarder. Furthermore, it is suggested that an interior vapor retarder would be undesirable unless an exterior vapor retarder was installed as well.

An effective wall must be vapor tight enough to protect against winter condensation, while being sufficiently vapor permeable during the summer to provide quick drying, thus the idea of a nylon-based vapor barrier membrane with varying permeability. The "smart" retarder acts like a conventional retarder at the interior side of an assembly during the heating season where humidity conditions are relatively low. However, the membrane can become as permeable as gypsum board when exposed to high relative humidity (Kunzel, 1999). Its vapor permeability is shown in Figure 2.1 as a function of relative humidity. The graph shows that at a relative humidity below 50%, the retarder acts as a low permeable barrier. However, above 90% relative humidity, the barrier becomes vapor permeable.

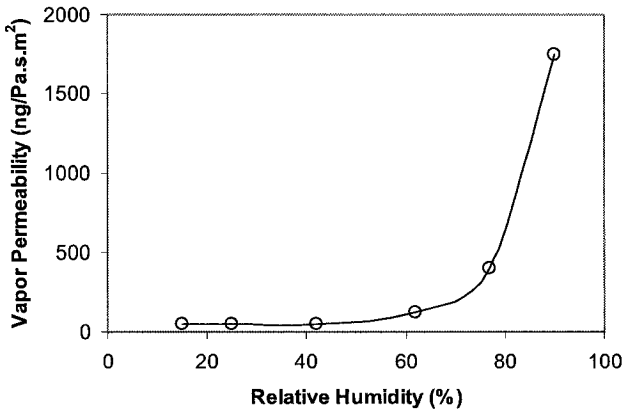

Figure 2.1 Permeability of nylon-based vapor barrier (Kunzel, 1999)

In a test conducted by Kunzel (1999), where the smart vapor retarder was implemented in an unvented cathedral ceiling, the membrane effectively reduced the moisture damage risk in the building envelope by increasing the moisture load tolerance of the assembly.

2.3.1.2 VENTED AIR CAVITIES

Straube and Burnett (1998) have shown that, on average due to solar radiation, the temperature of the air space behind the brick cladding can be 10°-30°C higher than the ambient air temperature. When temperatures increase, the water vapor content of the cavity air can decrease the density of air, which creates buoyancy effects that drive ventilation flow. This means that the movement of outdoor air, in and out of a cavity, will likely remove moisture rather than carry it in.

Salonvaara *et al.* (1998) studied 12 walls to investigate the hygrothermal behavior of different exterior sheathings and wall cavity ventilation between the sheathing and sidings. During warm outdoor conditions, walls with no ventilation demonstrated an increase in moisture contents in the wood specimens, where as, in ventilated walls, the bottom part of the wall slowly dried out. They concluded that wall cavity ventilation can improve the drying of walls. They further concluded that wall cavity ventilation cannot improve the drying out of moisture present in the insulation layer if the exterior sheathing has a low vapor permeance.

While conducting some tests to determine the moisture content and relative humidity in wall cavities, Sandin (1993) found that wide, well ventilated air spaces can significantly reduce the moisture transport inwards behind masonry sidings. TenWolde *et al.* (1986) also concluded that ventilated air spaces aid in preventing the entry of moisture into building assemblies. They argued that the ventilation in the air space creates a pressure equalization, which in turn deters moisture from being driven inwards towards the interior of an enclosure.

Pressnail *et al.* (2003) found that air cavities with increased ventilation rates or larger vent holes are more likely to prevent summer condensation. Furthermore, it was concluded by using the simulation tool, MOIST, that walls with an unvented air cavity

performed as walls without a cavity. Pressnail advises that if an absorptive cladding is used, a vented air cavity is needed within the assembly.

Hazleden *et al.* (2001), performed a series of tests to determine how building enclosures dry and their respective rates of drying. The objective of the experiment was to collect data on the drying capabilities of wood frame walls. Assemblies tested were based on commonly used stucco and wood-clad wall systems incorporating different types of vent areas, cavity sizes, sheathing materials and moisture barriers. The study included the parameters of the effects of drainage cavity width and vent area on drying. Hazleden determined that wall assemblies with cavities dry faster than assemblies without. In addition, plywood sheathing dries faster than OSB sheathing. Furthermore, it was noted that no difference in drying occurred between panels with building paper and SBPO (spun bonded polyolefin).

2.3.1.3 NON-ABSORPTIVE CLADDING

Preventing moisture from entering the cladding can greatly reduce the potential for solar driven moisture (Pressnail, 2001 and Kunzel and Kiessl, 1996). Incorporating within the building design features such as eaves and overhangs can protect the building surface but only to a certain degree. These design characteristics cannot protect against such factors as wind-driven rain.

Sandin (1993) suggests impregnating the surface of brick veneer cladding with a water-repelling agent. Impregnating masonry with such sealants as siloxane can also prevent the transport of moisture. A study performed by Al-Gahtani *et al.* (1999) found that some treatments raised the moisture content of masonry compared to untreated masonry. Chiovitti *et al.* (1999) performed a series of tests as per ASTM E 514 and RILEM Test Method 11.4 to evaluate the performance of water repellents and to develop effectiveness in reducing moisture penetration in brick veneer. The results proved, in general, to decrease the moisture content of the masonry. Kunzel agrees that such treatments can effectively repel rain water, but that, if not properly applied, can increase the moisture

content of the cladding. Furthermore, initial moisture within the brick can be trapped within.

2.3.2 Additional Related Work to Summer Condensation

Sherwood (1985) conducted a series of field tests on several different wall panel constructions for two years in a hot, humid climate. The panels were tested with and without interior penetrations such as electrical outlets to study the effects of air leakage. During the summer months, with outdoor average temperatures reaching upwards of 100°F, south facing walls constructed with wood sheathing resulted in greater moisture increases compared to northern exposed walls although the moisture content of the south facing wood framing did not exceed 12% during the summer. As the same constructions under winter conditions sustained no condensation, it was concluded that the walls work well in cold climates.

Hubbs and Hircock (2002) monitored several Vancouver residential constructions. It was observed that, after walls were wetted by rainfall followed by sun exposure, exterior sheathing moisture contents spiked. However, the elevated moisture contents decreased along with exterior temperatures acting on the cladding. It was suggested that a comparative study be performed to better understand the performance of assemblies for further knowledge.

2.4 Summary

The work presented above has provided insights on the occurrence of solar-driven moisture flows.

The use of a low vapor permeance membrane is still up for debate. Straube (2001) believes an interior vapor barrier should be omitted from constructions where summer condensation may occur and replaced with an interior paint finish, contrary to what Lawton and Brown (2003) suggest. Lawton and Brown noted that multiple paint layers applied directly to gypsum can elevate the sheathing moisture content without the presence of a polyethylene vapor barrier. The polyethylene barrier provides protection to

the moisture sensitive gypsum board which prevents mould growth during the heating season, while Levin (2000) suggests replacing the traditional vapor barrier with a more diffusive open material such as polypropylene fabric. TenWolde *et al.* (1986) consider that both an interior and exterior vapor retarder is needed. Tsongas and Olson (1995) believe that moisture penetrates building enclosures due to low vapor permeance of the exterior weather barrier paper.

Wilson (1965), Straube and Burnett (1998), Salonvaara *et al.* (1998), Sandin (1993), TenWolde *et al.* (1998) and Pressnail *et al.* (2003) all state that the inclusion of ventilated air cavities prevent moisture transport in wall assemblies and increase the drying potential. Unfortunately, there are still building envelopes being developed without the inclusion of a ventilated air cavity.

Preventing the accumulation of moisture within brick cladding has been tested using a siloxane sealant. Such an approach can prove to be damaging (Kunzel 1996).

The work performed to date is limited in scope and the data produced is scarce and difficult to analyze in detail due to lack of information on all conditions during the measurements. Furthermore, some conclusions are contrary to one another. The phenomenon of solar-driven vapor diffusion needs a more systematic investigation to understand and provide solutions to solve the problem. The following project presents aims at evaluating the magnitude of solar-driven vapor diffusion in walls. An existing small-scale set-up was used to first study the phenomenon. Then, a large-scale test set-up was designed to study the effect of solar-driven vapor diffusion in test specimens. The experimental procedures are detailed in the following chapters.

Chapter 3: Small-scale steady-state study of inward vapor flow

This chapter presents a first study on small-scale specimens, done to understand the magnitude of the flows and temperature, relative humidity and moisture content variations to be expected for walls subjected to solar-driven moisture flow. An existing set-up at the Katholieke Universiteit Leuven in Belgium was used (De Meulenaer, 2006).

3.1 Small Scale Experimental Setup

3.1.1 Test setup

The small-scale setup consists of eight horizontal specimens on a supporting frame (Figure 3.1). A hot box covers the specimens providing constant outside boundary conditions (Figure 3.2). The short sides of the support frame are open to the laboratory allowing conditioned air (constant temperature and relative humidity) to flow below the specimens. The hot box is heated by a closed-loop heating system, comprising of a heating chamber equipped with eight 250W heat lamps and a fan. The system is regulated by a thermostat. The 0.4 m x 0.4 m specimens are constructed within an insulated vapor tight Plexiglas frame, ensuring one-dimensional heat and moisture flow. Three different wall parameters are investigated: weather resistive barrier, interior finishing and inclusion/absence of a wooden stud.

3.1.2 Test protocol

A quantity of 1.5 liters of water is initially added to the masonry, leading to an equivalent moisture content of 105 kg/m^3 in the brick.

The experiment is divided into two phases: a wetting followed by a drying phase. During the wetting phase, the masonry remains covered with an aluminum plate, preventing drying of the masonry towards the outdoor environment. The drying phase begins following 17 days of wetting by removing the aluminum plates from the specimens. The

removal of the aluminum allows drying both towards the indoor and outdoor environment.

The loading conditions were steady state. The outside temperature was 40°C with an outside relative humidity of 15 %RH. A constant temperature of 18°C and 75% RH was used as the indoor climate.

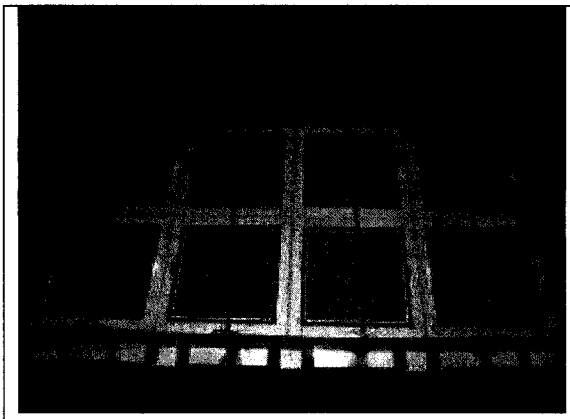

Figure 3.1 Test specimens on supporting frame with aluminum plates removed.

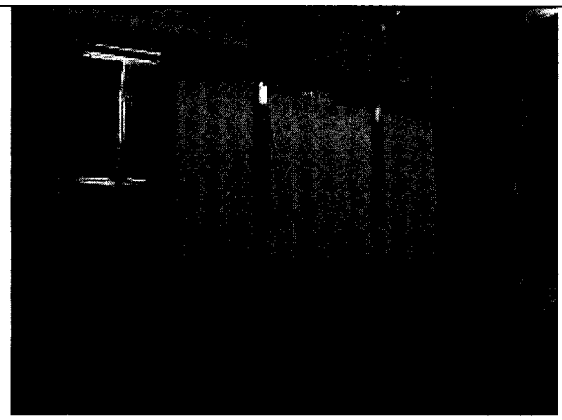

Figure 3.2 Hot box and heating system placed above test specimens.

3.1.3 Composition of Specimens

The specimens were based on typical North American wood frame construction. All of the assemblies included brick veneer cladding. From outside to inside, the walls were comprised of:

- Brick masonry – 90 mm
- Air space – 30 mm
- Weather resistive barrier
- OSB sheathing – 9 mm
- Mineral wool insulation with 38 mm x 89 mm spruce-pine-fir (SPF) stud in four specimens
- Gypsum board – 12.5 mm
- Interior finishing

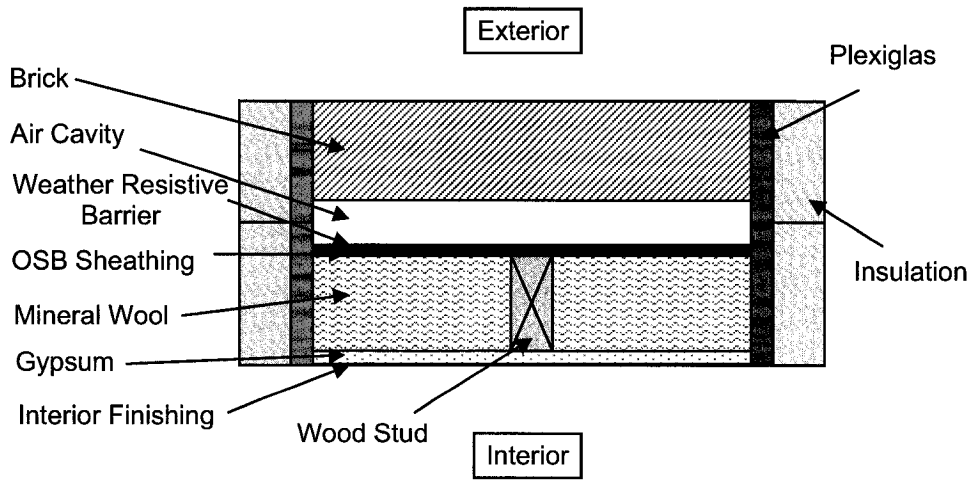

Figure 3.3 Typical small-scale wall assembly

The overall composition of the assemblies can be divided into three components: Brick, Weather Resistive Barrier & Sheathing and Insulation & Gypsum, seen in Figure 3.4.

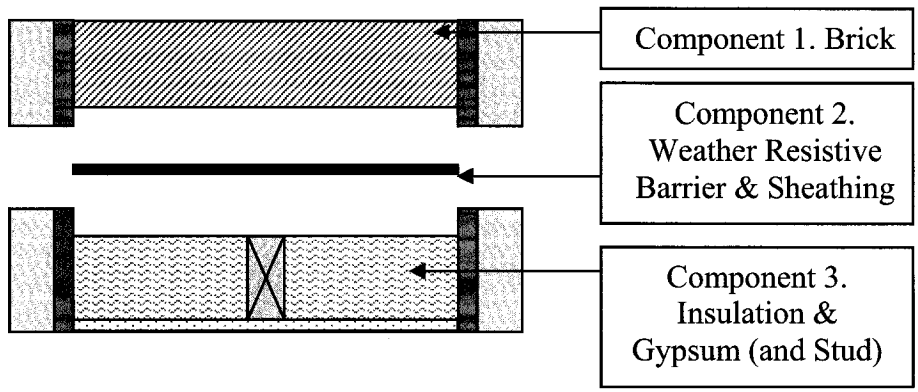

Figure 3.4 Parts of the Test Specimens

The test assemblies were all similar in construction with the following variations:

1) Interior finishing:
   - (a) Acrylic Paint (high vapor permeance)
   - (b) Vinyl Wall Paper (low vapor permeance)
2) Weather resistive barrier:
   - (a) Building Paper (low vapor permeance)
   - (b) Spun Bonded Polyolefin (high vapor permeance)
3) Presence or absence of wooden stud

3.1.4 Measurement Protocol

The samples were monitored with both gravimetric and electronic continuous measurements. Gravimetric measurements were done to monitor the accumulation of moisture while electronic probes monitored the conditions within the specimens.

3.1.4.1 Gravimetric Measurements

For the entire duration of the experiment, the assemblies were removed from the support and weighed at several time steps. The three components of the assemblies, shown in Figure 3.4, were weighed individually to establish their moisture contents. By doing so, the moisture content of the different assembly components could be determined. The frequency of measurements was limited to twice a week - every third and seventh day in a seven day cycle. In addition, four times over the course of the experiment, the individual weight of each assembly material was recorded: before the wetting phase, between the wetting and drying phases, at the completion of the drying phase and the oven dry weight of the materials. This involved completely dismantling the entire assemblies and weighing each material by itself.

A balance with an accuracy of 0.1 gram was used to determine the mass of the components.

3.1.4.2 Continuous Measuring

The temperature, relative humidity and moisture content were electronically monitored throughout the entire duration of the experiment at various positions within the test specimens.

Appendix E provides the detailed information for the sensor equipment used with calibration results.

3.1.4.2.1 Sensor Placement

The placement and orientation of the thermocouples (TC), along with the relative humidity probes (RH) and moisture pins (MC) were arranged so that all of the measuring

devices line up in the non-studded assemblies. This is to ensure a better collection of data for a one-dimensional analysis. Refer to Figure 3.5 for the sensor placements.

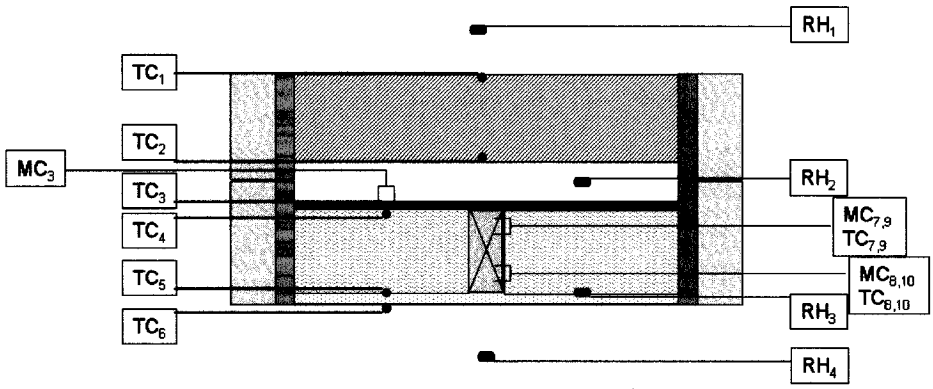

Figure 3.5 Sensor lay-out for small-scale specimen

3.2 Experimental Results

This section presents the experimental results of the eight wall specimens. Table 3.1 assigns a symbol and label to each of the eight walls. The measurements of the experiment includes temperature, relative humidity and moisture content throughout the samples as well as moisture accumulation in the gravimetric samples and individual materials as described in the measurement protocol.

Table 3.1 Wall Assembly Legend

Symbol	Label	Description
▬▬▬	B. Paper - Vinyl	Building Paper and Vinyl Wall Covering
▬▬▬	SBPO – Vinyl	Spun Bonded Polyolefin and Vinyl Wall Covering
▬▬▬	B. Paper – Acrylic	Building Paper and Acrylic Paint
▬▬▬	SBPO – Acrylic	Spun Bonded Polyolefin and Acrylic Paint
▬ ▬	B. Paper – Vinyl – Stud	Building Paper, Vinyl Wall Covering and Wood Stud
▬ ▬	SBPO – Vinyl – Stud	Spun Bonded Polyolefin, Vinyl Wall Covering and Wood Stud
▬ ▬	B. Paper – Acrylic – Stud	Building Paper, Acrylic Paint and Wood Stud
▬ ▬	SBPO – Acrylic – Stud	Spun Bonded Polyolefin, Acrylic Paint and Wood Stud

3.2.1 Environmental Conditions

The exterior temperature and relative humidity recorded throughout the experiment are the conditions within the hot box. The temperature within the hot box was measured to be 42.2°C ±0.5°C. The recorded hot box temperatures led to the desired surface temperature of 40°C for the brick. Furthermore, the low relative humidity, which fluctuated between 14.7% to 18.6% RH was due to the closed circuit heating system.

The interior temperature and relative humidity conditions were not as constant as the exterior ones. The lowest recorded temperature on the interior was 16.6°C while the highest temperature was 19.2°C. This is a difference of 2.6°C. The relative humidity ranged from 58.2% to 80.5%, so less constant than the exterior conditions. This fluctuation of 22.3% can be a result of the laboratory's HVAC system working in cycles and doors opening to the exterior environment due to regular occupant traffic.

3.2.2 Gravimetric Measurements

In the case of the specimens with acrylic paint interior finishing, the experiment lasted 45 days while the experiment lasted 80 days in the case of vinyl wallpaper specimens. The duration of testing varied because the drying rates of the assemblies with acrylic paint was observed to be much quicker than those with vinyl wallpaper.

3.2.2.1 Weight of Walls by Parts

The wall assemblies were deconstructed and weighed by components from the beginning to the end of the experiment every third and seventh day in a seven day cycle. Figure 3.6 presents the change in weight due to moisture in each wall assembly and Figure 3.7 to Figure 3.9 presents the weight variations for each of the three components.

It can be seen in Figure 3.6 that very little moisture was lost to the environment during the wetting phase since the graphs do not change much during the first 17 days of the experiment. Once the drying phase was started, moisture was permitted to evaporate to the exterior and diffuse through the other assembly parts. An obvious weight difference can be seen between the assemblies with and without studs. Figure 3.7 clearly shows that

once the drying was started, the moisture in the brick component quickly dried. The sheathing component, seen in Figure 3.8, accumulated moisture throughout the wetting phase and dried throughout the drying phase. The gypsum reacted differently than the sheathing component since it continued to accumulate moisture through the wetting phase and into the drying phase. As well, unlike the other components, two different, distinct patterns are observed in the gypsum depending on the type of interior finish.

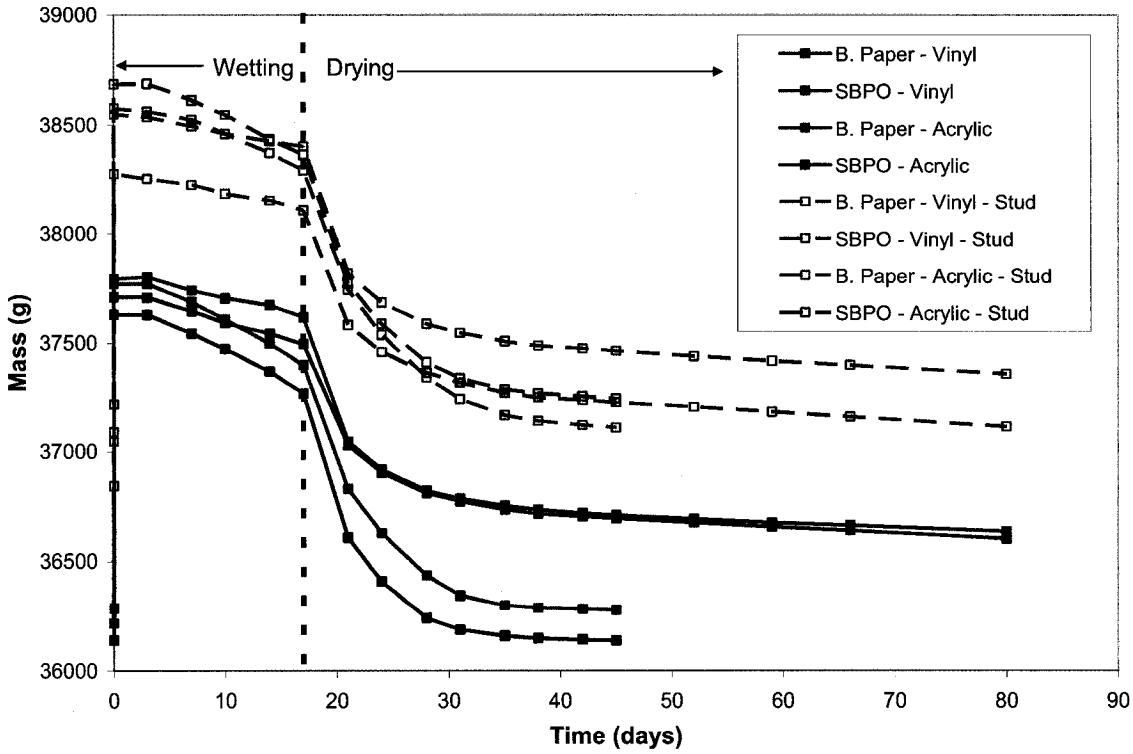

Figure 3.6 Total mass of all assemblies during full duration of test

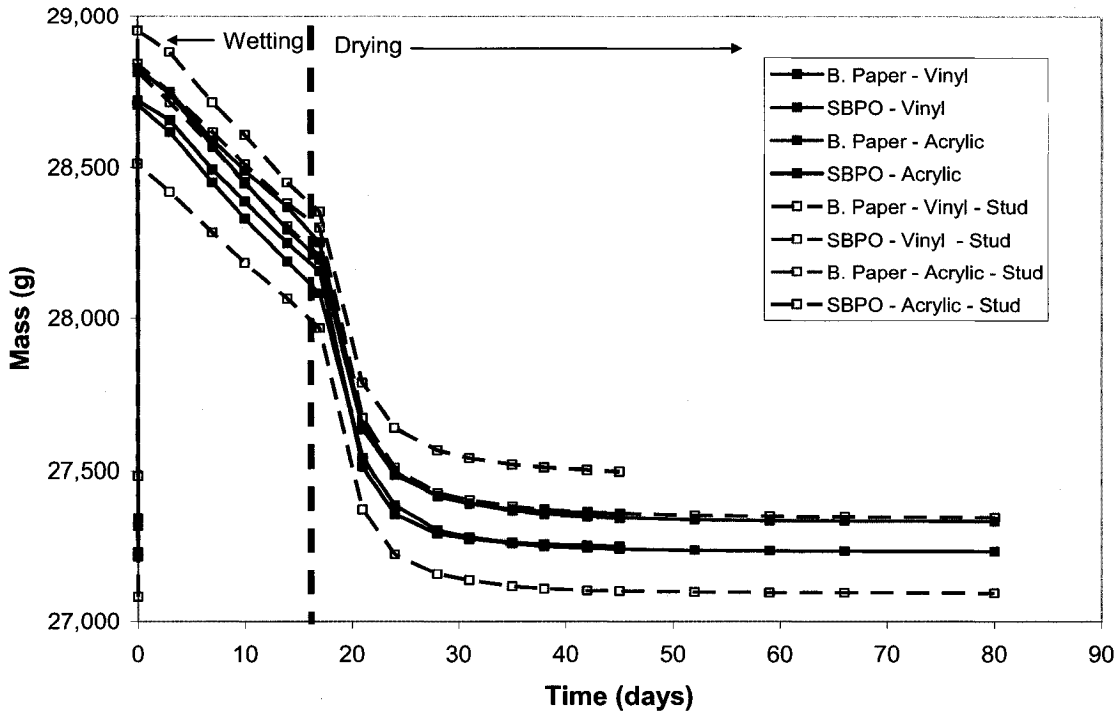

Figure 3.7 Mass of component 1 – Brick during full duration of test

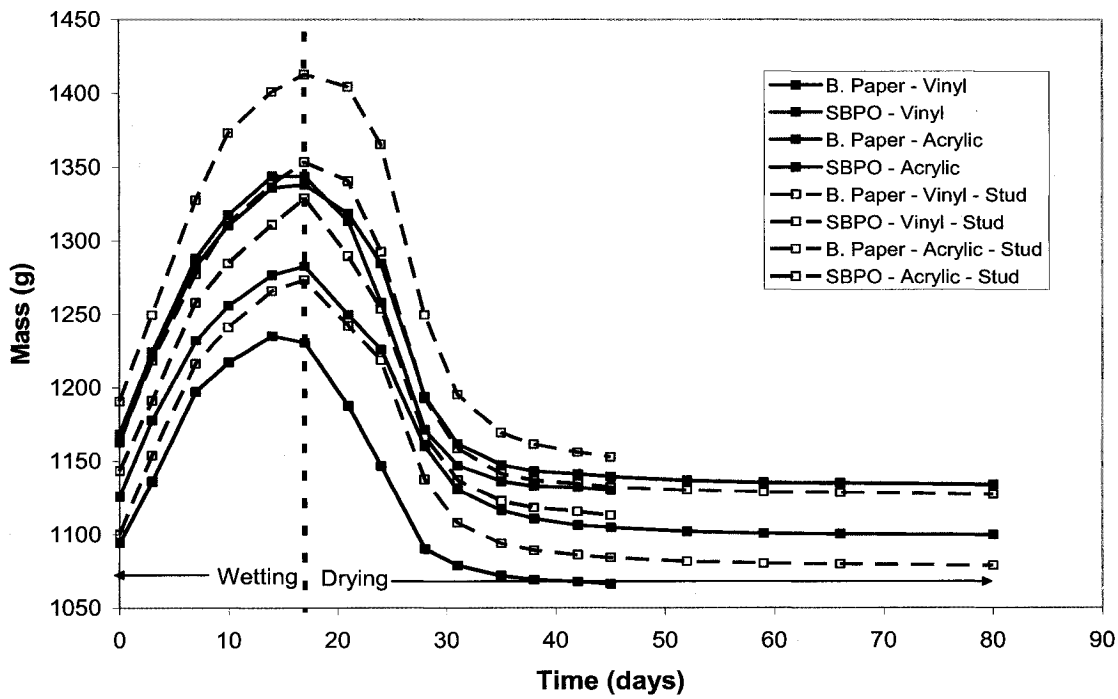

Figure 3.8 Mass of component 2 – Sheathing & WRB during full duration of test

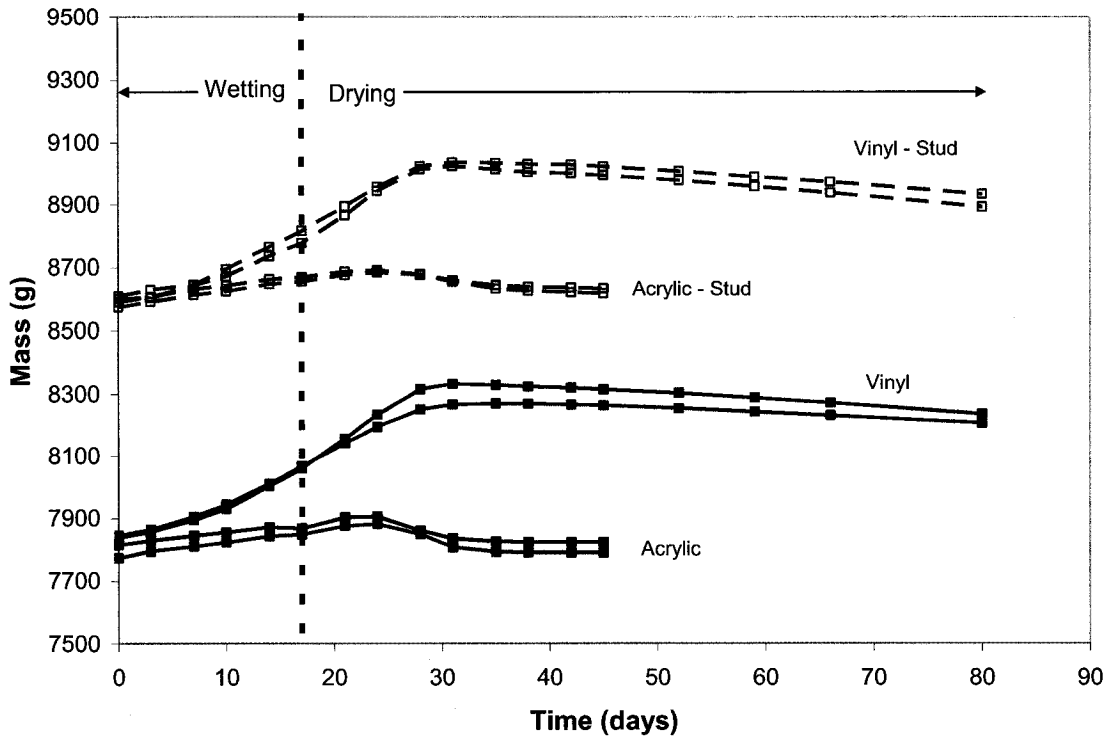

Figure 3.9 Mass of component 3 – Insulation & gypsum

Throughout the wetting phase and into the beginning of the dying phase, condensation, under the form of water droplets, was observed to lie on the sheathing paper at the regular deconstruction and weigh-ins. To prevent this build up of condensation from running off, it was collected with a wide tissue and weighed. In general, more moisture, about 17.5 g, was collected from the assemblies finished with building paper than those with spun bonded polyolefin (13 g). Once the brick components were dry, condensation was no longer observed. Refer to Appendix B for the amount of condensation accumulated and removed from each sheathing.

3.2.2.2 Mass of Individual Wall Materials

The following section focuses on the mass of the individual materials which make up each wall system. These weights were measured only four times throughout the entire experiment since this measurement required the complete deconstruction of the assemblies which could have influenced the moisture content within the assemblies. The

mass of the individual assembly materials was recorded before the walls were assembled at normal conditions, between the wetting and drying phase, at the end of the experiment and after the materials had been oven dried at 50°C for a week.

Obtaining the individual mass of these materials leads to a better understanding of the component behaviors in each assembly since the oven dry mass can be used to determine the moisture content in each layer of the assemblies with the following equation:

$$MC = (M_i - M_{dry})*100/M_{dry} \quad (3.1)$$

Where M_i is the instantaneous mass of the material and M_{dry} is the dry mass of the material.

All results and calculations are found in Appendix B.

3.2.3 Observations of Mold

Areas with mold were observed on the weather resistive barriers, the OSB, gypsum and between the vinyl wall covering and gypsum, seen in Figure 3.10 and Figure 3.11. Once noted, it is anyhow beyond the scope of this project to quantify or to further investigate this occurrence of mold.

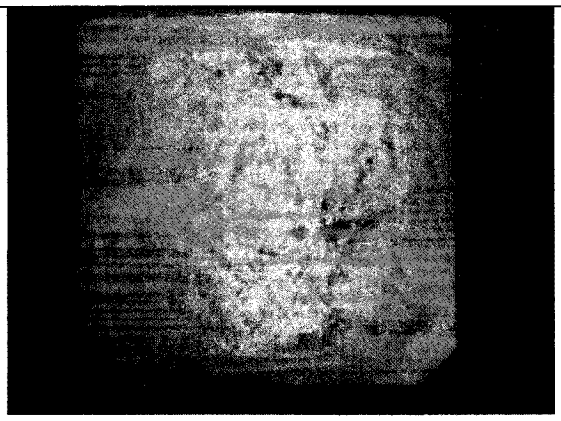

Figure 3.10 Mold observed on SBPO

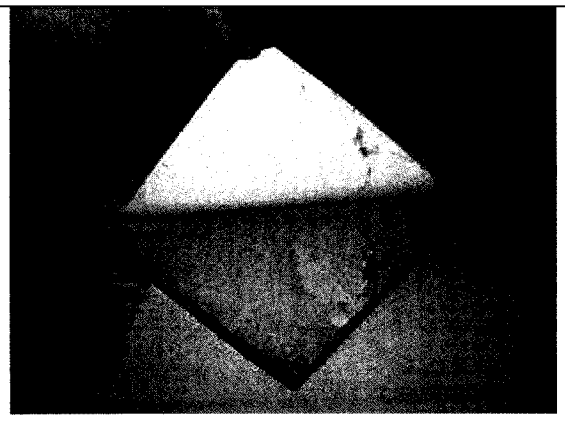

Figure 3.11 Mold observed between gypsum and vinyl wall covering

3.3 Observations and Conclusions

The following section analyzes the experimental results presented above. Material moisture contents are graphed. The individual materials are compared between assemblies to determine if wetting and drying patterns exist and whether material drying rates are dependent on adjacent materials.

3.3.1 Gravimetric Measurements

3.3.1.1 Moisture within Components

The moisture occurring in each assembly is presented below in Figure 3.12 where a large distinction can be made between the drying and wetting phases. Each assembly received approximately 1.5 L of water, absorbed in the brick at the beginning of the experiment. The exact determination of the added moisture is difficult due to some leaks through the brick (less than 10 ml). Over the duration of the test, the moisture dried out. The rate of the moisture leaving the assemblies is dependent on the duration of the wetting phase as well as the materials used in the assembly constructions. Since some materials have a higher permeance then others, assembly construction governs the drying rate of each specimen. At day 45, the specimens constructed with acrylic paint were nearly dry while the specimens with vinyl wall covering still contained about one third of their initial moisture.

In the wetting phase, moisture diffuses through the system to the inside. Such vapor movement is observed to be greater in the painted assemblies, signaling that moisture is capable of drying through to the interior when acrylic paint is used to finish the gypsum board while vinyl wall covering does not permit moisture to travel through as easily. The vaportight finishing prevents the assemblies from losing any significant amount of moisture during the wetting phase. Then, at the start of the drying phase, the moisture within the assemblies can exit to the two sides of the assemblies, i.e. the brick cladding side of the system and gypsum board side.

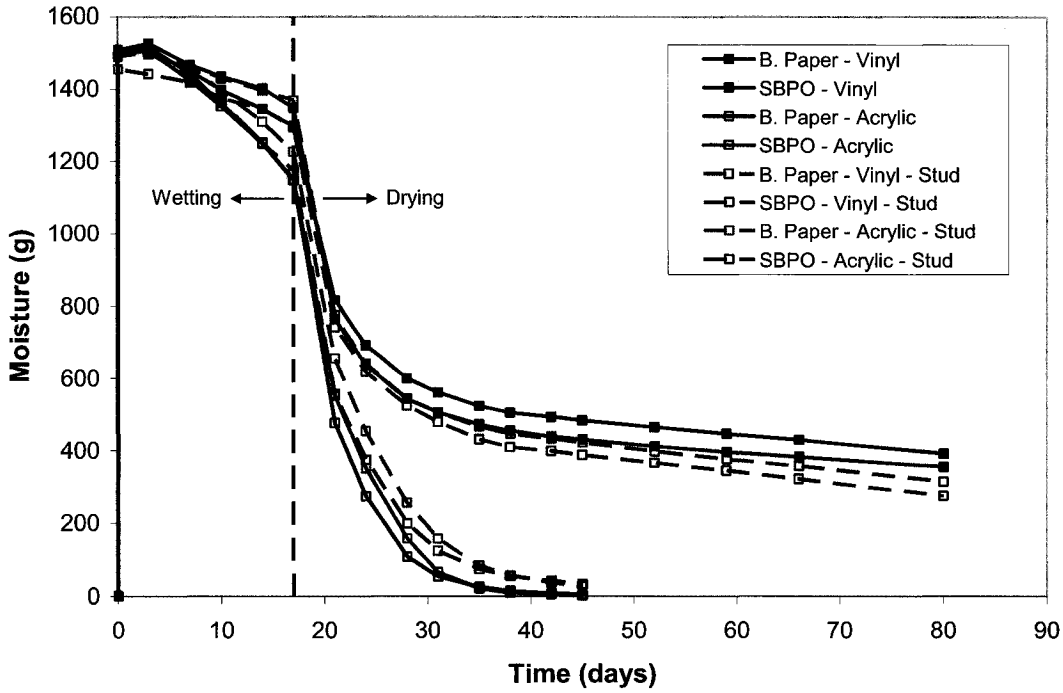

Figure 3.12 Total moisture accumulation in all assemblies

3.3.1.1.1 Moisture of Component 1

The moisture in component 1 is the amount of moisture found in the brick portion of the wall assemblies. Figure 3.13 describes the moisture trends within the brick, which are uniform throughout all of the test assemblies regardless of their material construction. During the wetting phase, upwards of 40 kg/m^3 (576 g) of moisture per wall is driven from the brick towards the interior. This moisture is absorbed by the other building components.

Once the drying phase is started, the brick dries first rapidly. It takes about 20 days for the brick to become nearly totally dry.

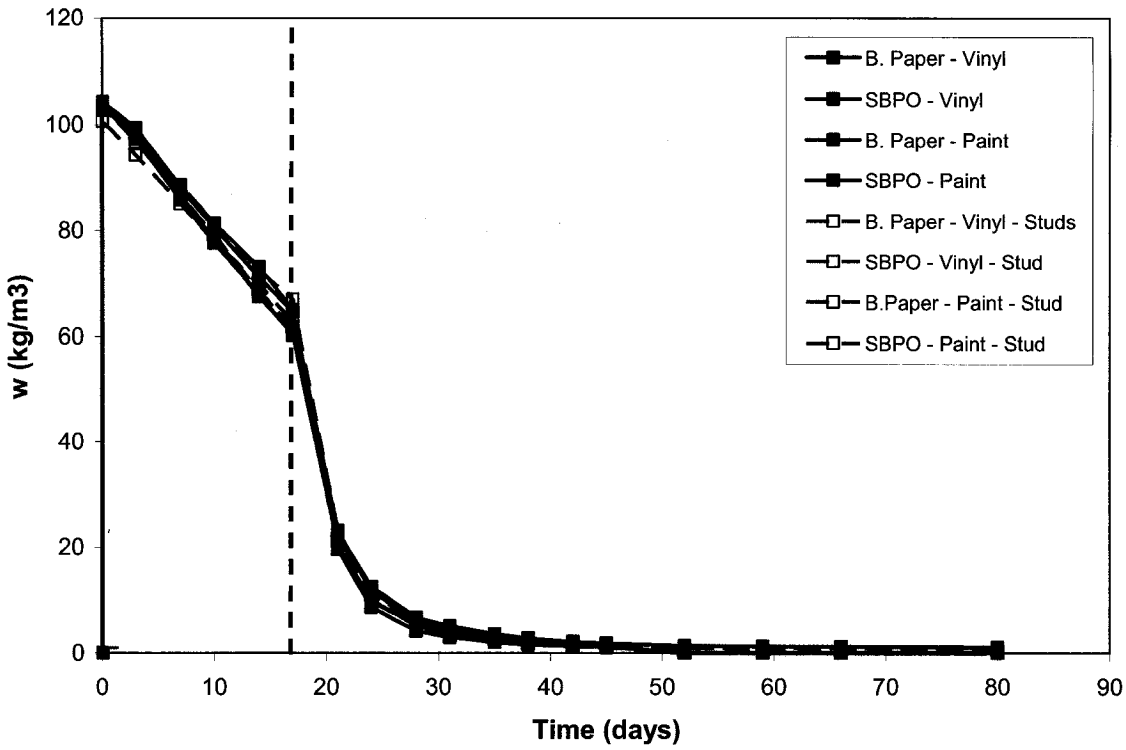

Figure 3.13 Moisture content in bricks - component 1

3.3.1.1.2 Moisture of Component 2

It is the OSB of component 2, consisting of the OSB and the weather resistive barrier, which absorbs the bulk of the moisture faced with this assembly section. The OSB sheathing, which is a non-homogeneous material, absorbs moisture in the range from about 120 kg/m^3 to 190 kg/m^3. All of the specimens constructed with a stud absorbed more moisture than without a stud.

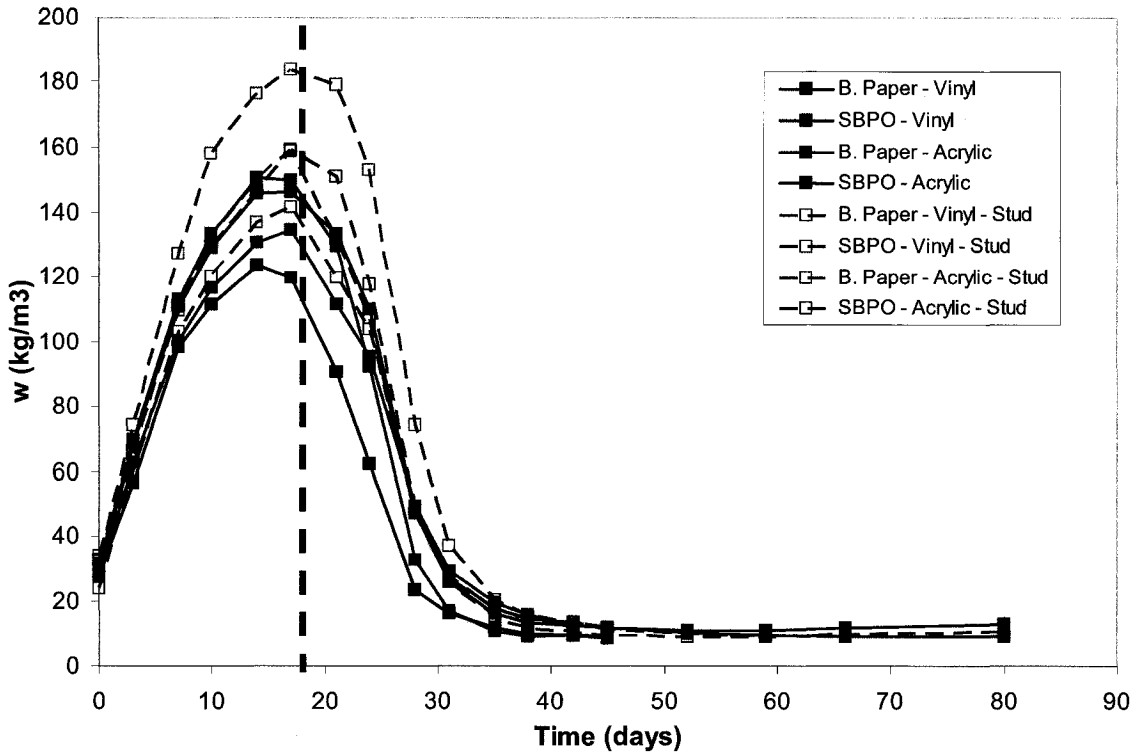

Figure 3.14 Moisture content in OSB sheathing

The weather resistive barriers have an impact on the moisture response of the OSB sheathings. Comparing the response of the assemblies finished with vinyl wall paper, all sheathings covered in building paper have somewhat greater measured amounts of moisture than when covered with SPBO. The same observation is noted when the assemblies are finished with acrylic paint. This indicates that, at high relative humidity, the building paper is slightly more vapor permeable than the SBPO, allowing for greater quantities of moisture to flow through. As a result, the sheathing covered with building paper may accumulate more moisture and equally more moisture will be allowed to dry out.

Studying the effect of the interior finishing on the OSB sheathings proves to be of interest. The assemblies finished with vinyl paper are more vapor tight thus leading to an increase in moisture within the sheathings. This trend is observed in all comparisons but between the SBPO – no Stud assemblies.

The final amount of moisture in all the individual sheathings is similar at the end of the experiment. The overall drying of the individual sheathing specimens over prolonged periods of time is not affected by the varying sheathing papers and finishing within the different specimens.

3.3.1.1.3 Moisture of Component 3

The interior side of the wall assemblies, component 3, consists of mineral wool insulation, gypsum board, interior finishing and depending on the specimen either the inclusion or absence of a wooden stud. The following section describes the amount of moisture accumulated in the section, primarily by the interior gypsum board.

Figure 3.15 clearly shows the two different responses of the gypsum board in terms of moisture content. Half of the assemblies accumulate up to 250 kg/m^3 of moisture while the other half accumulate up to 50 kg/m^3 moisture. As expected, the assemblies finished with the low permeable paper (VWC) accumulate more moisture than the assemblies finished with the highly permeable paint. Furthermore, the assemblies with the vinyl wall paper not only accumulate a significant amount of moisture, but also have difficulty in drying.

The moisture accumulation within the gypsum depends greatly on the permeance of the interior finishing directly applied to its interior facing side. The weather resistive barrier, although minimal, also has an effect on the moisture accumulation of the gypsum.

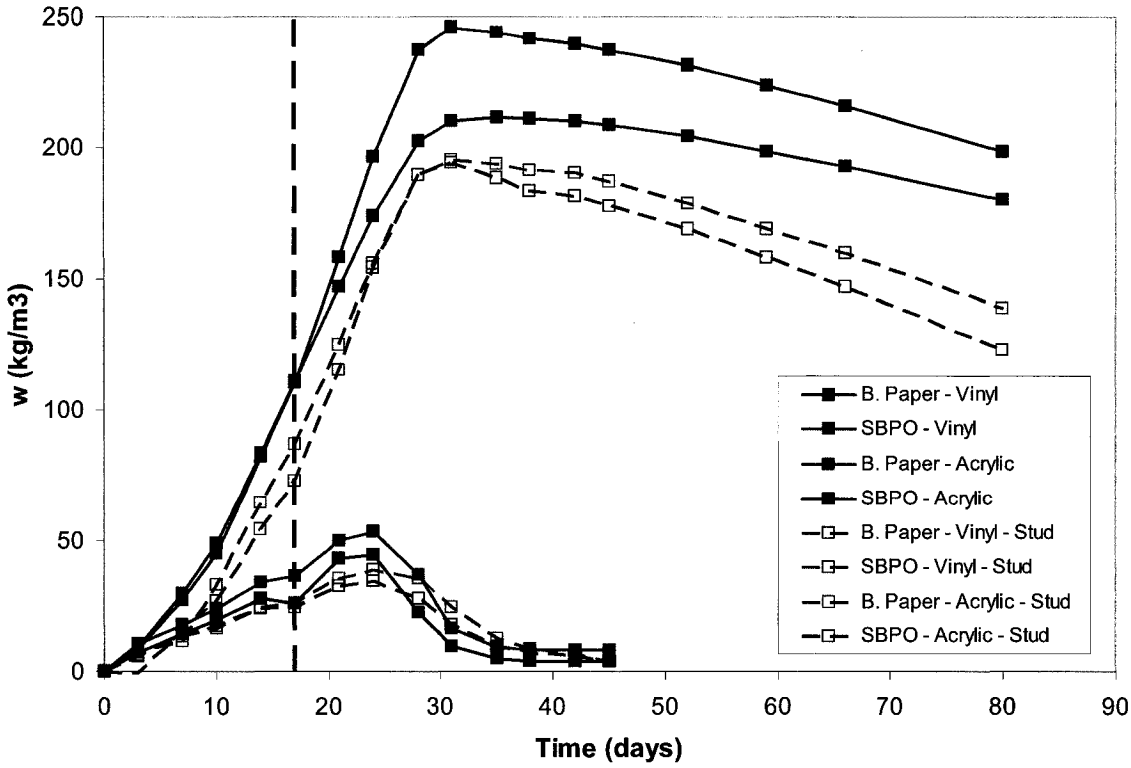

Figure 3.15 Moisture content in gypsum panels

Comparing the effect of the sheathing papers on the gypsum, while keeping the interior finishing constant, proves to be similar to that of the OSB. In all but the Vinyl –Stud assemblies, the gypsum boards with building paper accumulate a greater amount of moisture than when constructed with SBPO.

Furthermore, the blocking effect in terms of area of the wood studs induces an effect on the moisture behavior of the gypsum board. Referring to Figure 3.16, the inclusion of a wood stud decreases the moisture found in the gypsum panels. The stud points represent the amount of moisture found in the wood at specific times during the experiment. Two reasons explain the reduction in moisture present in the gypsum: a 10% reduction of gypsum surface area in contact with moisture due to stud, and moisture uptake by the stud. The moisture of the gypsum combined with the moisture of the adjacent wood stud equals the moisture within the gypsum panels constructed without studs.

Appendix B presents the effect of the moisture absorption by the wood studs on the moisture content of the gypsum specimens.

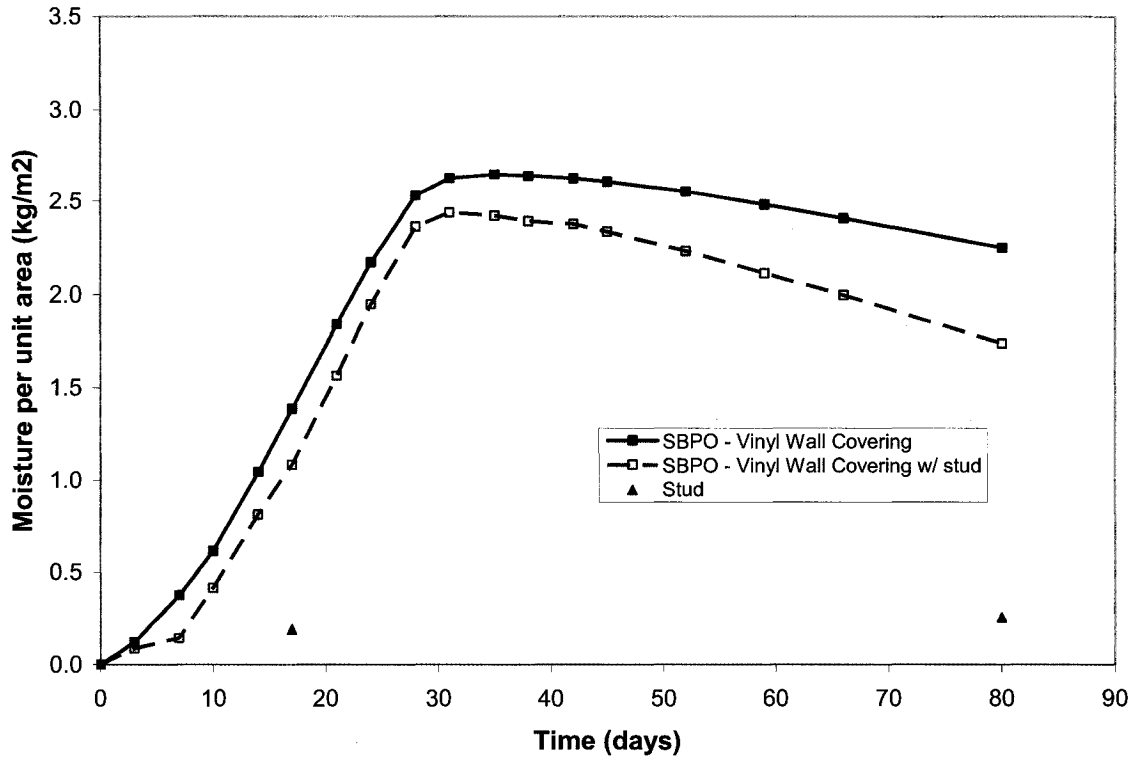

Figure 3.16 Example of effect of the presence of wood on the moisture accumulation per area in gypsum in one assembly with spun bonded polyolefin and vinyl wall covering

3.3.1.2 Comparison of Moisture Transport in three Materials

A relation between the drying rates of the brick, OSB sheathing and gypsum board is noted regardless of the inclusion/absence of wooden studs.

During the experiment, once the aluminum plates are taken off of the assemblies, the bricks quickly dry out towards the inside and outside. As the moisture dries from the brick towards the inside, moisture gets absorbed by the subsequent series of building components which make up the assemblies.

In the case of the OSB, moisture is accumulated during the wetting phase. The OSB sheathings begin to dry as soon as the assemblies are permitted to dry to the outside.

However, the drying rate of the OSB seems to be dependent on the drying rate of the brick and the OSB's only dry out once the brick has almost completely dried.

A different relation is seen between the OSB and gypsum. Unlike the OSB, the gypsum continues to accumulate moisture even after the assemblies are allowed to dry to both sides. When the aluminum plates are removed, the assemblies still have high relative humidity within the wall materials and cavities which are still exposed to vapor pressure differentials. These pressure differentials further drive moisture towards the inside of the assembly, thus into the interior sheathing.

Figure 3.17 shows that walls finished with vinyl have a maximum amount of moisture in the gypsum when the OSB is nearly dry on day 31. Figure 3.18 shows that the drying of gypsum occurs at day 24, one week earlier, in the assembly with acrylic paint, highlighting the maximum amount of moisture in the gypsum, which evidently is still while the OSB retains moisture. This explains that the acrylic paint covered assemblies allow for the interior sheathing to dry towards the interior, which is not the case for the VWC assemblies.

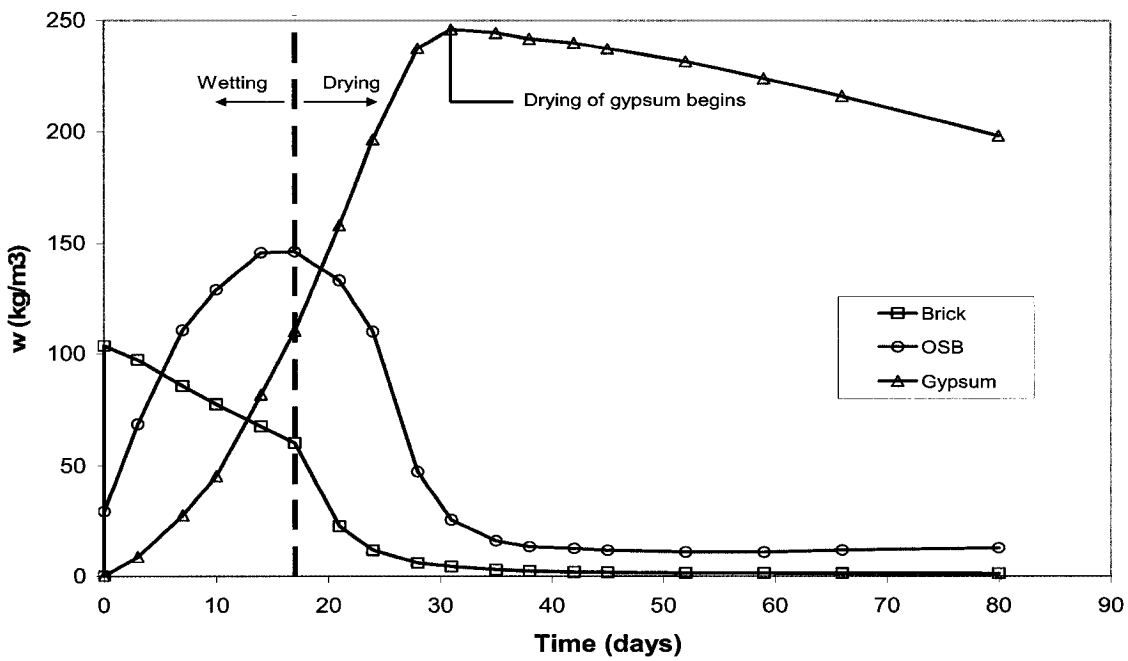

Figure 3.17 Moisture content in three components of the B. Paper - Vinyl assembly

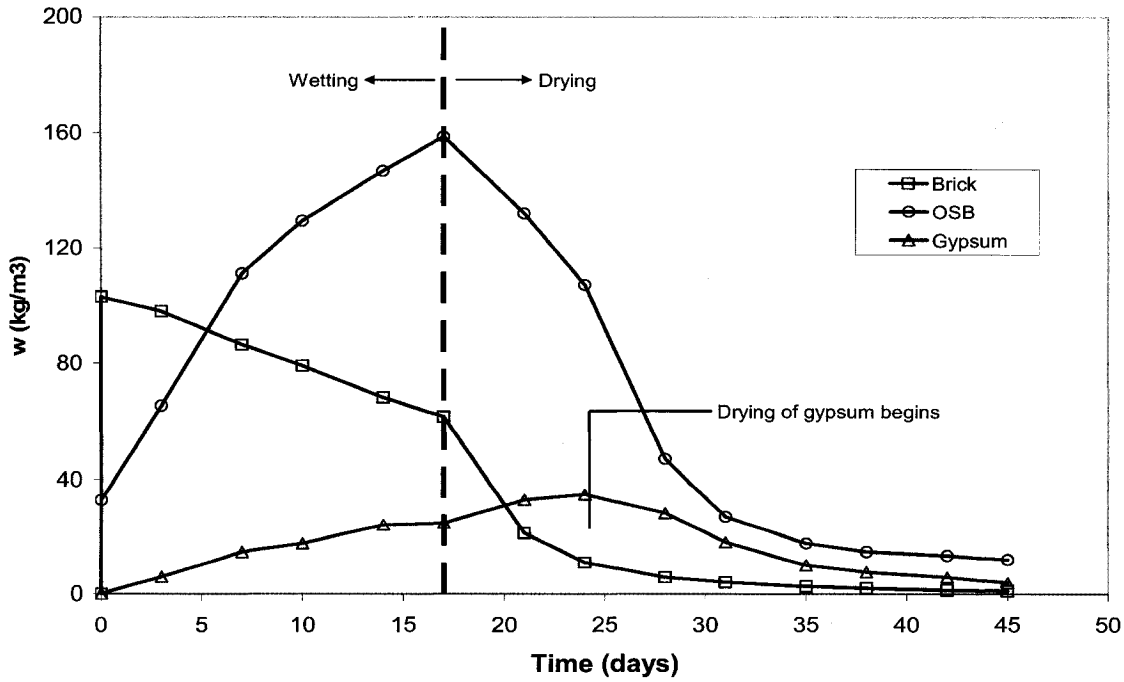

Figure 3.18 Moisture content in three components of the SBPO – Acrylic - Stud assembly

As previously explained, the gypsum covered with VWC can only dry once the OSB is nearly dry which is not the case with acrylic paint covered gypsum. Since the paint is vapor permeable, the gypsum can begin drying towards the interior even when the OSB still contains moisture where the VWC covered gypsum can mostly dry to the exterior. Furthermore, in the case of acrylic paint, both the OSB and gypsum are finished drying at almost the same time.

Table 3.2 Maximum measured moisture content in sheathings (kg/m^3)

Wall	MC in OSB	day	MC in Gypsum	day
B. Paper - Vinyl	139.84	17	246.00	31
SBPO - Vinyl	130.68	17	211.60	31
B. Paper - Acrylic	142.38	14	53.60	24
SBPO - Acrylic	119.14	14	49.00	24
B. Paper - Vinyl - Stud	150.30	17	193.80	31
SBPO - Vinyl - Stud	141.20	17	195.10	31
B. Paper - Acrylic - Stud	173.08	17	39.30	24
SBPO - Acrylic - Stud	149.23	17	34.70	24

Table 3.2 outlines the maximum measured moisture content in each sheathing component for all assemblies and at what day it is measured. The sheathings which accumulated the most moisture are shaded.

In the case of the OSB sheathing, all but two maximums are found to be at the end of the wetting phase just before the drying phase is commenced. The trend shows that the building paper covered OSB's accumulate more moisture than the spun bonded polyolefin covered sheathings.

The gypsum boards show different results. The maximum moisture contents are, as stated earlier, greatly dependent on the interior finishing. The maximum moisture is measured on day 31 for the vinyl finished gypsums and day 24 for the paint finished assemblies. Furthermore, the maximum amount of moisture is found to be in the gypsum panels from the assemblies without wood studs.

Refer to Appendix B for comparison graphs of the moisture behavior between materials for all assemblies.

3.3.1.3 Calculated Moisture Content of Individual Wall Materials

The SBPO had moisture content of up to 44.4% while the building paper measured moisture content as low as 22.9% which may have had an effect on the OSB sheathing. The sheathing covered with building paper had higher moisture contents than the SBPO covered OSB in all cases, by more than 7% moisture content difference. In addition, all OSB panels had an initial moisture content of about 4% due to the laboratory conditions where they were stored. By the end of the experiment, the moisture content of the OSB was lower than its initial laboratory conditions.

The vinyl wall covering influenced the moisture content of the mineral wool insulation by nearly one and half times in all assemblies compared to the acrylic paint finishes while the studs all saw similar moisture contents. The studs continued to accumulate moisture beyond the wetting phase, especially in the vinyl finished assemblies.

A difference in moisture accumulation is seen between the painted and vinyl covered gypsum panels. The vinyl covered gypsum panels are shown to have moisture content as high as 34.5% while the acrylic painted panels' moisture contents do not exceed 10%, about three and half times difference. The inclusion of the wood studs saw even lower moisture contents in the gypsum specimens.

All the experimental data-derived moisture content results are presented in Appendix B.

3.3.2 Interpretation of Continuous Monitoring Results

3.3.2.1 Moisture Content Probes Data

To measure the moisture content of the wood materials of each specimen, moisture content probes were used. Some malfunctions occurred during some periods of the test. These results were not accurately logged and have since been disregarded from the graphs. Also, note that the RH sensor for assembly B. Paper – Vinyl – Stud malfunctioned and no data was obtained for the relative humidity between the insulation and gypsum panel.

3.3.2.1.1 Moisture Content of OSB Sheathing

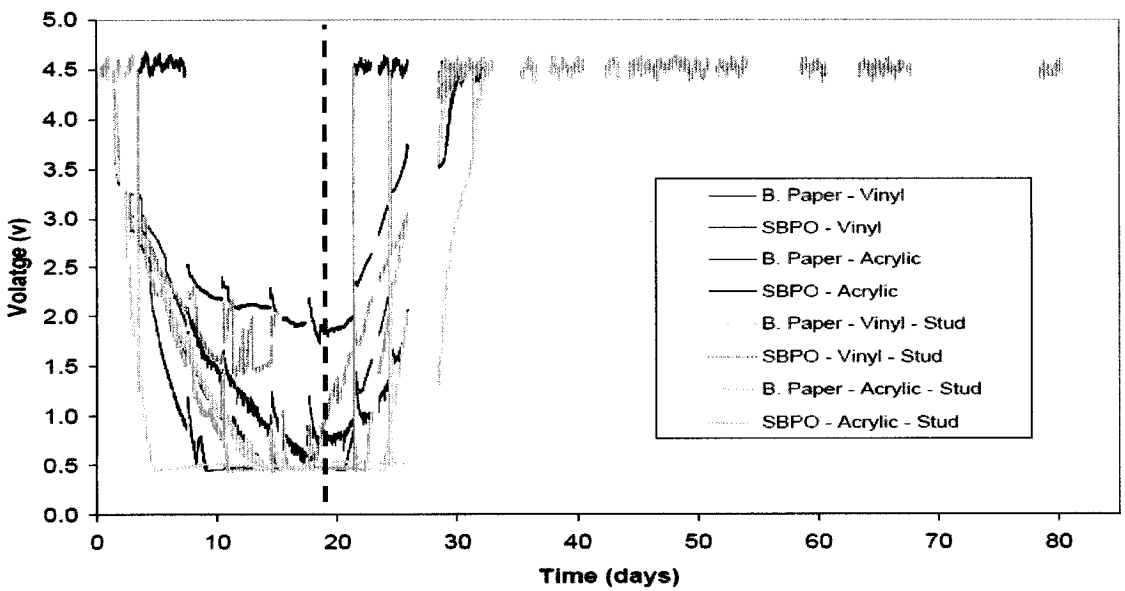

Figure 3.19 Moisture content probes voltage outputs of OSB

Since OSB is not a homogeneous material, and the moisture content probes used do not have a conversion table for the OSB used, the voltage outputs of Figure 3.19 are not providing actual moisture contents but rather offer an idea of what is taking place within them. The outputs shown in Figure 3.19 indicate the presence of moisture within the specimens.

In all but the 'SBPO – Acrylic' specimen, the moisture content reached excessive moisture levels in the sheathing. The results of the moisture pins confirm qualitatively the gravimetric results obtained from the OSB. As the conductance of the OSB decreases in Figure 3.19, the moisture content in the OSB increases as seen in Figure 3.14.

3.3.2.1.2 Moisture Content of Wood Studs

Each stud is equipped with four moisture content probes to map the moisture content at different locations and depths. The results displayed in Figure 3.20 represent the moisture content in the stud from sample 'B. Paper – Vinyl – Stud'. The moisture content probes 5.7 and 5.9 are on the OSB side of the stud while probe pairs 5.8 and 5.10 are adjacent to the gypsum panel. The results illustrate the moisture present in the stud where the moisture accumulation on the OSB side is relatively less than the gypsum side. Furthermore, moisture content probes 5.7 and 5.9 have no difference in moisture content regardless of their difference in penetration depth. However the moisture content on the gypsum side is dependent on the penetration depth.

The moisture content probe 5.8, which is 4 mm deep, reaches moisture content levels of 18% while probe 5.10, only 20 mm deep, reaches levels of 15%. While this is only a 3% difference, it shows that the wood stud accumulates different amounts of moisture depending on depth.

Refer to Appendix E for the moisture content probe locations in the S-P-F studs.

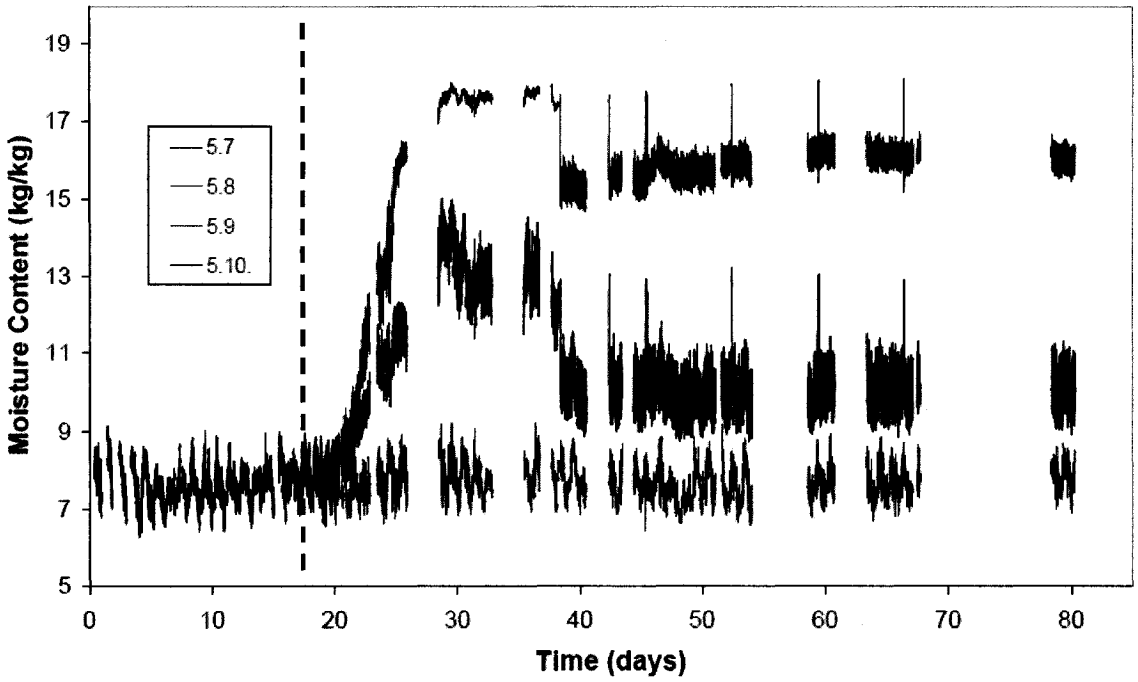

Figure 3.20 Electronic gravimetric moisture content of stud 'B. Paper - Vinyl - Stud' (kg/kg)

The moisture contents witnessed in the studs from the acrylic finished assemblies show almost no difference leading to two possible conclusions: the studs do not accumulate much moisture since the assemblies are much more vapor permeable, or the moisture content probes malfunctioned and were unable to properly record the outputs.

3.3.2.2 Relative Humidity Probes

Each specimen is equipped with relative humidity probes which monitor and record the conditions both in, above and below the specimens. The relative humidity within the air and insulating cavities are related to the moisture flow through assemblies and are discussed below.

3.3.2.2.1 Relative Humidity in the Cavity

The relative humidity measured in the air cavity, shown in Figure 3.21, explain,s that shortly after the onset of drying, the RH levels rapidly. At 30 days, after drying is allowed towards the outside, the relative humidity in the cavities stabilizes at about 25%

RH for the assemblies finished with vinyl wall covering. Where acrylic paint is used as the interior finish, the relative humidity levels in the cavities are slightly lower than those observed with the vinyl paper. Furthermore, the relatively more vapor permeable assemblies have a decrease in RH prior to their more vapor tight counterparts.

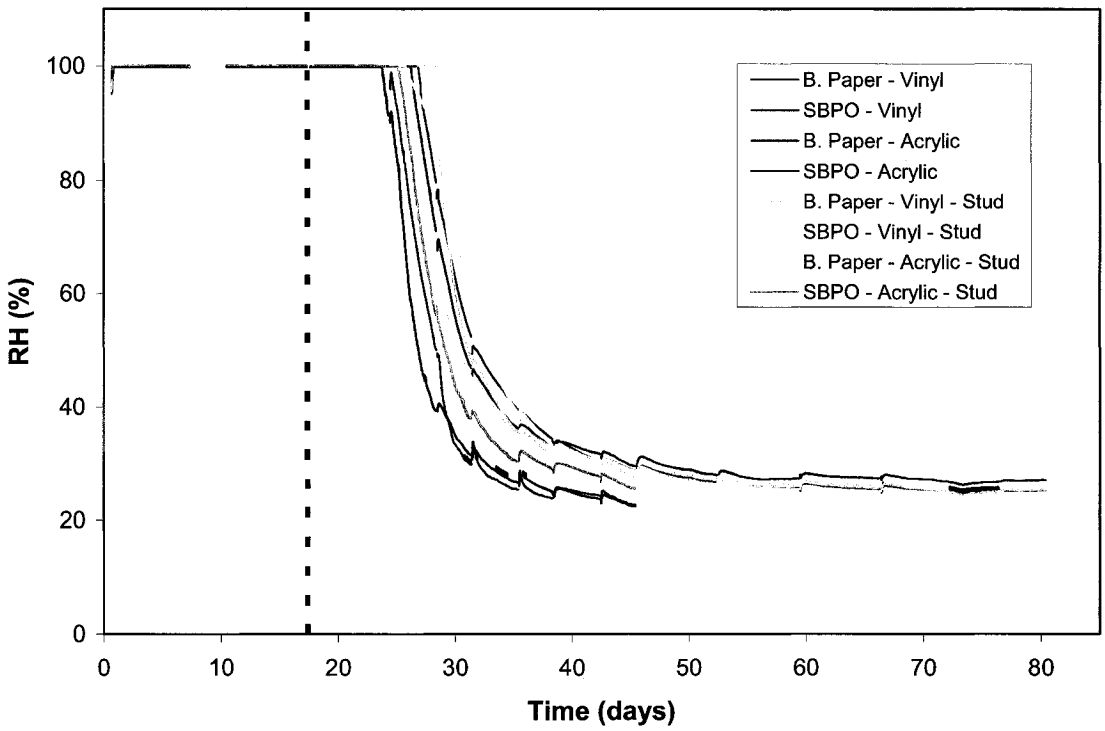

Figure 3.21 Relative humidity in cavity spaces during the whole duration of the test

3.3.2.2.2 Relative Humidity between Insulation and Gypsum Board

The measured relative humidity between the insulation and gypsum board is shown in Figure 3.22. The probe was placed on the exterior surface of the gypsum board and embedded with mineral wool. It is seen that the specimens finished with vinyl wall paper maintain an RH level near 100%. Conversely, the specimens with acrylic paint show a decrease in RH after drying is promoted to the exterior.

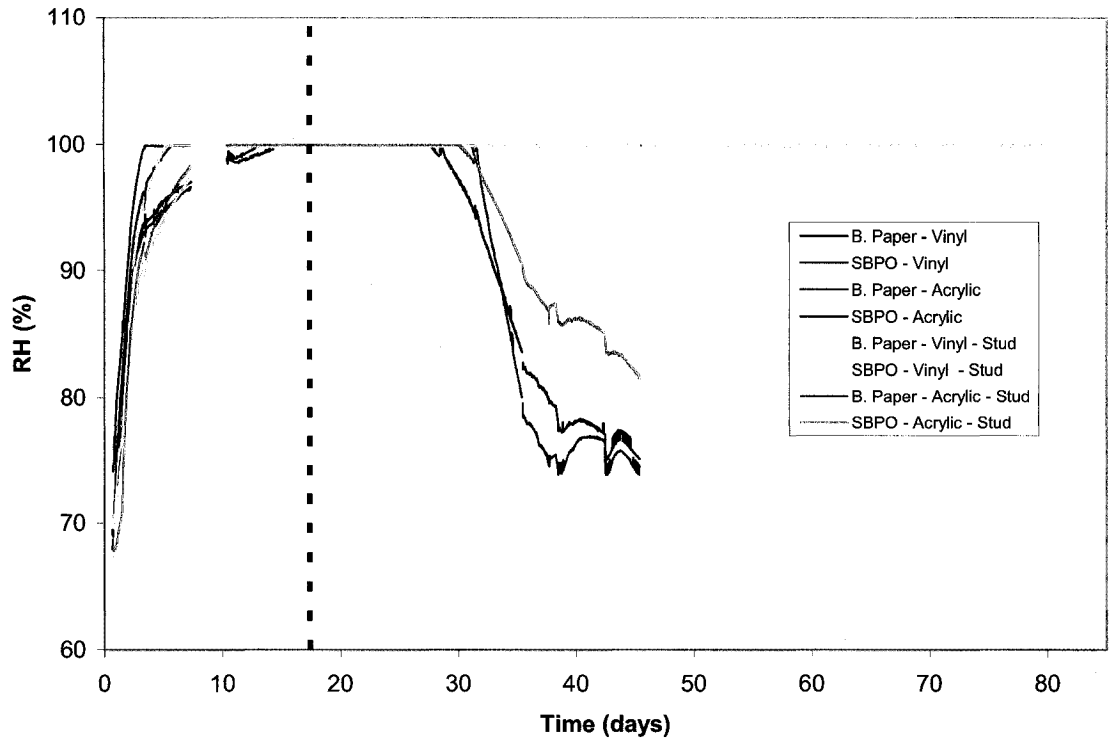

Figure 3.22 Relative humidity in the insulation close to the gypsum during the whole duration of the test

3.4 Simulation Results

The following section presents the modeling work performed to simulate and predict the outcome of the four wall specimens without a wood stud tested in the experimental set-up. The parameters used to simulate the wall assemblies are based on the environmental conditions of the laboratory experiment as well as the material properties which were tested in the lab or found in literature.

All simulations were conducted using a multidimensional hygrothermal simulation tool, HAMFEM. An acronym for Heat Air Moisture Finite Element Method, HAMFEM is a hygrothermal simulation model that calculates heat, air and moisture transfer through building components. It was developed at the Katholieke Universiteit Leuven (KULeuven) in Belgium. The software can be used to calculate transfer in 1, 2 and 3 dimensions using either atmospheric or user-defined boundary conditions. Further

information on the software is presented in Janssen et al (2006). The assembly descriptions, assumptions made and material properties for the simulations are fully explained in Appendix D.

The results of the one-dimensional simulations are based on 1.5 liters of water initially added to the brick specimens, while the rest of the materials are at the laboratory conditions. All units are shown in either kg for assembly sections and kg/m^3 for individual materials.

3.4.1 Total Moisture Content

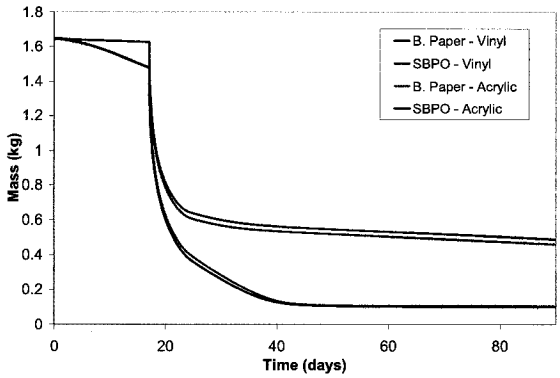

Figure 3.23 Total moisture mass - simulation

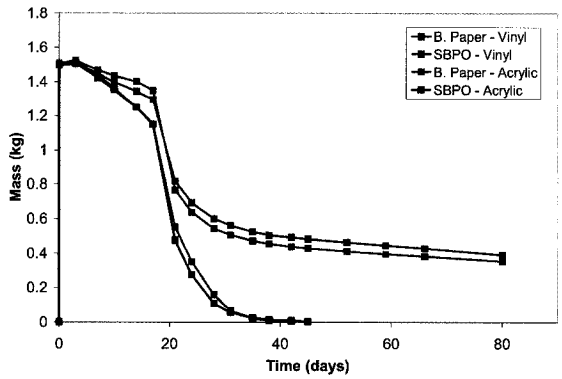

Figure 3.24 Total moisture mass - experimental

Referring to Figure 3.23, a clear difference in moisture during both the wetting and drying phase can be seen between the vinyl and paint finished assemblies. During the wetting period, the moisture remains nearly constant in the vinyl finished walls while the painted walls show a slight loss in moisture during that same period due to their respective permeabilities. When the drying phase is introduced, all assemblies show a sharp and rapid decrease in moisture. However, shortly after drying, the vapor tight assemblies have an abrupt decrease in moisture loss while the relatively vapor open assemblies continue to evacuate moisture at a rate which gradually decelerates compared to the latter. The assemblies constructed with building paper retain a slightly larger amount of moisture than those with spun bonded polyolefin.

A similar trend to Figure 3.23 is observed in the experimental results seen in Figure 3.24. The paint finished assemblies have a different response to the moisture as do the vinyl finished assemblies. Although the simulation results have smoother trends, some

experimental error can be assumed during the periodic disassembly of the specimens during gravimetric weigh-ins.

3.4.2 Moisture Content of Bricks

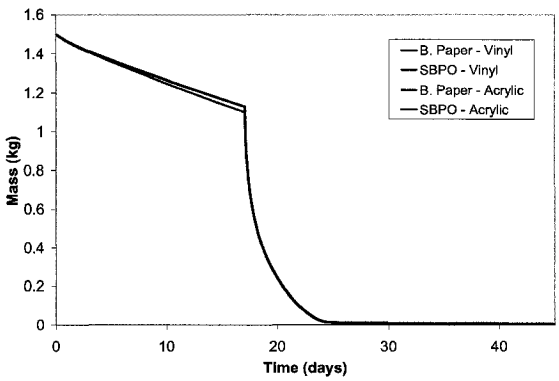

Figure 3.25 Total moisture in bricks - simulation

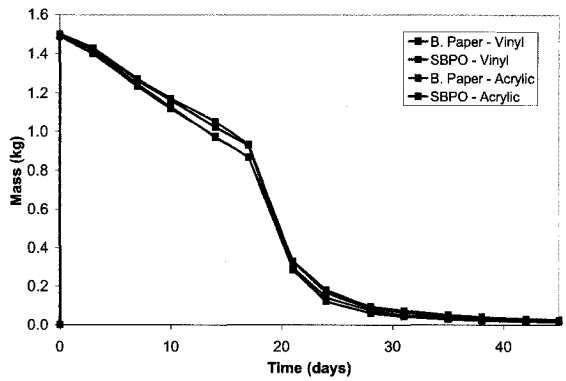

Figure 3.26 Total moisture in bricks - experimental

The simulated moisture within the brick remains quite constant for all of the different wall assemblies. As observed in the experimental results, once drying is allowed to the exterior, a significant loss of moisture is witnessed in all of the assemblies. The majority of moisture stored within the brick is lost to the environment while only a fraction of the stored moisture is driven towards the interior.

The simulation results in Figure 3.25 compared to Figure 3.26 both show that the weather resistive barrier has a alight effect of the drying rate of the bricks. The bricks from the building paper covered sheathing assemblies lose more moisture during the wetting phase than the spun bonded polyolefin assemblies; however these differences are not significant. These results show that the building paper is more vapor permeable allowing more moisture to diffuse through and into the subsequent building layers.

The simulation conducted with brick assumes that the entire material is a uniform matrix and does not take into consideration the use of mortar. Modeling with mortar is more complex and beyond the scope of these simulations.

3.4.3 Moisture Content of OSB Sheathing

Figure 3.27 depicts the moisture in the OSB sheathing within the wall assemblies for the duration of the test. The moisture within the sheathing is dependent on the weather resistive barrier, where the use of building paper increases the moisture in the OSB compared to the assemblies with spun bonded polyolefin.

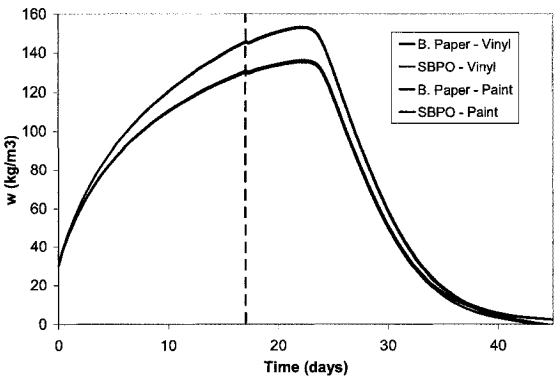

Figure 3.27 Moisture in OSB - simulation

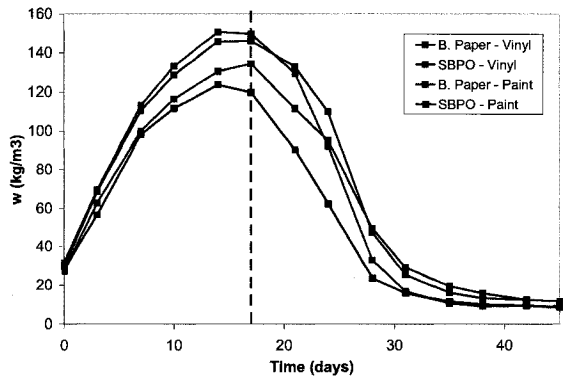

Figure 3.28 Moisture in OSB - experimental

The experimental results of the OSB in Figure 3.28 show a large variation in the response of the material depending on the construction. Although the trends of each assembly OSB are not as uniform as the simulation, the building paper covered OSB sheathings accumulate more moisture. Furthermore, the experimental result trends are symmetrical along the x-axis at their peak. This characteristic is not distinguished in the simulation results where the OSB continues to accumulate moisture in the drying phase. The difference between the simulation and experimental results is related to hysteresis. Accounting for hysteresis in the model proved to be difficult and beyond the scope of this research. Nevertheless, the results of the simulation are somewhat representative of the experimental results.

3.4.4 Moisture Content of Gypsum

As expected, the vapor-tight assemblies have a far greater accumulation of moisture than the relatively vapor open assemblies seen in both Figure 3.29 and Figure 3.30. It is clear that the permeability of the interior gypsum finishing plays a role on the moisture flow from the brick through to the interior. The relatively high permeability of the paint

prevents the accumulation of moisture in the gypsum while allowing it to dry out at a relatively fast rate. Relative to the highly permeable paint, the low permeable vinyl paper increases the accumulation of moisture in the gypsum while decreasing the evacuation of the accumulated moisture.

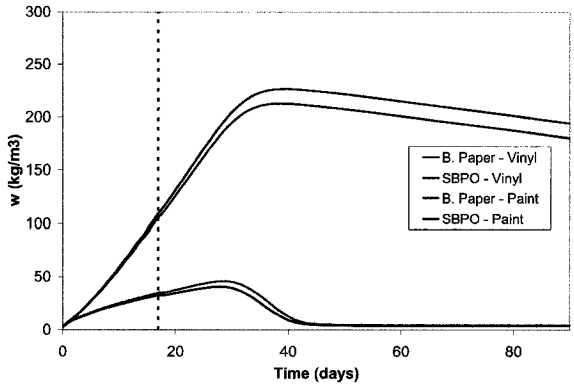

Figure 3.29 Moisture in gypsum - simulation

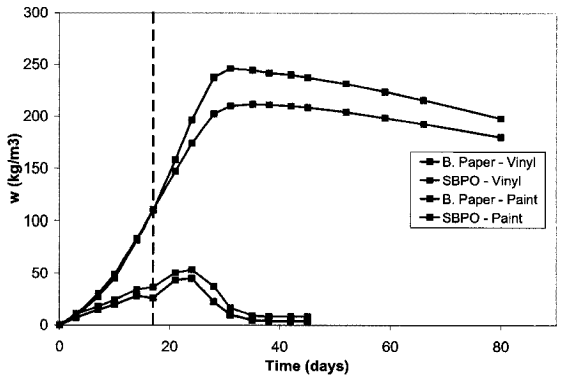

Figure 3.30 Moisture in gypsum - experimental

Figure 3.30 shows that the gypsum has the largest variation to moisture behavior in response to the interior finishings. The simulated results present a good representation of the gypsum behavior.

3.5 Conclusion

The small-scale test with constant thermal loading shows that, due to a relatively high temperature gradient, an important vapor flow is generated to the back wall, wetting the OSB, mineral wool and gypsum board. Moisture accumulation in gypsum board covered with a vapor-tight vinyl wall covering is much higher than the accumulation of moisture by gypsum board with vapor permeable paint. The acrylic paint finishing reduces the moisture content of the gypsum board by up to 5 times under the tested conditions.

It was shown that the type of weather resistive barrier slightly changes the wetting and drying behavior of the brick, OSB and gypsum board. Covering the OSB sheathing with spun bonded polyolefin slightly decreased the moisture accumulation of both the interior and exterior sheathings compared to building paper.

The presence of a wood stud leads to lower moisture content of the back wall, as the wood stud blocks and absorbs possible flow to the gypsum board. However, in the case of vapor open finishing, the hygroscopic behavior of the wood stud leads to prolonged moisture contents of the back wall.

During the testing, the moisture content of OSB and gypsum board were too high in all cases producing moisture related problems. However, these results show the behavior of wall systems under constant high-temperature gradients, which are not representative of reality. The following chapter presents a method to perform an experimental process under cyclic conditions for large-scale specimens.

Chapter 4: Large-Scale Cyclic Loading Study of Inward Vapor Flow

The aim of the project was to reproduce the solar-driven moisture flow, which occurs under specific summer conditions in a large-scale specimen. This chapter presents the design of the experimental setup to study this phenomenon, its construction and its use on a full test.

4.1 Needs and Objectives

Solar-driven vapor transport may impose a heavy wetting load on building assemblies. The previous chapter presented results that clearly demonstrate that such moisture flows may in fact be induced by high thermal gradients. The results of this wetting load were observed in the previous chapter. However, the small-scale experimental results for test specimens under constant loading detailed in the previous chapter are not representative of realistic field conditions.

The next step of this research project was to develop a greater understanding of the nature and significance of solar-driven inward vapor transport through the investigation of moisture accumulation of different large-scale wall assemblies under summer conditions in a hot and humid climate. Through comparative testing, the role of different materials used in the envelope assembly can be further understood under summer loading conditions. No setup has been designed to date which can characterize the moisture movement through large-scale wall assemblies exposed to summer loading and such a setup is required for this testing.

The development of a large-scale experimental setup is the focus of this chapter. The experimental setup was designed to specifically address solar-driven vapor diffusion under cyclic conditions. The setup is needed to monitor the moisture flow across a large-scale specimen. This is done by recording independently the change of mass of the cladding and the back wall. Given the mass variations of the back wall, the total amount of moisture entering the envelope can be recorded and studied.

4.2 Overall Set-up as First Designed

Large-scale wall assembly specimens (1.2 m x 2.4 m) are to be wetted and then exposed to high temperature cycles to simulate rain and sun exposure. The test specimen is divided into two components, suspended independently. The interior surface of the test specimen is facing the interior of a test hut, reproducing interior air conditions. Refer to Figure 4.1 for the overall setup as first designed and Figure 4.2 for the actual setup as built.

The setup is composed of five main parts:

Part 1: Test Hut

A test hut is used to reproduce indoor conditions. The test hut includes an opening large enough to receive 1.2 m x 2.4 m test specimens. The interior conditions are regulated with an air conditioning unit.

Part 2: Spraying System

A wetting setup consists of an array of spray nozzles on a spray rack to wet the specimens. By calibrating the system, an even distribution of water on the specimens was achieved.

Part 3: Solar Radiation System

A radiation system aims at heating the wall specimens uniformly. The radiation system comprises an array of lamps placed within a reflective box.

Part 4: Brick cladding with suspension and mass system

Part 5: Back wall with suspension and mass system

A weighing system is designed and implemented to continuously weigh the suspended wall specimens. Two weighing systems are implemented in the support of the outer cladding and insulating back wall of the test wall specimens. The weighing system

consists of a lever arm with low-friction ball bearings mounted to an overhead crane. The ends of the lever arm are used to support the test specimen and a respective counter weight. The counter weight relieves the dead weight of the wall so that any mass change in the system can be accurately measured with the use of a load cell.

The spaces between the back wall and the brick and the test hut are sealed with a light polyethylene sheet to control the flow of moisture to the environment.

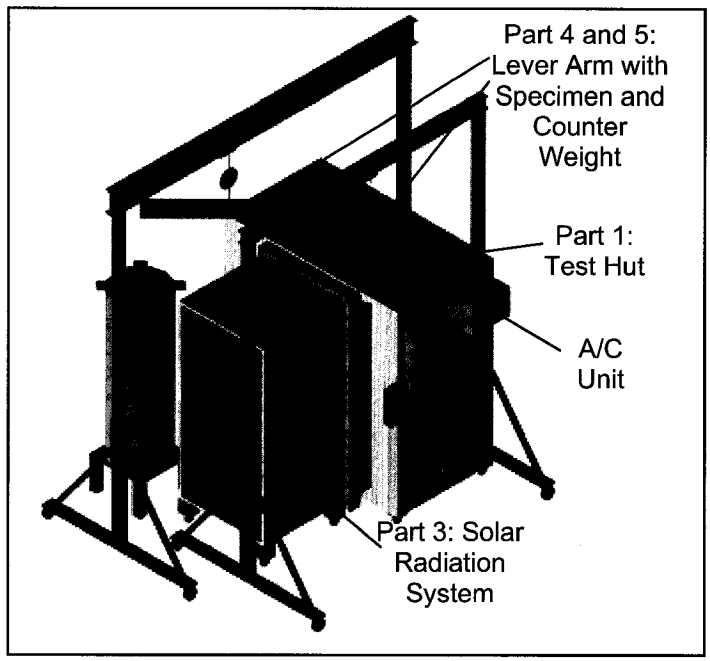

Figure 4.1 Overall setup as first designed

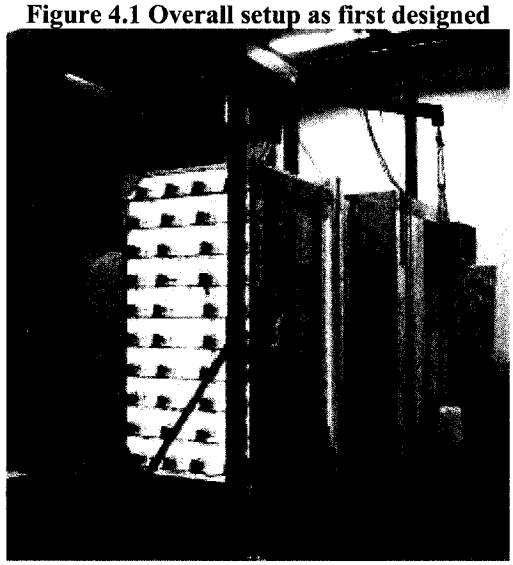

Figure 4.2 Overall setup during operation

4.2.1 Development of Experimental Procedure

With no existing standard for such an experiment, the conditions of the test were designed for this particular investigation. Interior as well as exterior conditions had to be produced, based on the climatic conditions of Charleston, South Carolina in southeast USA. Charleston is located in a hot and humid climate which sees a large amount of wind driven rain and solar exposition, ideal conditions for vapor diffusion under high thermal gradients.

4.2.1.1 Environmental Conditions

One of the driving factors that allow solar-driven vapor diffusion to occur is a cooled interior. In order to properly observe such an event, an air-conditioned environment was required to act on the interior surface of the wall specimens. In the case of the setup, a test hut was constructed to maintain the interior climate acting on the specimens. The temperature of the hut was set to 16°C, which was the 'interior' temperature for the experiment.

The 'exterior' conditions required more significant development. A surface temperature of at least 50°C was desired for the cladding of the specimen. A radiation system was developed to uniformly heat test specimens.

The specimen, as seen in Figure 4.3, is sandwiched between to the cooled interior conditions of the test hut from one side and exterior radiative heat on the other.

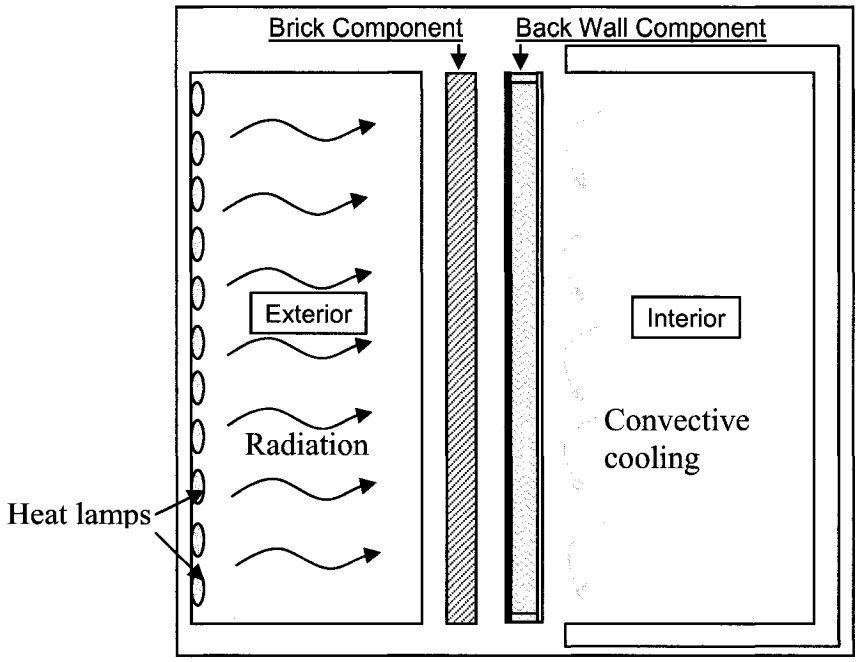

Figure 4.3 Section view of loading conditions on wall specimen

4.2.1.1.1 Interior Environment - Test Hut

A test hut with overall dimensions of 2.6 m x 1.45 m x 2.7 m high is constructed to maintain indoor conditions during solar driven moisture transfer tests. The hut is developed to include a large opening in one of its elevations large enough to receive the 1.2 m x 2.4 m test specimens. Test panels to be studied are placed in front of the opening where they are exposed to both the interior and exterior conditions of the hut. The opening to receive the test panels is 1327 mm wide, seen in Figure 4.4. A door is installed in one of the walls of the hut.

Table 4.1 Dimensions of Test Hut

	Exterior	Interior
Length	2.6 m	2.32 m
Width/Depth	1.45 m	1.2 m
Height	2.7 m	2.4 m

One of the major factors influencing solar driven moisture is the thermal gradient between the interior and exterior environmental conditions. To maintain specific conditions acting on the interior and exterior of the wall assemblies, both heat and airflow through the hut envelope are minimized. Mineral wool is used to insulate the hut while

silicone sealant prevents the passage of air through joints between the interior and exterior and one-part polyurethane foam is used to seal gaps.

Several openings are made in the walls of the hut. These openings and holes are placed to allow for instrument wiring passing from the interior to the exterior of the hut. Another opening is made to house the air conditioning unit, used to cool the interior environment acting on the test specimens.

An A/C unit, Panasonic CW-XC120VK, is the make and model of the A/C unit which is placed in the upper part of the wall opposite to the door (Figure 4.5). The dimensions of the unit are 560 mm (22.1") x 375 mm (14.9"). The minimum rated temperature capacity, as per the manufacturer, is 16°C (60.8 F) with a cooling capacity of 3370 W (11,500 Btu/h).

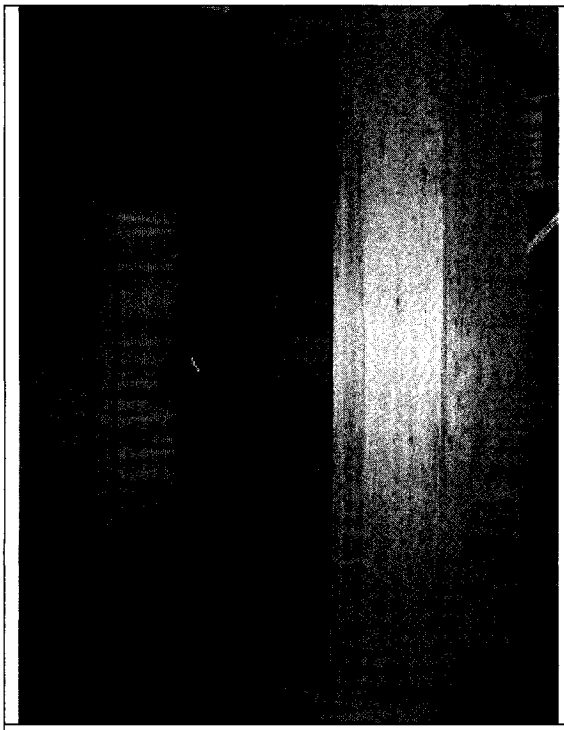

Figure 4.4 Opening of test hut to receive samples

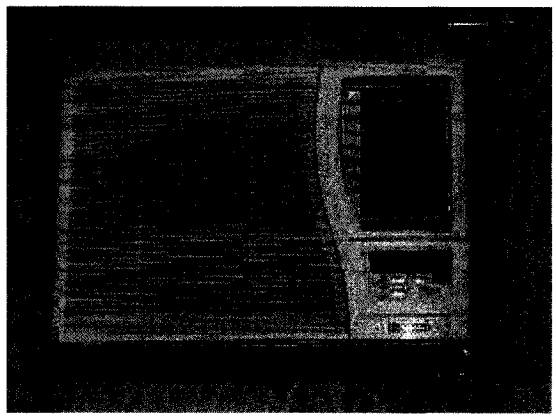

Figure 4.5 A/C unit

4.2.1.1.2 Exterior Environment - Wetting System

A wetting system is designed to simulate cladding wetted by rainfall using sprayer nozzles mounted to a moveable rack. During a test, this rack is used before the heating system to wet the test specimens to controlled amounts of moisture.

Standard residential gardening spray nozzles are selected as the means of water distribution. Eight nozzles, which are calibrated as per ASTM E-547, are used to supply the flow and spray area required for the experiment. The nozzles were placed on a spray rack in a manner that allows the test specimens to be evenly wetted by creating a film of water that runs over the brick façade. Through preliminary testing, the ideal arrangement of nozzles to obtain such results was achieved at a spraying distance of 1.5 m from the brick plane. The spray rack is equipped with four casters for mobility.

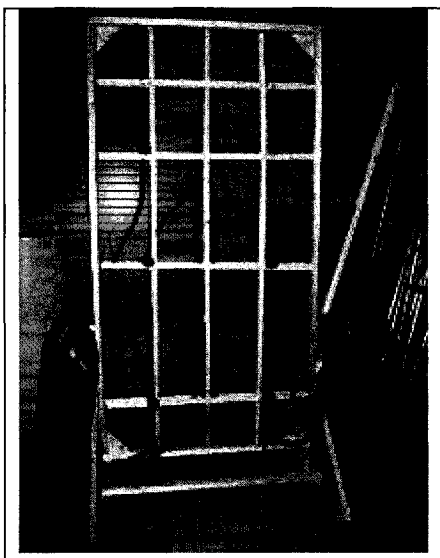

Figure 4.6 Spray rack system

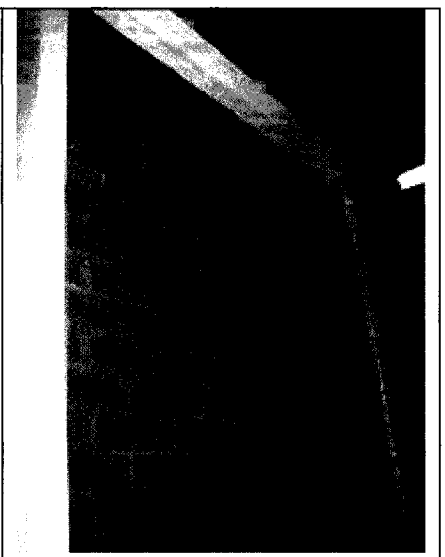

Figure 4.7 Wetting of brick façade

4.2.1.1.3 Exterior Environment - Radiation System

A radiation system, to simulate solar heat, was constructed and used to heat the exterior surface of the cladding of test specimens. The radiation system combines heat lamps housed in a reflective box.

In a previous experiment to simulate sunlight, Bosschaerts et al (2003) used 575-Watt heat lamps. It was found that obtaining a uniform irradiated surface is difficult, in particular with standard light bulbs. Nevertheless, heat lamps are chosen as the source of the heat for the radiation system. The lamps produce heat and are small enough to be configured in a variety of array configurations to achieve the desired heat distribution required for the purposes of the experiment. The Sylvania 175-Watt Par 38 Heat Lamp was selected.

The use of 40 heat lamps can sufficiently heat the test samples uniformly to a minimum of 50°C. The lamps are placed in a simple series of rows and columns within a reflective box with inner dimensions 48" x 50" x 8' high. The box is open from both the front and back. The front is open so that the test specimens can receive the heat generated by the lamps while the back is open for airflow to pass over the lamps and prevent overheating as well as convective heating of the specimens. The interior of the box is lined with aluminum sheet, which acts as a reflector concentrating the heat on the given surface while preventing energy loss to the environment. The bottom of the reflective box rests on four casters for mobility.

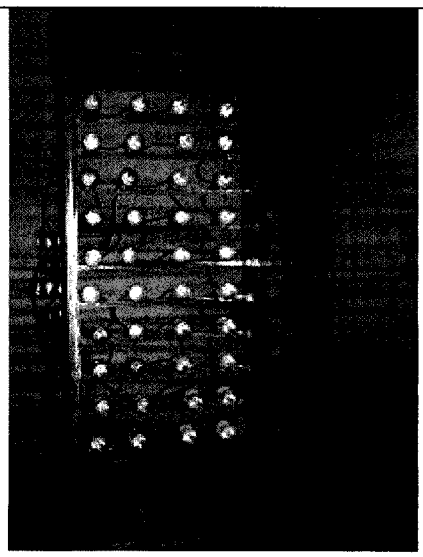

Figure 4.8 Light Box (Interior View) with lamps before optimization of layout

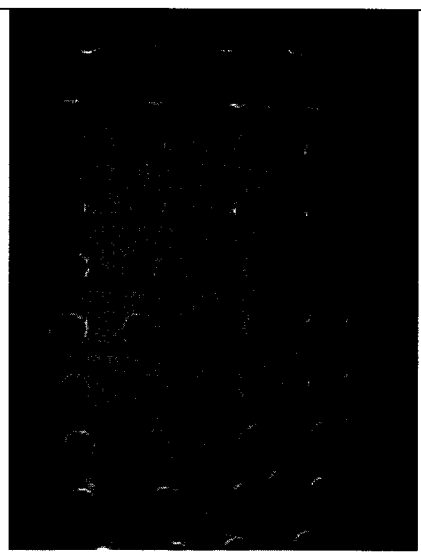

Figure 4.9 Heat lamps acting on test specimen in final optimized layout

4.2.1.2 Composition of Specimen

The specimen used in the experimental procedure was based on typical North American wood frame construction, as seen in the small-scale experiments. The assembly included brick veneer cladding. From outside to inside, the wall is comprised of:

- Brick masonry – 90 mm
- Air space – 20 mm
- Weather resistive barrier
- OSB Sheathing – 9 mm
- Mineral wool insulation / SPF stud – 38mm x 89 mm
- Gypsum board – 12.5 mm
- Inside finishing

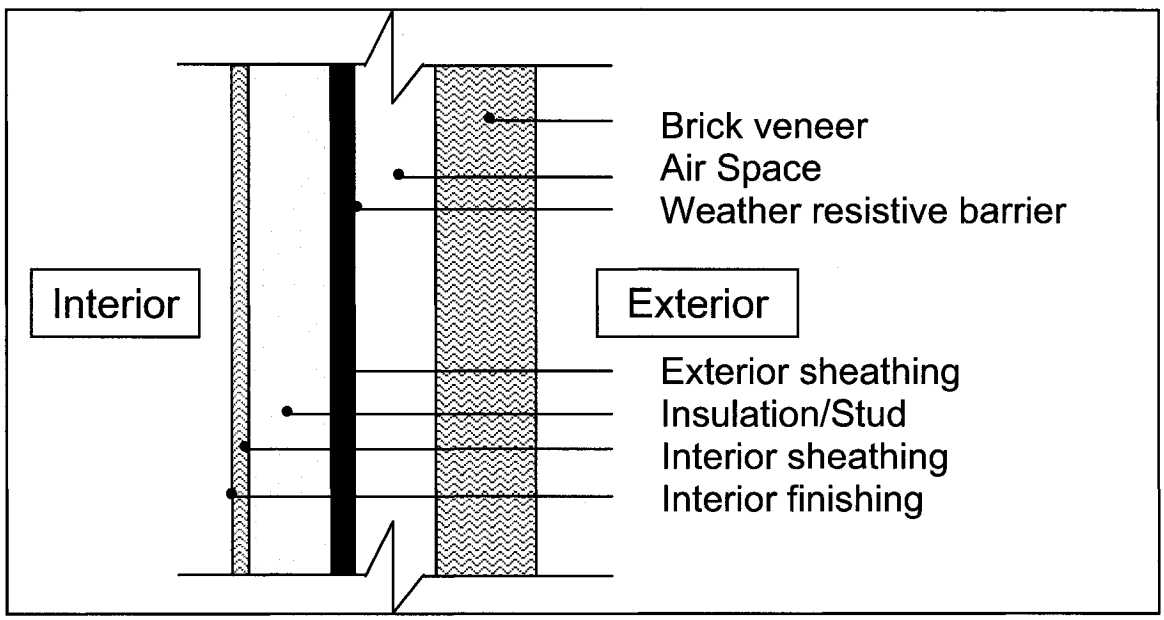

Figure 4.10 Test specimen assembly

The overall composition of the assembly can be divided up into two separate components:

1. Brick wall
2. Insulated back wall

The brick component consists of only brick veneer, while the remaining elements comprise the insulating back wall. The brick veneer is enclosed in a steel frame while the back wall is framed by wood studs. The two portions are combined and a 20 mm air space is formed between the walls, shown in Figure 4.11.

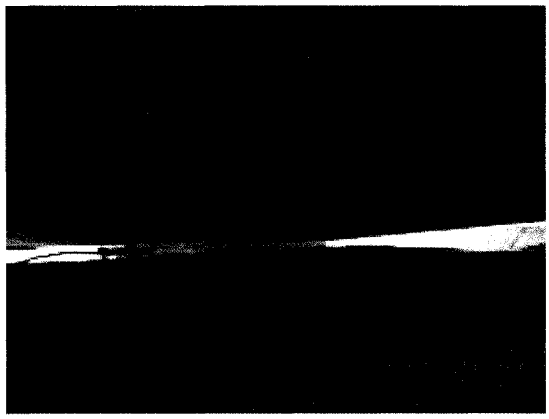

Figure 4.11 Air cavity between brick veneer and insulating back wall

The wall assembly used to validate the experimental setup, which related to one of the small-scale specimens, was composed of:

- Interior finishing:
  - Vinyl Wall Paper (low vapor permeance)
- Weather resistive barrier:
  - Spun Bonded Polyolefin (high vapor permeance)

4.2.2 Loading Protocol

The loading protocol acting on the specimens consists of alternating periods:

1. wetting phase
2. drying phase

4.2.2.1 Wetting of the Cladding

To correlate the small-scale with the large-scale experimental results, the brick cladding was wetted to the same moisture content as imposed in the small-scale experiments, i.e.

105 kg/m^3. Hence the spraying system is stopped when a quantity of 27 liters of water is present within the brick wall by the end of each wetting period, which was achieved in about 10 to 15 minutes of wetting. The amount of water absorbed by the brick cladding is monitored directly by the data acquisition system. Once the wetting system was turned off, it is replaced by the heating system.

4.2.2.2 Drying of the Cladding

When the desired moisture level was achieved in the cladding, the wetting system was removed and the heating system put in place. The heating system allowed drying to occur while the moisture was driven inwards. The heating system is applied for eight hours. Then the rest of the drying phase consisted of 16 hours without radiation. Timers were implemented to ensure eight hours of radiation.

The total wetting and drying cycle of 24 hours was repeated until a significant amount of moisture was observed within the back wall. Once a significant amount of moisture was witnessed, the drying cycles (eight hours of radiation and 16 hours without radiation) were repeated until the specimens returned nearly to their initial dry states. This part of the test was required to verify a sufficient drying potential of wetted assemblies would allow for good moisture performance.

4.2.3 Measurement Protocol

The samples were monitored through gravimetric and continuous measurements.

4.2.3.1 Gravimetric Measurements

In the case of this experimentation, two gravimetric methods are employed: the two wall components are considered to be gravimetric specimens, and small material cut-outs taken from the interior sheathing and the wooden studs are also used as gravimetric samples. For the entire duration of the experiment, the assemblies are continuously weighed and recorded using a weighing system. The masses of the wall components allow for the total moisture accumulation in the assembly to be known over time.

Furthermore, the cut-outs from the interior sheathing allow for the measurement of the moisture accumulation at specific locations within the back wall.

4.2.3.1.1 Entire Wall Gravimetric Samples

A specific weighing system was devised to support and weigh large-scale test specimens. The system was comprised of several components, which allowed for the test specimens to be continuously measured. Different research performed by Forintek and Straube (2007) used a similar system.

The system components are as follows:

- Gantry crane
- Lever arm
- Counter weight
- Load cell

The crane is used to suspend all components of the weighing apparatus including test specimens. The lever arm, which is suspended by the crane, acts as a balance supporting a wall specimen and respective counter weight in mid-air. Employing a load cell, which is anchored between the counter weight and the anchor weight, measures any mass change acting on the specimen in question. This system is shown in Figure 4.12.

The load cells were connected at one end to the bottom of the corresponding steel table and at the other end to a counterweight, shown in Figure 4.13. The load cells respond to tension and convert the loads acting on them into an analogue electrical signal. These signals are recorded continuously to a computer through the Agilent 34970A data acquisitioner.

Refer the Appendix A for complete details on the weighting system.

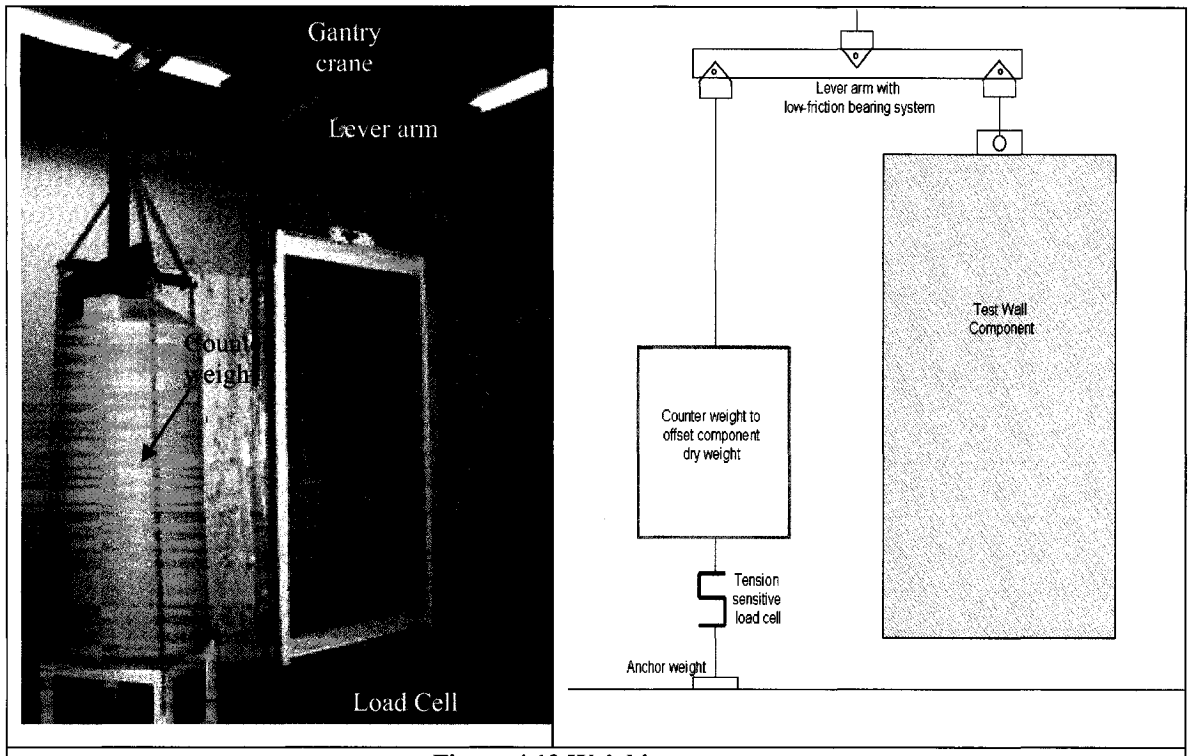

Figure 4.12 Weighing system

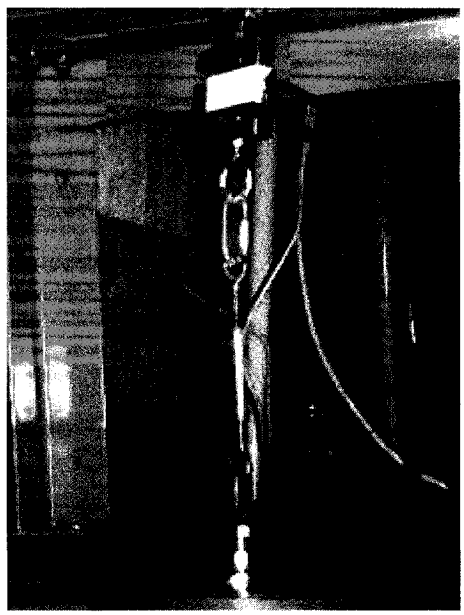

Figure 4.13 Load cell installation

4.2.3.1.2 Small Sample Gravimetric Samples

Besides measuring the entire moisture gain in the wall, two small gravimetric interior sheathing and stud samples are studied. Each material observed is taken from two

locations: top and bottom of the wall specimens. Studying samples taken from opposite vertical locations enables better mapping of the moisture movement through the wall due to solar driven vapor diffusion.

Two 15 cm x 15 cm square samples of gypsum board are cut out of the 12.5 mm thick interior sheathing 30 cm from the top and bottom of the wall. The specimens are equipped with a handle that allows them to be removed from the back wall for quick weigh-ins with the least amount of disturbance to the overall wall setup. A hole cut out for one the gypsum gravimetric samples can be seen in Figure 4.14.

In addition to the gypsum samples, two wood samples, 12.5 mm x 12.5 mm x 38 mm, are cut out of the wood studs to follow the moisture accumulation. These wood samples are located at the same distances from the top and bottom of the wall as are the gypsum samples. Little flaps are cut out of the gypsum allowing the stud specimens to be accessed. A stud sample is depicted in Figure 4.16.

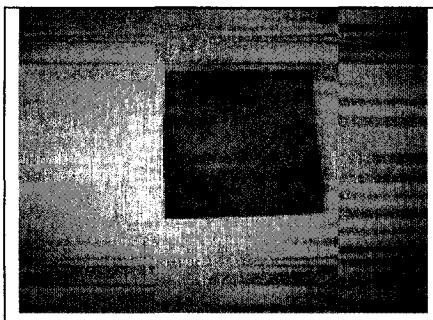

Figure 4.14 Gypsum gravimetric hole in interior

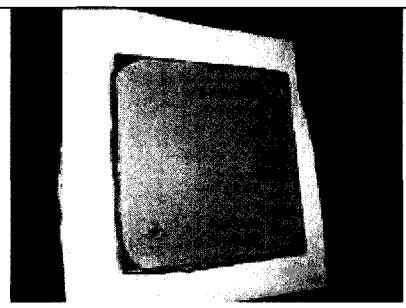

Figure 4.15 Gypsum gravimetric sample

Figure 4.16 Stud gravimetric sample

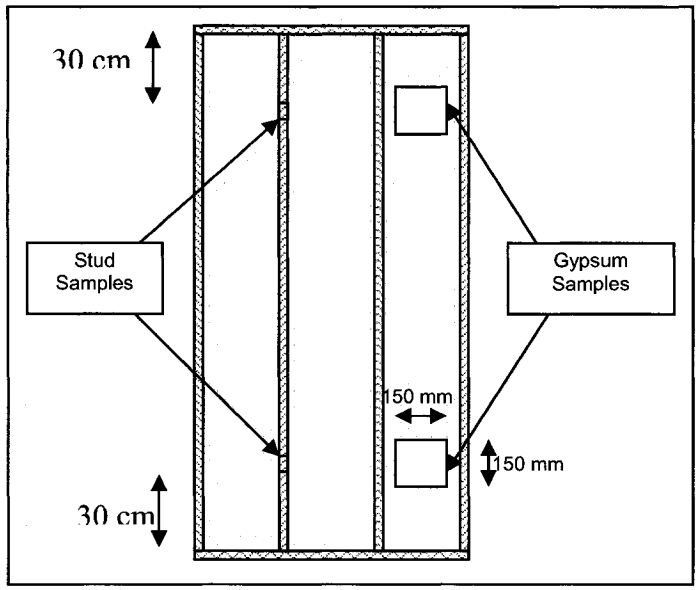

Figure 4.17 Gravimetric sample locations

All openings in the interior sheathing around the gravimetric samples are sealed with a tight tape to prevent air leakage. The readings are taken periodically throughout the entire experiment to observe any moisture patterns that cannot be seen by weighing the entire wall specimen as a whole. A balance with an accuracy of 0.01 grams is used to weigh the components.

The moisture content in the OSB sheathings is monitored using electric resistance moisture content pins (MC). The placement of the moisture pins can be seen in Figure 4.18. The measurement output is recorded manually using a transducer manufactured by Delmhorst.

4.2.3.2 Continuous Monitoring

The temperature and relative humidity were electronically monitored throughout the entire duration of the experiment at various positions within the test specimens. Refer to Appendix E for the sensor equipment used with calibration results.

4.2.3.2.1 Sensor Placement

The placement of the thermocouples (TC), along with the relative humidity probes (RH), was arranged so that the measuring devices line up. The moisture pins in the OSB were also placed along the same orientation. All of the relative humidity probes along with the corresponding thermocouples were placed at the exact center of the specimens. In addition, to verify whether even conditions were achieved, thermocouples were placed 30 cm from the top and bottom of the wall specimens as were the moisture pins in the OSB. Refer to Figure 4.18 for the sensor placements.

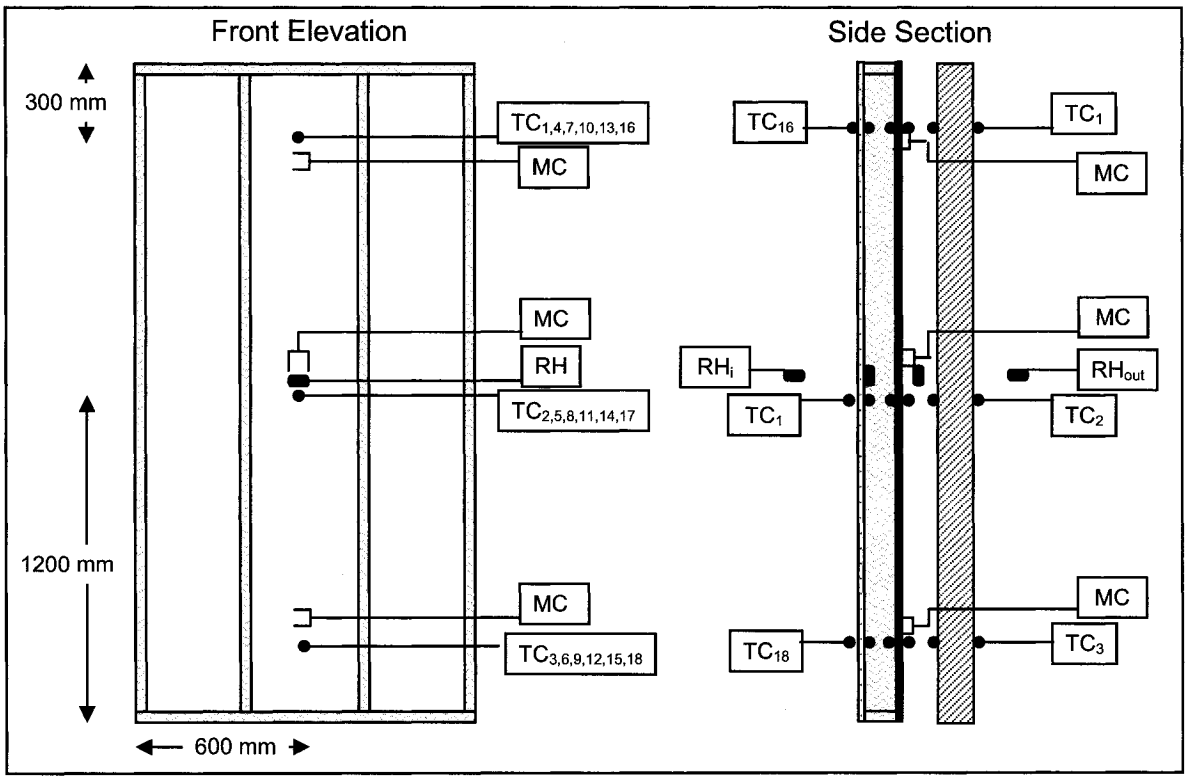

Figure 4.18 Sensor placement for large-scale specimen

4.3 Implementation of the design

Implementation of the setup resulted in some challenges and setbacks. During preliminary testing, many observations were noted and corrections made to minimize any experimental errors. Several points must be noted in consideration to the experimental setup, which aims at recreating solar-driven vapor diffusion through building enclosures.

4.3.1 Setup Geometry

Combining all of the elements of the experimental setup required a significant amount of planning and design. From the selection of the cranes to the orientation of the lever arms and the width of the air cavity, modifications to the design were performed.

The clear span of the cranes was required to fit the reflective box, two wall components, the test hut and enough space to allow the reflective box and wetting system to be moved interchangeably without disturbing the test specimens.

The original design of the lever arms was modified to include swivels at the pivot points which enable the wall components and respective counter weights to be suspended in different planes. Installing swivels at the fulcrum and end pivot points of the lever arms prevented the weighing system from conflicting with other parts of the test setup.

4.3.2 Preliminary Test Results

Once the experimental setup was completed, a preliminary test was conducted to assess the parameters and procedures of the experiment of this project.

The test specimen was subjected to a wetting period followed by simulated solar radiation. Throughout the monitoring phase, gravimetric sampling was recorded and the moisture content of the gypsum and studs were measured.

The wetting and radiation systems were implemented as per the loading protocol for a 24-hour loading period. The temperature and relative humidity profiles through the assembly showed ideal testing conditions with a single wetting and heating cycle where the relative humidity in the air and insulating cavities reached upwards of 96% and 82% respectively.

The gypsum and stud gravimetric samples were weighed periodically during the eight hours of radiation following the wetting. No mass increase was observed in the stud specimens since the duration of the experiment was short and not enough moisture was introduced into the system. However, the gypsum samples did show a slight uptake of

moisture. Table 4.2 shows the mass change of the gravimetric gypsum samples during the preliminary test.

Table 4.2 Preliminary test results

Time (hours:minutes)	0	2:20	3:20	4:40	7:20
Top Sample (g)	204.49	204.52	204.58	204.64	204.99
Bottom Sample (g)	204.76	204.97	204.98	205.02	205.03

Less than 1 gram of moisture is observed to accumulate in the gypsum specimens during the drying phase of the experiment. Nevertheless, an increase in moisture is present. Through a series of wetting and drying cyclic periods, it is believed that a significant presence of moisture will be witnessed in the insulating back wall.

4.3.3 Wetting System

To get significant results a larger amount of moisture is required to be added to the reservoir cladding. Since the sprayer nozzles are on a mist setting, a lot of moisture was dispersed into the environment, which can in turn become deposited on the counter weights leading to errors. To contain the sprayed moisture, an impermeable membrane was used to temporary enclose the space between the spraying system and the test walls. Once the wetting was complete, the membrane was removed. However, the runoff of water within the area between the spraying system and the hut enclosed by the membrane influenced the mass of the back wall. During the wetting periods, small amounts of moisture become deposited on the exterior perimeter of the back wall adding upwards of 100 grams additional mass. This additional mass cannot be accounted for since it eventually evaporates into the laboratory environment.

4.3.4 Weighing System

The weighing system for the overall mass of the two wall components was extremely sensitive and picked up the slightest change in mass. A number of occurrences can influence the results of the weighing systems which are directly linked to both the brick veneer and back wall.

The small gravimetric samples were removed from the back wall and weighed every few hours. This procedure involved the entry into the test hut and the disruption of the experiment. Slight disturbances occurred in the overall mass of the back wall gravimetric samples when the small gypsum and stud gravimetric samples were measured. Continuously weighing the gypsum and stud samples influenced the readings measured by the load cell.

Air circulating within the laboratory disturbed the extremely sensitive weighing apparatuses, causing oscillating mass readings in the walls. These disturbances were unpreventable under the laboratory conditions.

A calibration of the weighing systems was done to determine their accuracies. A series of known masses were loaded and then unloaded on the systems. The brick wall weighing system, loaded up to 32 kg, returned errors no greater than 1.75%. The back wall weighing system, which saw mass variations up to 8 kg, returned errors as high as 3.34%. Refer to Appendix A for complete details of the weighing system calibration.

4.3.5 Air Cavity

The air cavity, as explained earlier, is present between the two wall components. Sealing the perimeter of the air cavity from the environment proved to be difficult. Finding a method to prevent moisture from escaping the cavity, while not inducing load transfer on either wall, proved to be near impossible. It was decided that a light, impermeable membrane would seal the cavity. Care had to be taken into consideration since the membrane came into contact with both the cladding and insulating back wall. Any tension within the encasing membrane could influence the mass outputs of both walls.

During experimentation, liquid water accumulated on the encasing membrane at the bottom of the air cavity. Not only did this add extra mass to both wall components but eventually led to a break in the seal of the membrane. It was then determined that the wall cavity will include a bottom ventilation to allow for the drainage of the liquid water from within the assembly.

Furthermore, condensation is seen to accumulate on the inside of the membrane since it is not insulated from the laboratory conditions. During the gypsum and stud gravimetric weigh-ins, the back wall is slightly disturbed causing the condensate within the air cavity to shift and drain. This ultimately affects the mass measured by the load cells for either wall component.

4.3.6 Limitations

In addition to the above discussed challenges, this experimental setup has several limitations compared to actual field conditions. They are listed below:

- The wetting of the brick is uniform, where as this may not be the case for brick veneer cladding on a building exposed to wind driven rain. The wetting method used is intended to distribute a controlled uniform moisture load across each assembly. Furthermore, the cladding is repeatedly wetted between drying periods to recreate cyclic wetting and drying which may or may not be representative of the field.
- The specimens in this study are not subjected to air pressure forces or wind gusts that would be present in the field. The specimens are only exposed to air convection and radiation.
- The radiative heat flow acting on the specimens is constant for eight hour periods assuming no cloudy periods which may or may not be reflective of the heat acting on surfaces in the field.
- The test specimen does not include any envelope penetrations (such as windows, doors, vents, balconies, etc).

4.4 Running of a Test

Refer to Appendix F for a detailed step-by-step procedure for the running of a test.

4.5 Experimental Results

This section presents the experimental results of the test wall examined with the setup. The measurement of the experiment includes temperature, relative humidity and moisture content throughout the sample, as well as moisture accumulation in the gravimetric samples and the entire wall components as described in the experimental protocol.

The figures representing all experimental results can be found in Appendix C.

4.5.1 Environmental Conditions

The simulated exterior temperature and relative humidity throughout the experiment are the conditions within the reflective box. The air temperature within the reflective box was recorded to be 20°C during the night and reached about 40°C during the eight hours of radiation. Radiation of the lamps led to the desired surface temperature acting on the brick during simulated sun radiation. The low relative humidity of 8.5% measured during heating was due to the high temperature. The relative humidity within the laboratory, which depended on the outdoor conditions, fluctuated between 11% and 34% when the lamps were off.

The interior temperature was kept more constant than the exterior and fluctuated between 16.4°C during the day and 14.3°C at night while the radiation system was off. The relative humidity within the test hut was not controlled and varied between 18.9% and 70.1% RH. It is believed that the varying relative humidity within the test hut was due to air leakage from within the material interfaces which were not sealed.

4.5.2 Gravimetric Measurements

4.5.2.1 Mass of Small Gravimetric Samples

The mass of the gypsum samples are presented in Figure 4.19 while the results of the studs are seen in Figure 4.20. The gypsum specimens show two different accumulation and drying rates. The top gypsum sample accumulates almost 12 grams more moisture than the bottom. This is a good indication that the moisture uptake across the interior

sheathing is not uniform. It is also noted that the mass of the samples remains quite uniform and constant for the first eight days of the experiment. Once the bottom of the air cavity is ventilated, the top gypsum sample begins to accumulate more moisture that the bottom.

The stud specimens however show a more uniform increase in moisture. Shortly after the wall assemblies are exposed to moisture, both samples begin to show an increase in mass. Roughly seven days after the wetting is terminated, the studs begin to decrease in mass.

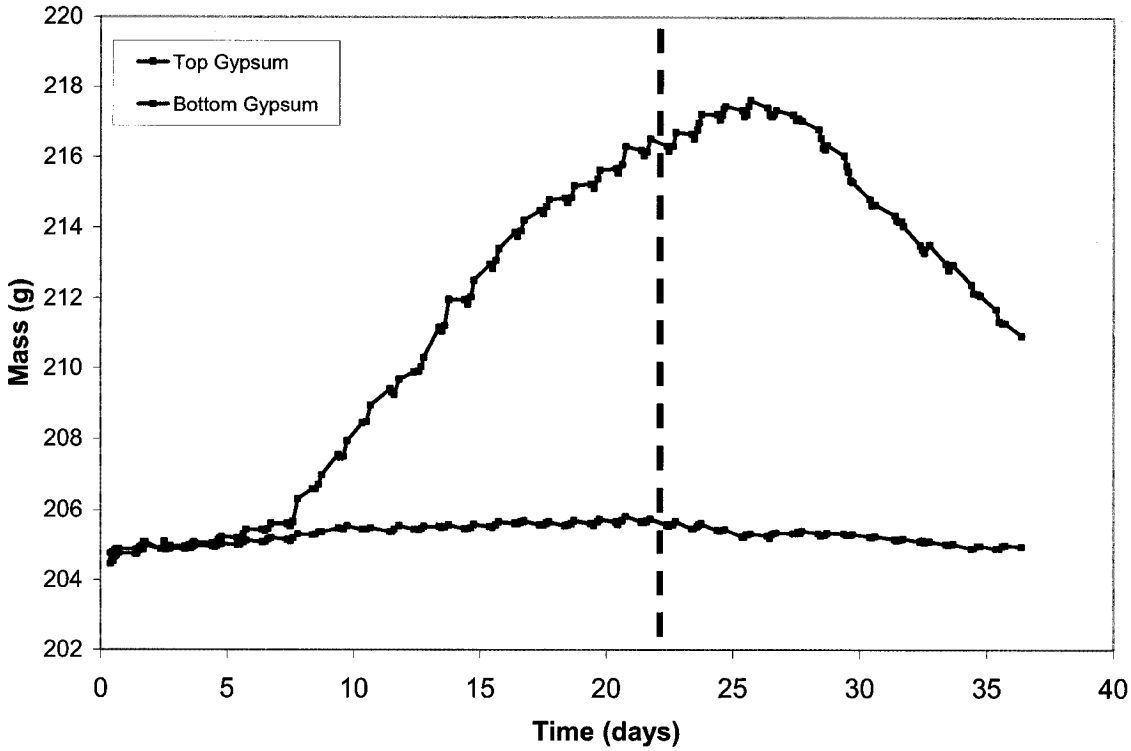

Figure 4.19 Mass of gravimetric gypsum samples

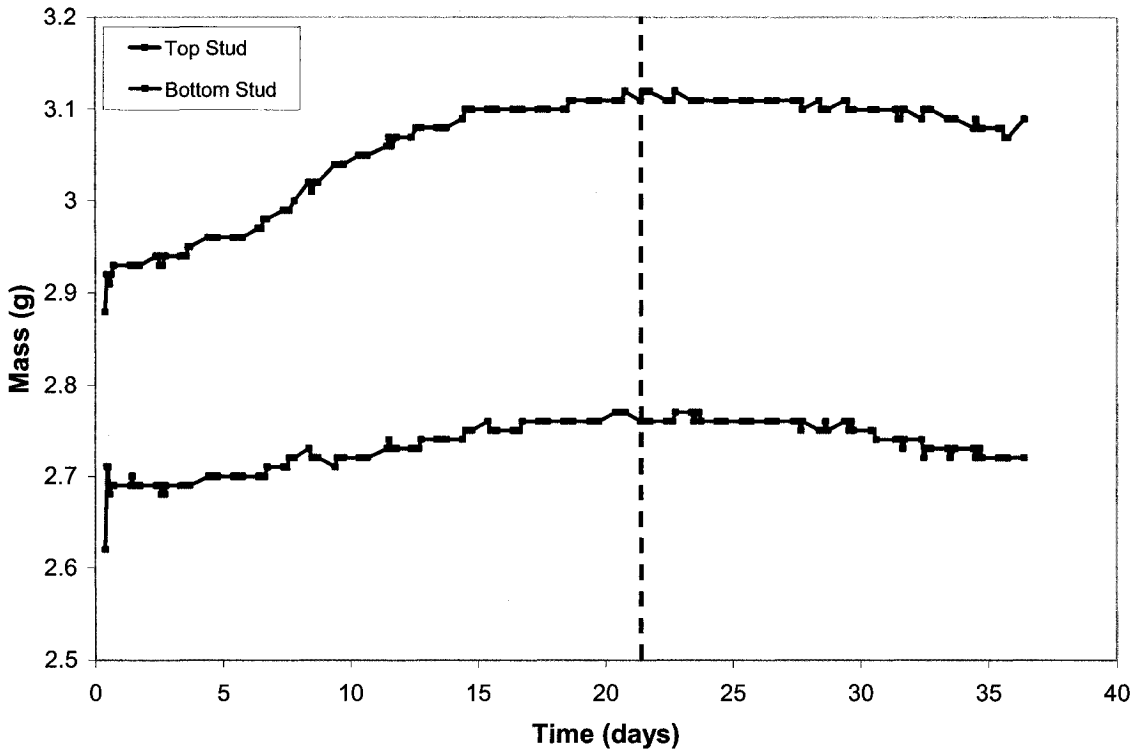

Figure 4.20 Mass of gravimetric stud samples

4.5.2.2 Mass of Large Wall Components

The brick and back wall components are continuously weighed and measured throughout the experiment with the designed weighing systems. The results of both the brick and insulating wall are presented in Figure 4.21 and Figure 4.22 respectively. The mass refers to the increase in moisture as measured by the load cells and do not reflect the actual masses of the wall components themselves.

The moisture accumulation within the brick component rises every day during the wetting regime. The moisture within the brick steadily decreases almost immediately during the first eight hours of radiation followed by a slower decrease in moisture for the following 16 hours when the wall is not exposed to radiation.

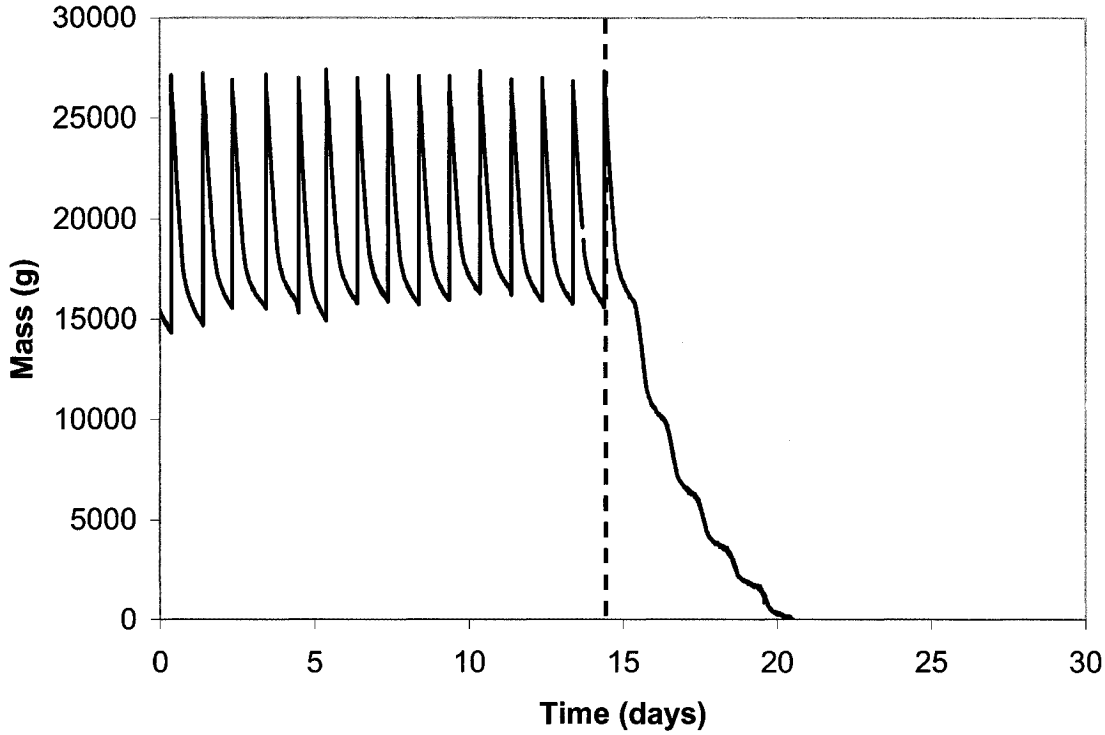

Figure 4.21 Mass of brick wall component

The trend in Figure 4.22, which illustrates the moisture accumulation within the insulating back wall, behaves differently. Unlike the brick, the back wall comes into contact with much less moisture at every wetting event. However, the back wall retains much of the moisture that comes into contact with it. It is also noted that while the brick component of the wall specimen is exposed to radiation, the vapor pressure drives acting on the back wall are increased. The increased vapor pressure is denoted by the oscillating peaks in the graph.

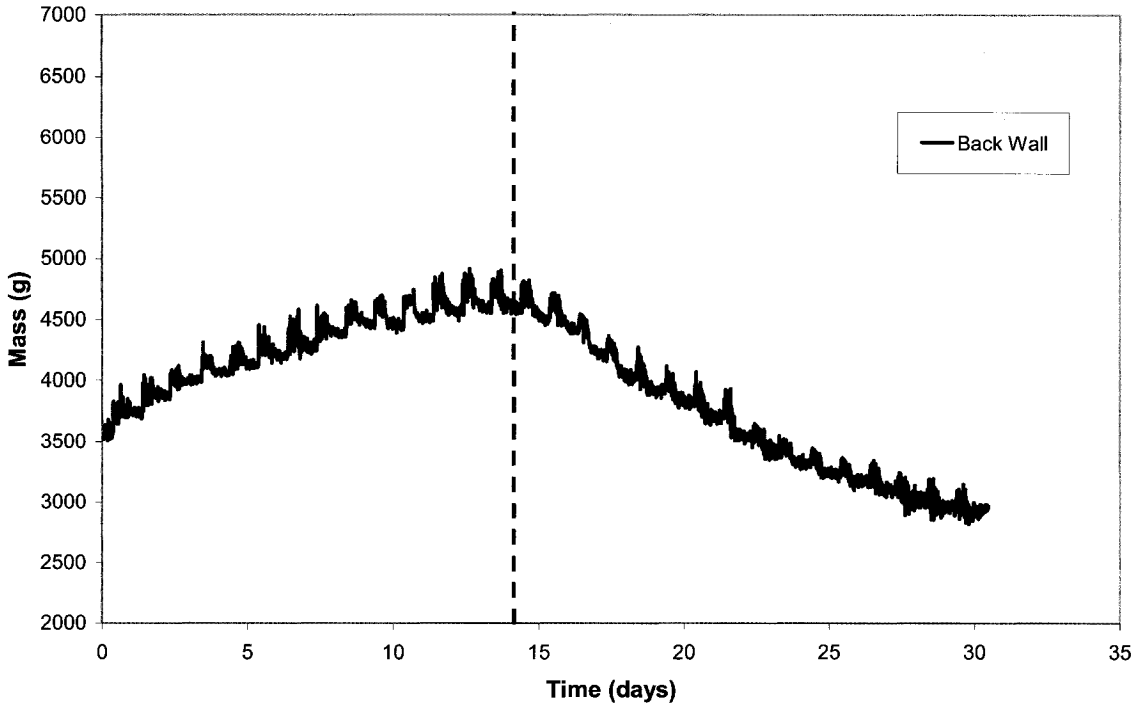

Figure 4.22 Mass of back wall component

4.6 Observations

The following section analyses the experimental results obtained and aims at validating the results with simulations. Correlations with the small-scale experiment are also explored.

4.6.1 Gravimetric Measurements

4.6.1.1 Moisture within Brick Component

Figure 4.21 depicts the moisture within the brick component of the test specimen. After a daily wetting period, 27 liters of added moisture is present in the system. Then, when the brick has been exposed to cyclic radiation for a 24 hour period, roughly 13 liters of moisture remain within the brick. Taking into account the initial moisture content the brick had, in reality, about 34 liters of moisture following every wetting period. By day 30, most of the moisture within the brick had been evacuated.

4.6.1.2 Moisture within Back Wall Component

The moisture accumulation within the back wall is seen to increase by increments which are influenced by the wetting and radiative cycles exposed to the brick component. Referring to Figure 4.36, the amount of moisture accumulated by the back wall was upwards of 1500 grams.

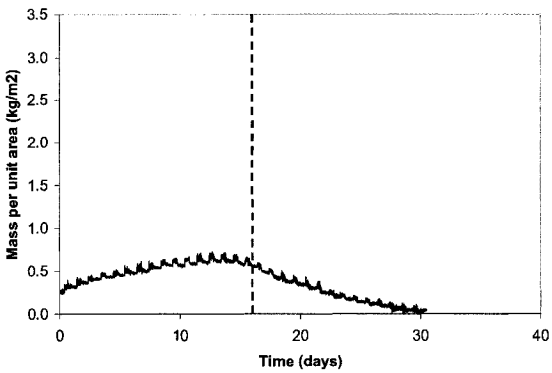

Figure 4.23 Moisture content of back wall in large-scale test

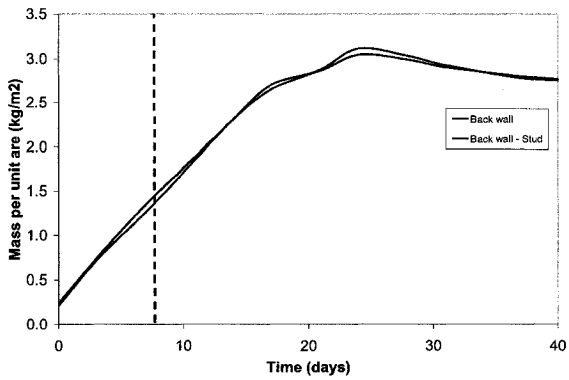

Figure 4.24 Moisture content of small-scale SBPO – Vinyl back walls

Comparing the large-scale results with the observed small-scale results in Figure 4.24, the trends are similar. Although the large-scale test specimen was subjected to cyclic loads compared to constant loads for the small-scale test specimens, the large-scale test specimen was exposed to multiple wetting periods. The difference in loadings exposed to each assembly can explain the difference in moisture accumulated by each wall component.

4.6.1.3 Moisture within Gypsum Sheathing

Figure 4.25 illustrates the moisture accumulation within the gypsum, independent from the other back wall materials.

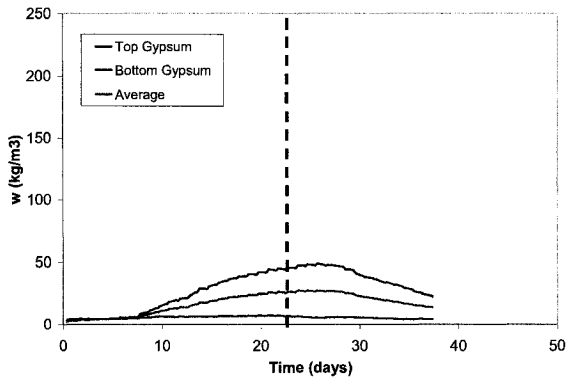

Figure 4.25 Moisture content of gypsum samples in large-scale test

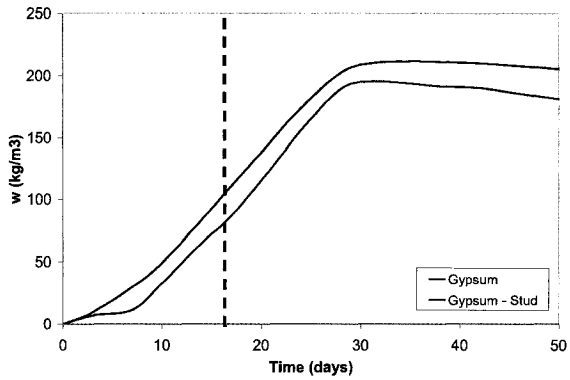

Figure 4.26 Moisture content of small-scale SBPO – Vinyl gypsum specimens

Two very different trends are observed between the gypsum samples above. The top gypsum sample accumulates over 10 times more moisture than the bottom sample leading to the conclusion that the moisture accumulation across the sheathing is not uniform. It is believed that unexpected wetting of the top portion of the exterior sheathing was related to the increased moisture present in the top gypsum.

Comparing the large-scale results with the small-scale results which included a wood stud in the construction, in both cases, the accumulation of moisture at the beginning of the experiment is minimal. After several days, both the small and large scale gypsum specimens begin to accumulate moisture at a larger rate. It is believed that the wood within the assembly first accumulates moisture introduced to the system, followed by the gypsum.

Comparing the large-scale results to the small-scale results, it seems that the gypsum has an easier time evacuating moisture under cyclic loading versus constant heating.

4.6.1.4 Moisture within Wood Studs

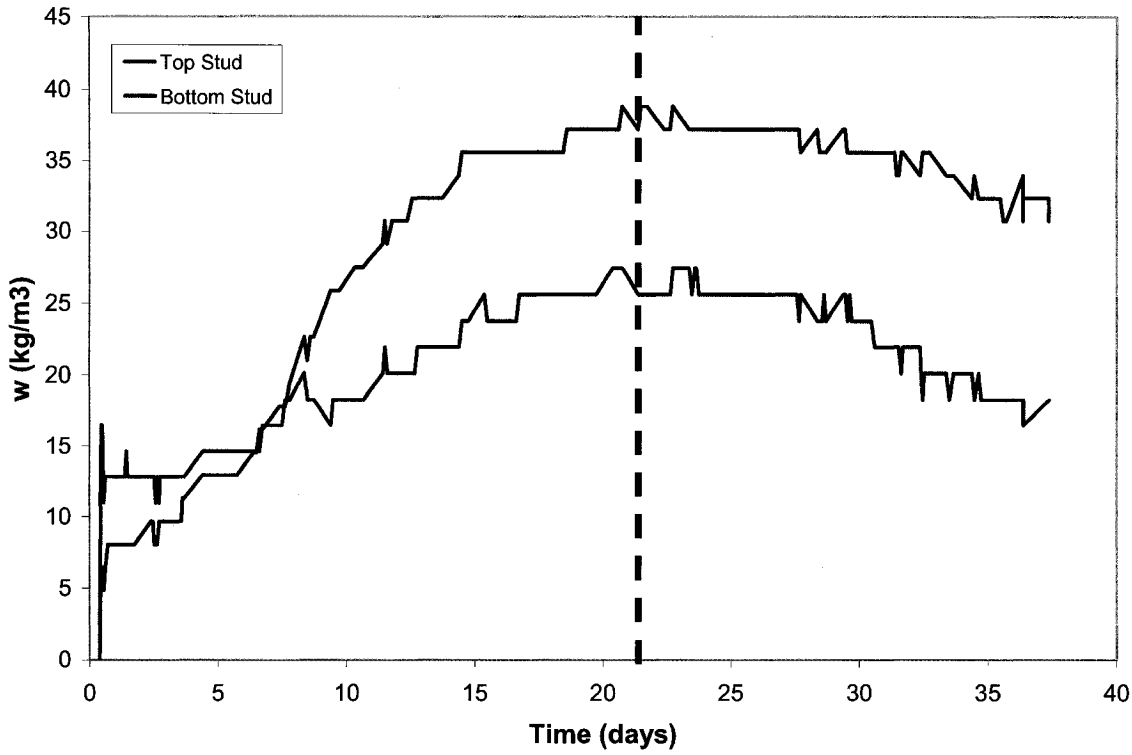

Figure 4.27 Moisture content of stud samples in large-scale test

The above figure describes the moisture content of the wood stud samples. Initially, the bottom stud accumulates more moisture than the top stud. However, at day eight, the top stud begins to have an increase in moisture absorption rate over the bottom stud. Once the two studs reached their respective maximums, they began to dry at the same rate. The top stud reaches 38.8 kg/m^3 while the bottom stud has a maximum of 27.5 kg/m^3, a difference of about 11 kg/m^3. The difference in moisture accumulation between the top and bottom studs is another indication that the wetting of the back wall is not uniform.

4.6.2 Interpretation of Sensor Outputs

4.6.2.1 Moisture Content Probes

The moisture content of the OSB sheathing was recorded several times per day. It was observed that the measured moisture content in the OSB sheathing was greatest at the top while the middle location of the OSB fell in between the top and bottom readings. This is

another good indication that the moisture accumulation within the back wall was not uniform. The top portion of the back wall saw greater moisture loads than the bottom.

The moisture content readings vary depending on the wetting of the brick cladding. Initially, before the cladding is wet, the moisture content in the sheathing is low. Following wetting and some exposure to simulated solar radiation, the moisture content across the sheathing increased. By the end of a radiation exposure cycle, the moisture content across the sheathing decreases. This pattern is observed throughout the wetting and drying cycles.

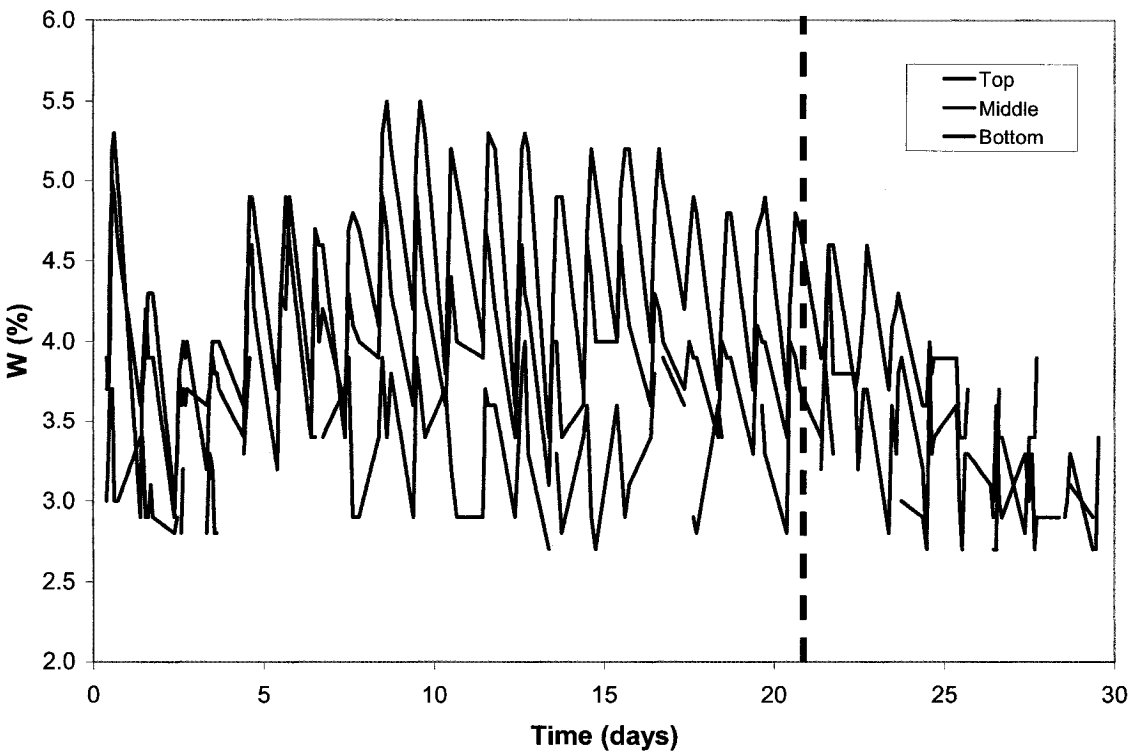

Figure 4.28 Electronic moisture content for OSB in large-scale test

The moisture content at the bottom portion of the sheathing was not always recorded. It is believed that either the moisture pins were in contact with the glue of the sheathing which influenced errors in the readings or the moisture content was too low to be measured.

One week after the wetting regime ended, no more moisture was measured within the OSB sheathing. Although a minute amount of moisture may have still been present in the sheathing, the measuring device would have been unable to record it.

4.6.2.2 Relative Humidity Probes

Relative humidity probes were used to monitor and record the relative humidity in and on both sides of the specimen. The conditions within the air and insulating cavities are related to moisture flow through assemblies and are discussed below.

4.6.2.2.1 Relative Humidity in the Air Cavity

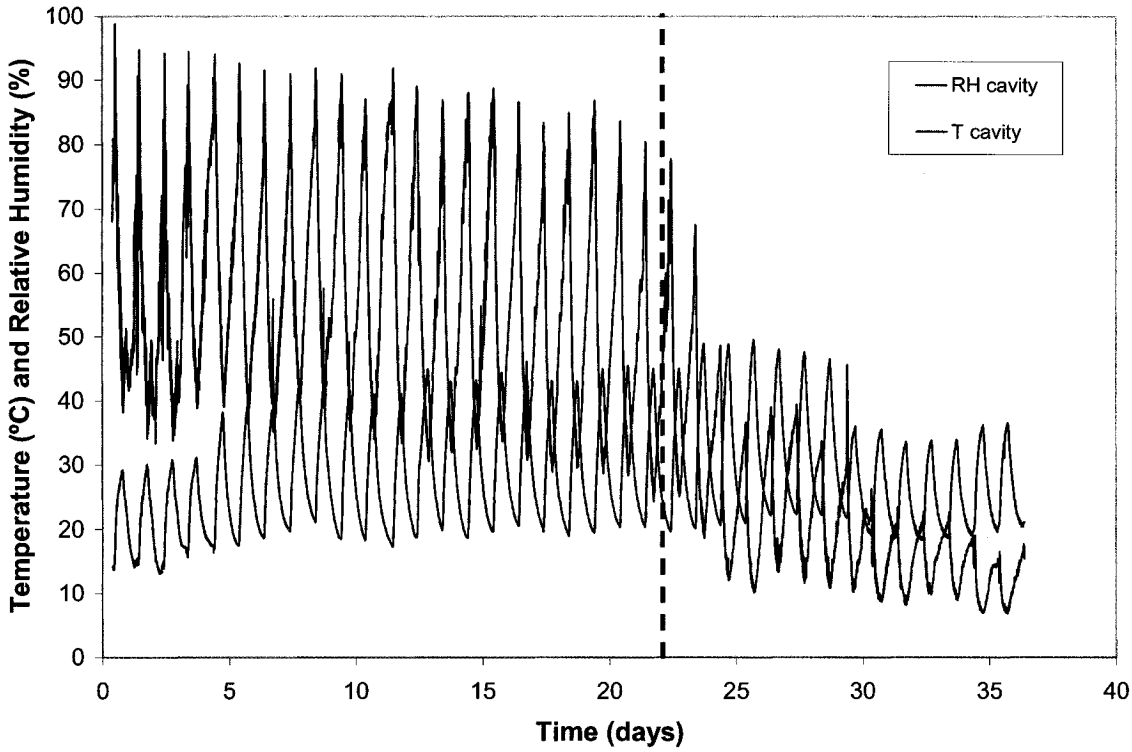

Figure 4.29 Exterior and air cavity temperature and relative humidity

The conditions found in the air cavity, shown in Figure 4.29, show that, following the wetting of the brick cladding and radiative heating, the RH level increases. The RH within the cavity reaches upwards of 90% RH, while after the cladding is exposed to a radiative cycle, the RH decreases to 35%. The RH level, which is observed to vary

depending on radiation exposure, begins to decrease shortly after the wetting regimen ends.

4.6.2.2.2 Relative Humidity between Insulation and Gypsum Board

The relative humidity within the insulating cavity has a delayed response when compared to the air cavity RH. During the first few wetting and drying cycles, the RH in the insulating mineral wool close to the gypsum increases. The relative humidity cycles reach a plateau at day 15 where they vary between 76% and 85% RH. Five days after the wetting regime ends, at day 25, the relative humidity decreases. The decrease in RH at the insulation-gypsum interface is more abrupt than the increase observed at the beginning of the experiment.

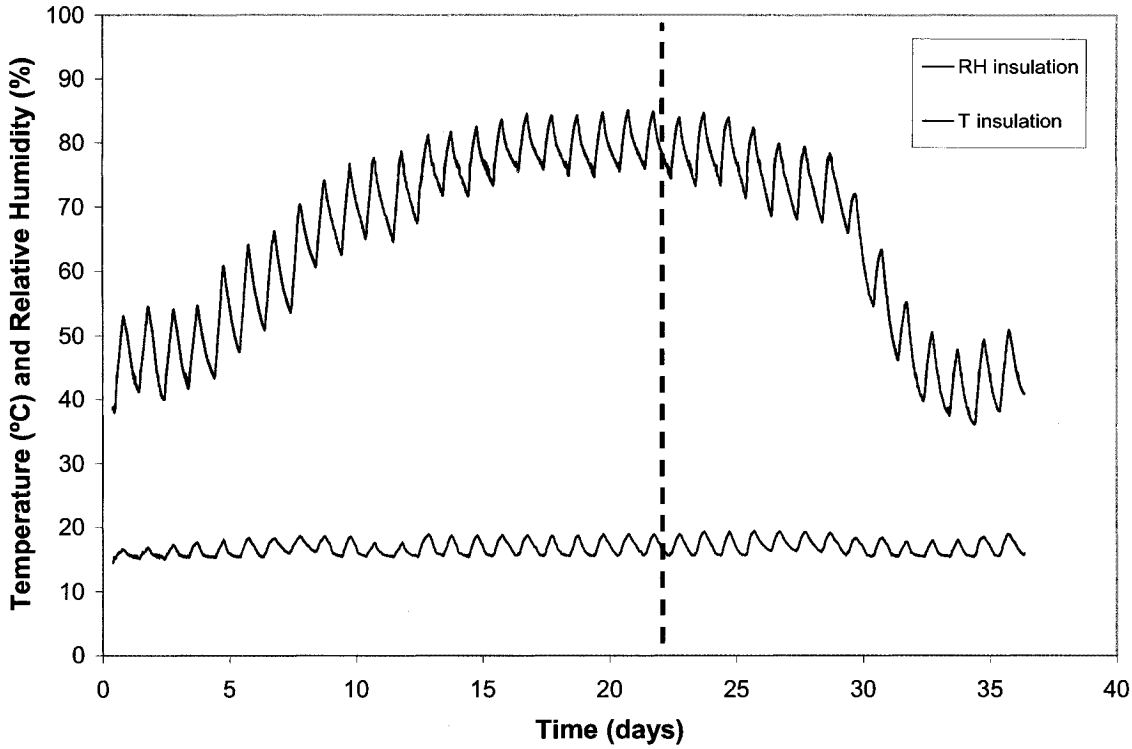

Figure 4.30 Relative humidity between insulation and gypsum

4.6.2.3 Experimental Conditions Acting Across Test Specimen

The following section aims at better understanding the environmental conditions acting across the test specimen for a typical cyclic loading period with and without wetting.

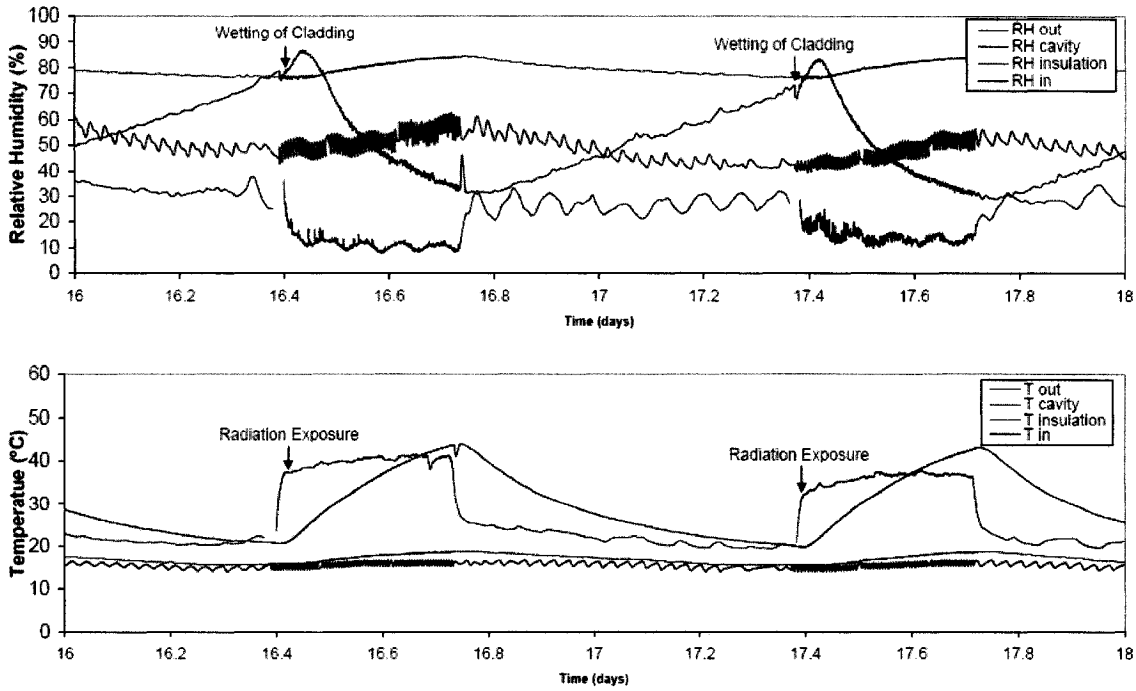

Figure 4.31 Experimental conditions across assembly with wetting

The results of Figure 4.31 present the conditions across the test assembly for two days during the wetting regimen. The arrows indicate the two times when the specimen was wetted and exposed to radiation. The outside relative humidity, within the reflective box, drops immediately once the specimen is exposed to simulated solar radiation and increases to the laboratory RH level once the radiation is stopped. The temperature at the same location is about 40°C in the reflective box during radiative heat exposure and decreases to about 20°C for the following 16 hours where radiation is stopped. The relative humidity within the air cavity peaks at 85%RH shortly after the wetting of the cladding and then decreases to 30% as the wall assembly is exposed to radiation. The cavity RH proceeds to increase once again as the heat lamps are off. The air cavity temperature increases shortly after the cladding is under radiation and decreases shortly after the lamps are turned off. The maximum temperature recorded within the cavity is roughly 5°C above the temperature recorded in the reflective box but decreases to the same temperature within the box in the following 16 hours. While the indoor and insulating cavity temperature remain quite constant throughout each period, the relative humidity does not. The indoor relative humidity varies throughout the day as does the humidity within the insulating cavity. While the indoor RH varies between 50% and

60%, the insulating cavity RH fluctuates between 80% and 90%. Both increase as the assembly is exposed to radiative heat for eight hours and decrease during the following 16 hours when not exposed to radiation. It is clear that the inclusion of radiative heat increases the inward vapor drive.

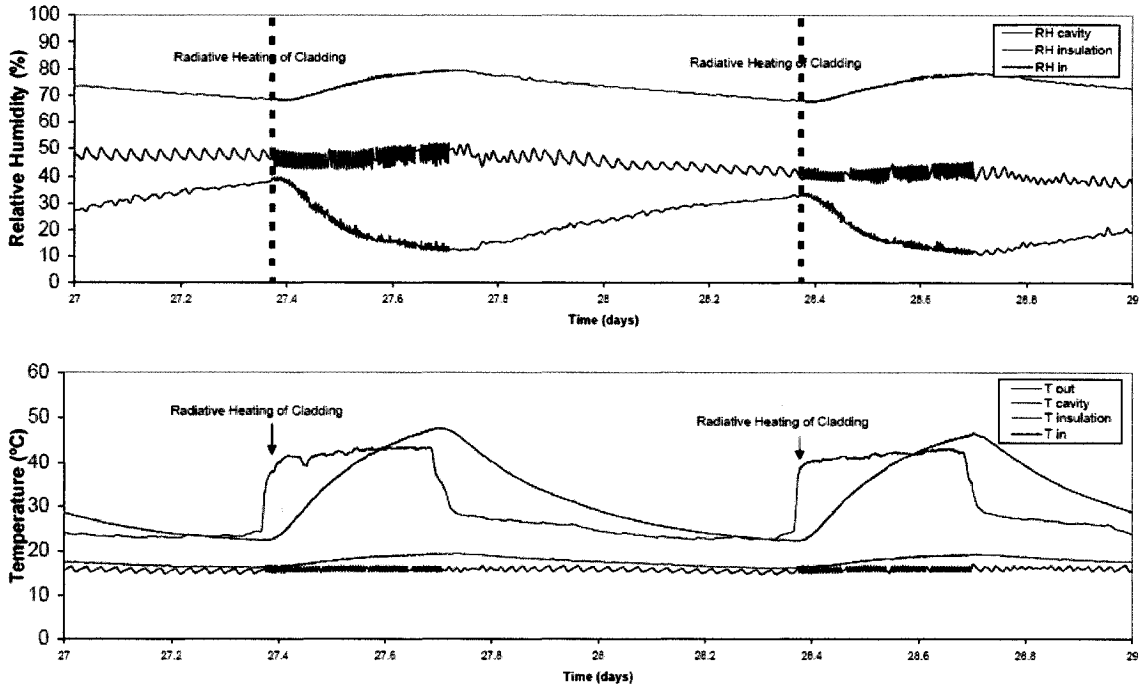

Figure 4.32 Experimental conditions across assembly without wetting

Several days after the completion of the wetting regime, the conditions within the assembly change. As seen in Figure 4.32, the relative humidity within the insulating cavity decreases by about 1% RH in one drying cycle while a decrease of roughly 4% RH is seen within the interior. The maximum relative humidity in the air cavity decreases by about 5.5% during one cycle while decreases down to the laboratory RH during times without radiation. The temperatures across the assembly remain the same as observed during the wetting regime in Figure 4.31.

4.7 Simulation Results

The experiment was simulated using the previously discussed model in chapter 3. The comparison of the experimental and simulation results aimed at evaluating whether the

experimental setup was recreating the expected effects of solar-driven vapor diffusion on large-scale test specimens under cyclic loading. Since the materials used for the large-scale specimen were similar to those used in the small-scale experiment, all material properties were kept the same. The boundary conditions which represent the loadings acting on the specimen were modified to reflect the conditions seen in the laboratory. It must be noted that the temperature and relative humidity in the laboratory were not constant. Due to lower occupancy overnight and on weekends, the HVAC system load was reduced during these times. In addition, since the laboratory is directly linked to the exterior, the outdoor climate has an effect on the boundary conditions. These variations are not taken into account in the simulations, but rather constant temperature and relative humidity are assumed. The simulations are carried out by imposing surface temperatures of 50°C and 20°C during radiation and without radiation exposure, respectively.

4.7.1 Moisture Content within Wall Components

4.7.1.1 Moisture Content of Brick Component

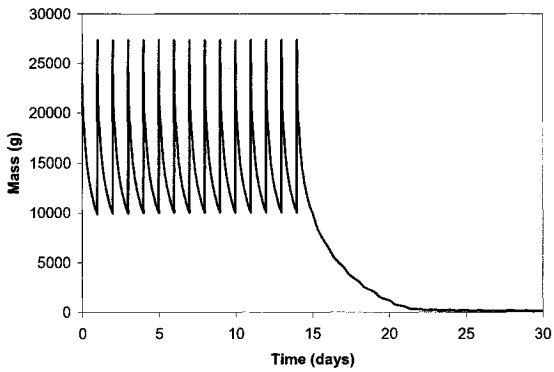

Figure 4.33 Mass of moisture in brick - simulation

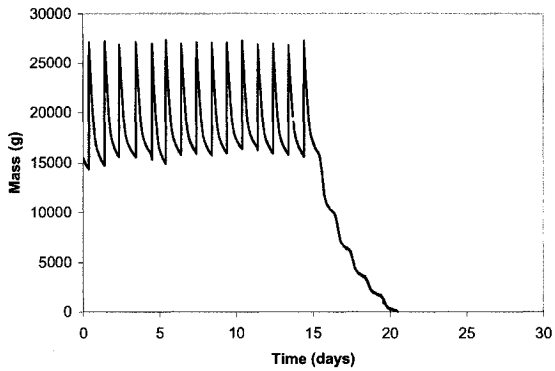

Figure 4.34 Mass of moisture in brick – large-scale experimental

For the simulation, at every wetting period, 27 kg of moisture is added. After a period of 24 hours, which includes eight hours of radiation exposure, followed by 16 hours no radiation, roughly 10 kg of moisture remain in the brick, while about 15 kg remained in the brick in the experiment. Once the wetting regime is terminated and the system is allowed to dry under cyclic conditions, the brick dries in about eight days.

4.7.1.2 Moisture Content of Back Wall Component

The modeled back wall component is made up of the weather resistive barrier, OSB sheathing, mineral wool insulation, gypsum sheathing and vinyl wall covering while the experimental specimen includes wood studs in addition to the preceding mentioned materials.

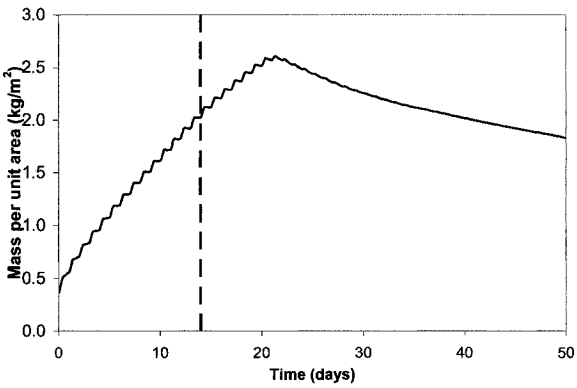

Figure 4.35 Mass of moisture per area in back wall - simulation

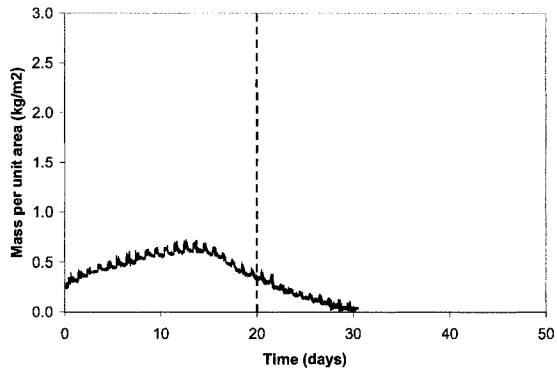

Figure 4.36 Mass of moisture per area in back wall – large-scale experimental

The simulation results, seen in Figure 4.35, show a relatively constant stepwise increase in moisture within the back wall component. The moisture continues to accumulate in the assembly several days after the completion of the wetting regime to a maximum of 2.6 kg/m^2. The initial decrease in moisture, seen at day 21, is due to the drying of the sheathing, while the constant rate of moisture loss seen from about day 36 is predominantly due to the gypsum.

As seen in the simulated results, the moisture accumulation seen in Figure 4.36 during the wetting regime was also stepwise. The accumulation rate within the specimen was greater during times of radiation exposure compared to no radiation. Unlike the simulation, the test specimen ceased to accumulate moisture once the wetting regimen ended. Although, globally, drying continued for a period of days following the wetting and drying cycles, moisture content increases daily in the specimens. It is understood that the relative humidity in the air cavity and the remaining moisture in the brick component are the main causes for this trend.

4.7.1.3 Moisture Content in Gypsum

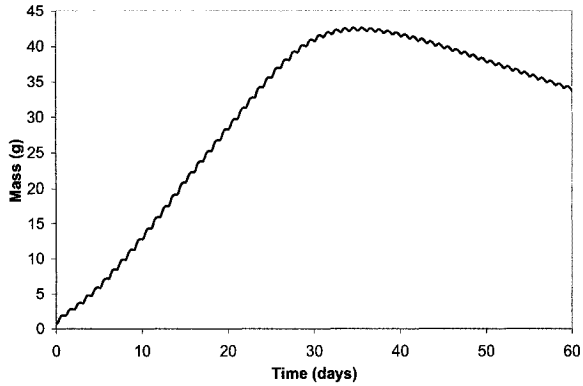

Figure 4.37 Mass of moisture in gypsum - simulation

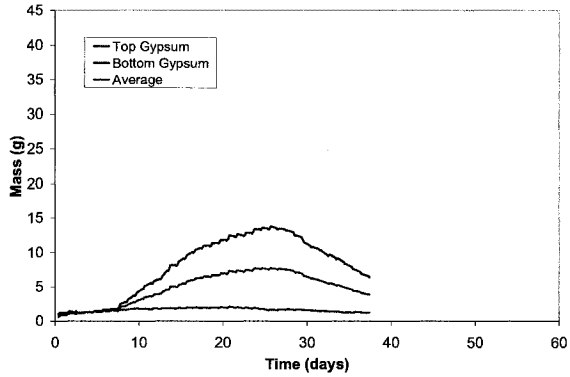

Figure 4.38 Mass of moisture in gypsum - experimental

An average, taken from the top and bottom gravimetric gypsum samples in Figure 4.38, has a similar trend to the simulated result presented in Figure 4.37. The simulation returns a maximum of 42.5 g of moisture content compared to 13 g in the top gypsum sample.

4.8 Conclusion

The construction of an experimental setup to simulate solar-driven vapor flow through large-scale test specimens under cyclic loading was done. The results of the testing done on one large-scale test specimen were carried out and the results were presented. Cyclic loading on the test specimen shows that, due to a relatively high temperature gradient resulting in a high vapor pressure gradient, an important vapor flow is generated to the back wall, wetting the OSB, mineral wool, stud framing and gypsum board.

It is shown that the experimental setup with the simulated environmental loading conditions can reproduce trends similar to the ones observed in the small-scale test setup. Although the magnitude of the moisture accumulated between the large and small-scale specimens is not the same, the setup can be used to carry out a series of comparative analyses on various large-scale wall constructions.

The simulation results only offer a first approximation of the processes seen the large-scale tests. The results obtained from the simulation differed in magnitude to the experimental results for several reasons. One of the most influential reasons was due to

the opening of the bottom of the air cavity which enabled condensed moisture to drain out of the system. The air cavity was not insulated along the perimeter allowing heat transfer to the laboratory environment, which influenced an increase in condensation within the air cavity, which was not taken into account in the model. In addition, three-dimensional heat and mass flow took place in test specimen where the simulations were one-dimensional. This three-dimensional flow, for instance, involved the wood stud framing, which was not included in the model.

Comparing the results of the large-scale test to those observed in the small-scale test, one can note that the differences between the two are as those observed between the large-scale test and simulation result. The small-scale test included a well insulated air cavity to ensure one-dimensional heat and moisture flow. Furthermore, air leakages between the material interfaces in the small-scale experiment were minimized while not in the large-scale experiment.

However, the environmental conditions within both the large and small-scale experiments produce similar results. The relative humidity measured at the gypsum surface was at levels above 80% RH for the constant loading experiments. The same levels, however cyclic, were observed in the large-scale cyclic testing. This similarity is a good indication that the experimental procedure is capable of recreating solar-driven vapor diffusion through large-scale test specimens.

Chapter 5: Conclusion

This investigation of moisture movement through the building envelope supports the importance of testing and the need to advance the current state of knowledge of mass transport in building envelope systems. With new building material products being repeatedly introduced to the industry, the moisture movement within building envelopes may be affected. Current research deals with experimental setups, both controlled and field tests, to study the interaction of actual assemblies with climatic conditions. These results can be used to validate modeled work to perform advanced simulations of heat, air and mass transfer in wall assemblies.

This project studied the moisture movement and accumulation in lightweight wood-framed wall assemblies with brick veneer exposed to simulated solar radiation from an experimental approach on small-scale test specimens. A second experimental approach was developed and implemented to determine if the results can be duplicated in large-scale test specimens. A heat and mass transfer model was applied in the data analysis. This project developed a better understanding of the nature and significance of solar-driven inward vapor diffusion through the investigation of the hygrothermal performance of different wood-framed wall assemblies under summer conditions, with considerations of a hot and humid climate for loading and assembly design.

The results of the small-scale experimental procedure return several conclusions. Although the weather resistive barriers had a minimal effect on the exterior and interior sheathings, some observations are made. The permeability of one weather resistive barrier is directly influenced by the relative humidity within the system, resulting in the building paper becomes less vapor tight relative to the spun bonded polyolefin at high relative humidity. During occurrence of higher relative humidity, the OSB sheathing is observed to accumulate more moisture when covered with building paper relative to the SBPO due to the difference in the vapor permeabilities. At lower relative humidity levels, the sheathings dry at relatively the same rate. Similar occurrences are observed in the gypsum sheathing.

The influence of the interior finishing on the moisture flow through the assemblies is far more noticeable relative to the weather resistive barrier. The use of a relatively vapor tight finishing, as the vinyl wall covering, can greatly increase the moisture content of the interior sheathing which can be highly susceptible to moisture related problems. The more vapor open acrylic paint resulted in less severe moisture contents within the gypsum sheathing. Since the interior gypsum is highly sensitive to moisture and susceptible to mould growth, highly impermeable interior finishings are undesirable in residential constructions exposed to such vapor flows.

The large-scale experimental procedure results, when compared to the small-scale and simulation results, prove to be interesting. Similar trends are observed with the exception of a difference in moisture content magnitude within the back wall. Since the loading procedures are different, exact comparisons cannot be made. Nevertheless, cyclic loading on test specimens is more realistic, when compared to real climatic conditions. The test specimen used to validate the large-scale experimental procedure was subjected to similar levels of relative humidity and temperature gradients through the system as the small-scale specimens with the same composition. It is concluded that wall assemblies exposed to cyclic loading conditions see less severe moisture contents across the construction as well as improved drying capabilities.

5.1 Contributions of the Research

The experimental research has advanced the field of study of moisture movement through building envelopes through the following contributions:

- Implementation of an existing test procedure to study the behavior of small-scale wall assemblies subjected to constant loading conditions and production of a set of experimental data on moisture patterns of eight wall assemblies. The experiment was continuous for a period of 80 days. The data collected includes temperature, relative humidity and moisture content.

- A comparative analysis of the influence of three wall parameters – permeance of weather resistive barrier, the presence of hygric buffering and the permeance of interior finishing using experimental and modeling results.
- Development, design and construction of a test procedure to study the behavior of large-scale wall assemblies subjected to cyclic loading conditions.
- Production of experimental data on moisture patterns of a wall assembly. The experiment was continuous for 39 days.

5.2 Recommendations for Future Work

Through this work, a greater understanding of future work has come to attention. Some suggestions for future work with the existing experimental procedure are:

- Determine method to insulate air cavity from laboratory environment without affecting measurements.
- Inclusion of more relative humidity and temperature probes to better map the conditions across the assembly.
- A more efficient and accurate way to simulate wetted cladding without disrupting measurements.

Some suggestions for future related work are:

- Simulated loading conditions must be more accurately calibrated to reproduce exact repetitive conditions.
- The influence of various absorptive cladding materials on the overall hygrothermal performance of the building envelope could be studied.
- The selection of alternative vapor retarders which prevent the occurrence of envelope failures subjected to various climates could be studied.
- Year-round field testing in various climates done on wall assemblies to better understand their hygrothermal performance could be performed.
- Further modeling could be done to perform parametric analyses of wall assemblies.

References

ASHRAE Handbook Fundamentals 2001

Al-Gahtani, A.S., Ibrahim M., Almusallam A.A., (1999) *Performance of Concrete Surface Treatment Systems,* Concrete International, Vol. 21, pgs 64-67

Anderson, N.E., (1987) Summer Condensation in an Unheated Building, *Nordic Symposium on Building Physics*

Bomberg, Brown, (1993) Building Envelope and Environmental Control: Part 1- Heat, Air and Moisture Interactions *Construction Canada* 35(1), p. 15-18

Bosschaerts, W., Suy, O., Marinus B., (2003) Test renewable energy equipment: Space Heating and Warm Sanitarian Water Production Setup of a Test Facility *European Journal of Mechanical and Environmental Engineering*, VOL 48; PART 2, pages 109-120

Carmeliet, J. and De Meulenaer, M. (2006) Moisture problems in lightweight structures in warm, humid climates, Katholieke Universiteit Leuven

Chiovitti D., Gonçalves M., Renzullo A., (1999) *Performance Evaluation of Water Repellents for Above Ground Masonry*, Durability of Building Materials and Components, Vol. 1, pgs 560-567

Hazleden (2001), Envelope Drying Rates Experiment, *Canadian Mortgage and Housing Corporation*

Hubbs and Hircock (2002) Building Envelope Performance Monitoring

Hutcheon. N.B. (1953) Fundamental Considerations in the Design of Exterior Walls for Buildings, Division of Building Research, DBR No.37

Janssen, H., Blocken, B., Carmeliet, J., (2006) Conservative Modeling of the Moisture and Heat Transfer in Building Components under Atmospheric Excitation, *International Journal of Heat and Mass Transfer*

Kumaran, M.K., Lackey, J.C., Normandin, N., van Reenen, D., (2006) Vapor permeances, air permeances, and water absorption coefficients of building membranes, *Journal of Testing and Evaluation*, pp. 241-245

Kumaran, M.K., Lackey, J.C., Normandin, N., Tariku, F., van Reenen, D., (2002) A Thermal and Moisture Transport Property Database for Common Building and Insulating Materials *ASHRAE Research Project 1018-RP*

Kunzel (1999) Flexible Vapor Control Solves Moisture Problems of Building Assemblies, J.Thermal Envelope & Building Science, Vol 23 July 1999, p95-102)

Künzel, H.M. and Kiessl, K., (1996) 'Drying of brick walls after impregnation',*Internationale Zeitschrift für Bauinstandsetzen* 2 pgs.87–100.

Lawton, Mark D., Brown, William C., (2003) Considering the Use of Polyethylene Vapour Barriers in Temperate Climates

Levin, P., (2000), "Moisture in constructions with loose-fill insulation and no vapour barrier", *Nordic Journal of Building Physics*, June.

Ojanen, T., Ahonen, J., (2005) Moisture Performance Properties of Exterior Sheathing Products made of Spruce Plywood or OSB, *VVT Working Papers 22*

Pressnail K., Timusk J., Kan L., Dong B., Kan V. (2003) In search of a wall for all season: controlling sun driven moisture, University of Toronto, *9th Canadian Conference on Building Science and Technology,* Vancouver

Roels, S., Janssen, H., Carmeliet, J., de Wit, M., (2006) Hygric buffering capacities of uncoated and coated gypsum board, *3rd International Building Physics Conference*, Montreal, Canada, pp.27-32

Salonvaara, M. H., Ojanen, T., Kokko, E. and Karagiozis, A. N., (1998) Drying capabilities of wood frame walls with wood siding, Thermal Performance of the Exterior Envelopes of Buildings VII, Clear water Beach, Florida, pp. 165-177.

Sandin, Kenneth (1993), "Moisture Conditions in Cavity Walls with Wooden Framework", *Building Research and Inf.*, vol 21, no. 4

Sherwood, Gerald E., (1985) Condensation potential in high thermal performance walls-hot, humid summer climate. Res. Pap. FPL 455. Madison, WI: US Department of Agriculture, Forest Service, Forest Products Laboratory.

Straube, J.F. (2001) The influence of Low-Permeance Vapor Barriers on Roof and Wall Performance, *Proceedings of Thermal Performance of Building Envelopes VII*, Clearwater Beach, Florida

Straube, J.F., Smegal, J., (2007) The Role of Small Gaps Behind Wall Claddings on Drainage and Drying, *Proceedings of the 11th Canadian Conference on Building Science and Technology*, March

Straube, Burnett (1997) Field Testing of Filled-Cavity Walls, *ICBEST Proceedings,* Bath, U.K.

Straube, J. F. and Burnett, E. F. P., (1998), "Drainage, ventilation drying and enclosure performance", *Thermal Performance of the Exterior Envelopes of Buildings VII*, Clear water Beach, Florida, pp. 189.

TenWolde, A. and Mei, H.T. (1986) Moisture movement in walls in a warm, humid climate," Presented at ASHRAE/DOE/BTECC Conference in Clearwater Beach, Florida

Tobiasson (1989) Vapor retartders to control summer condensation. *Thermal Performance of the Exterior Envelopes of Buildings IV*, ASHRAE

Tsongas, G. and Olson, J., (1995) Tri State homes: a case study of extensive decay in the walls of older manufactured homes with exterior vapor retarder, *Thermal Performance of the Exterior Envelopes of Buildings V*I, Orlando, Florida, pp. 207-218.

Wilson, A.G. (1965) Condensation in insulated masonry walls in summer. RILEM/CIB Symposium Moisture Problems in Buildings, Helsinki.

Appendix A: Large-Scale Cyclic Loading Experimental Development and Setup

A.1 Large-Scale Weighing System

A system was developed to non-destructively monitor the moisture movement across wall assemblies. The weighing system is composed of a gantry crane, lever arm, counter weight and load cell. The lever arm is supported upon a pivot point (fulcrum), thus two equally weighing objects can be balanced and suspended. With a secure enough lever arm, large-scale wall specimens can be suspended in air and their increase in moisture over time can be measured.

Supporting the Lever Arms

Gantry cranes were selected to suspend the test specimens above the ground with the use of a trolley and hoist. Two cranes were utilized: a one and three ton capacity. Each crane has an adjustable height between 12 and 15 feet. The one ton crane has an overall span of 12 feet while the three ton crane has a span of 15 feet. Figure A.1 and Table A.1 further explain the crane dimensions.

Selection of the cranes was based on the size of the test hut, thickness of test specimens and depth of the reflective box. Since the test hut, wall specimens and reflective box are to be placed between the gantry crane supports, the crane's clear span, D, needed to be large enough. A trolley and hoist, both accompanied by the gantry crane, link a lever arm to the crane.

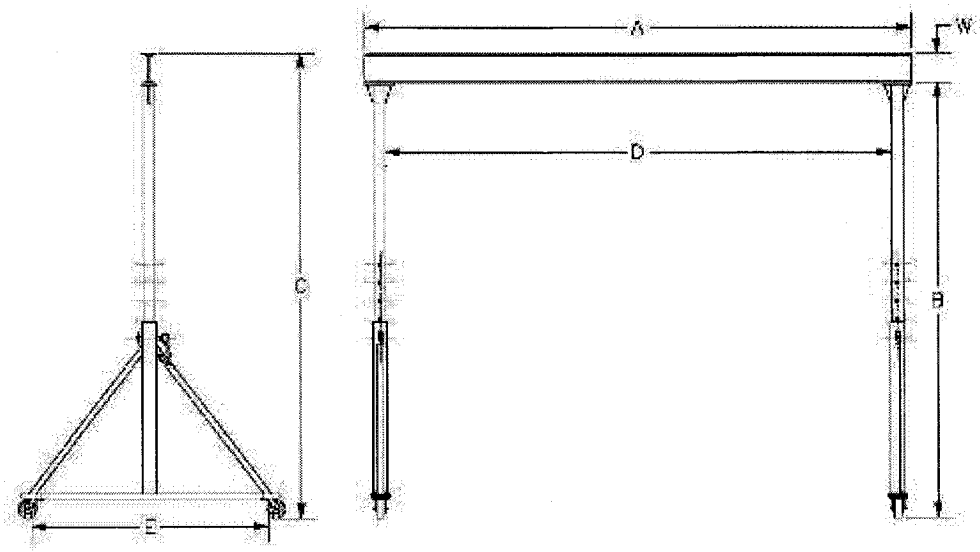

Figure A.1 Gantry crane

Table A.1 Gantry crane dimensions

Capacity	1 Ton	3 Ton
A	12'	15'
B	12'-15'	12'-15'
C	12'-6" – 15'-6"	13'-16'
D	10'-9 5/8"	13'-6 ½"
E	78"	78"
W	6"	12"

Lever Arms

The lever arm is the core of the weighing system. The arms balance the specimens in equilibrium, where two objects are hung at an equal and opposite distance from the central fulcrum. When the lever is level in the horizontal plane, both objects at either end of the lever are the same mass.

Two lever arms are constructed of hollow rectangular steel tubes (1.7 and 1.5 m long) with three pivot points (or axles). The center pivot (fulcrum) located at the midpoint of the beam is connected to the crane, while the two other pivot points support a wall and respective counter weight. Frictionless ball bearings make up the pivot points of the lever arms to allow the specimens to move freely. During experimentation, when an assembly changes mass due to loss/gain of moisture, the specimens will either slightly shift upwards or downwards. Figure A.2 shows a lever arm suspended by a hoist while balancing two equal masses.

Figure A.2 Brick lever arm

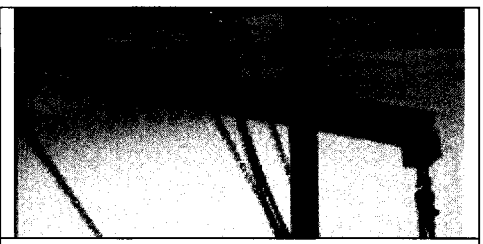

Figure A.3 Back wall lever arm

Counter Weights

The brick cladding framed with steel channels, is estimated to weigh approximately 735 kg when dry. Various insulating back walls comprised of studs, insulation and sandwiched between interior and exterior sheathing are estimated to weigh less than 75 kg. Two counter weights are needed for each wall component where their masses can be easily adapted to the varying components. By suspending the components in equilibrium, mass changes to the systems can easily be measured without knowing the overall mass of each wall component. Water tanks, with sealable screw-top orifices are used as the varying counter weights. A 200-gallon (760 L) tank is used for the brick wall and two 20 L jugs are used for the insulating back walls. Included in the counter weights are steel tables, which support the tanks from below and link the counter weights to the lever arms

using steel chains and ½" shackles. The tables are 53 cm x 53 cm x 43 cm high and 69 cm x 69 cm x 53 cm high.

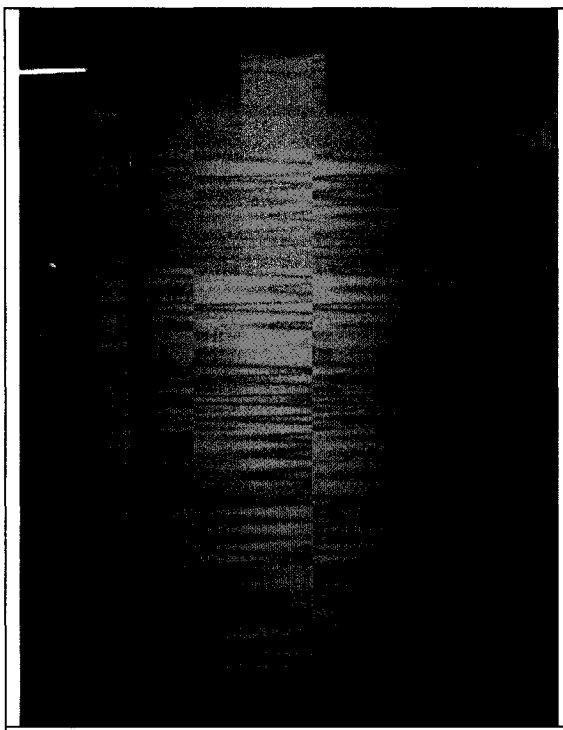

Figure A.4 200 gallon counter weight

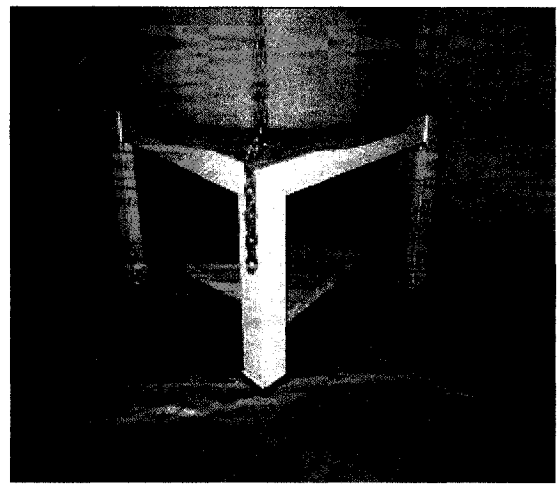

Figure A.5 Steel table supporting counter weight

Measuring Mass Change

The changes in mass, actually variations in moisture content, is monitored and measured with a tension sensitive load cells connected to a data acquisition system and computer.

Two different load cells are selected for the different wall sections. A load cell's capacity is inversely related to its accuracy, thus it is significant to use appropriate load cells with mass capacities that correspond to the moisture accumulation in each wall component. Through preliminary moisture uptake testing, it is estimated that at capillary saturation, the brick wall may accumulate 54 kg (120 lbs) of moisture. However for the purposes of this experiment, the cladding will be subjected to about half the saturation amount, hence a 45 kg (100 lbs) capacity load cell is selected. The Celtron STC-100 has a rated load of 45 kg with an ultimate load of 135 kg. In the case of the back walls, a load cell with capacity of 11 kg (25 lbs), seen in Figure A.6, is selected. The Omega LCCA-25 has a rated load of 11 kg with an ultimate load of 34 kg. Each load cell has an accuracy of ±0.03% full scale.

The load cells were applied to read the tension between the support tables and fixed weights placed on the ground. The steel tables were designed so that the load cells can easily be affixed from the top end. The bottom ends of the cells are connected to anchor weights, which equal the capacity of the load cells. These load cells are delicate, expensive pieces of equipment that can malfunction permanently if used beyond capacity.

Since the anchor weights are no greater than the cell capacities, in the event that the cells are submitted to a force beyond their capacity, damage will be prevented. A clear implementation of a load cell placed between a steel table and weight is seen in Figure A.7.

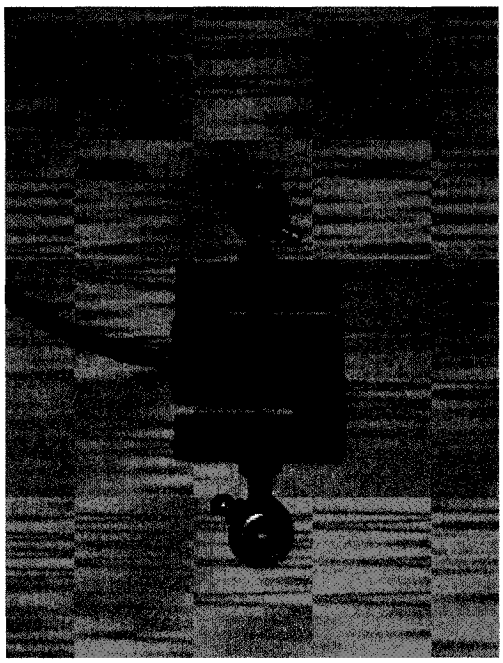

Figure A.6 11-kg capacity load cell

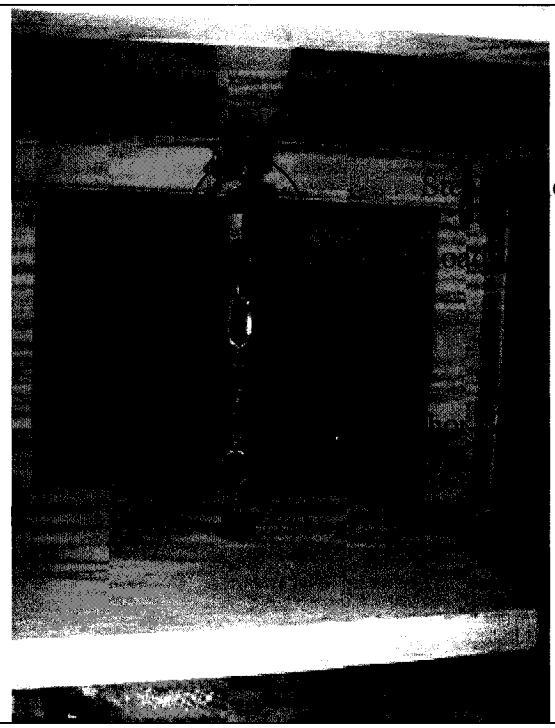

Figure A.7 Installation of load cell

Calibration

The weighing systems for each wall were calibrated to determine their accuracies. Each wall was independently loaded with incremental known masses to their rated maximum capacities. Once the maximums were reached, the systems were unloaded in increments. The actual and measured masses were then compared to determine the accuracy of the systems. Below, in Figure A.8, are the outputs of the overall loading applied to each weighing system.

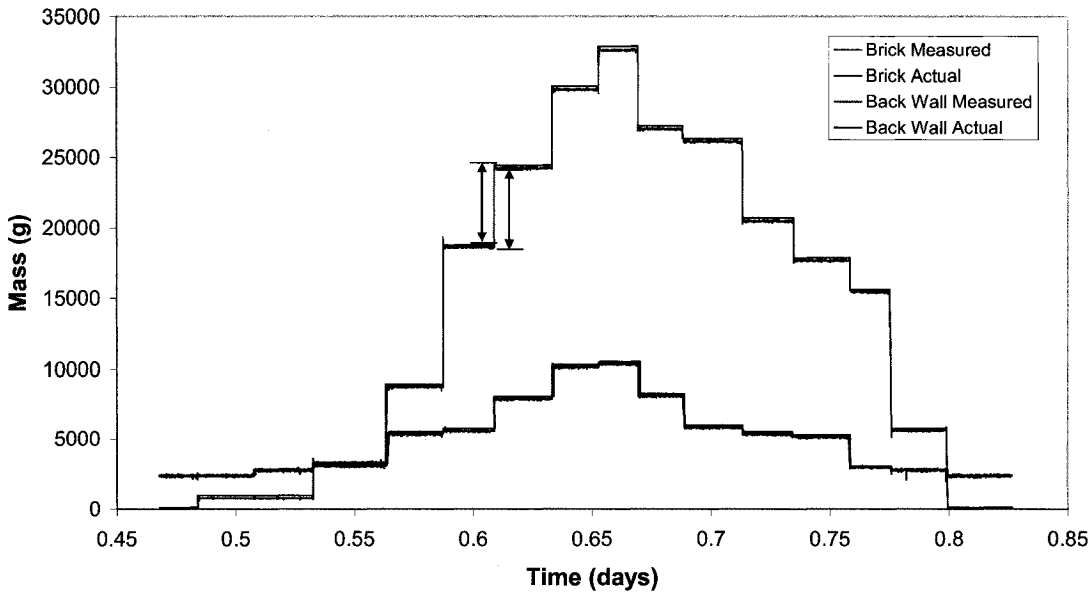

Figure A.8 Weighing system calibration results

The brick wall was loaded in steps to about 34 kg, while the back wall to 8 kg. Referring to the relative errors in Table A.2 and Table A.3 the brick wall system has greatest error at lower masses, while the back wall has a relatively constant error throughout its entire loading scale. The relative error was calculated by dividing the difference in masses by the actual mass.

Table A.2 Brick wall weighing system calibration

Cumulative Measured Mass (g)	Cumulative Actual Mass (g)	Relative Error (%)
113.00	113.00	0.00
818.62	1020.00	19.77
3082.52	3288.00	6.27
8773.55	8928.00	1.73
18651.89	18790.00	0.74
24353.88	24434.00	0.33
29820.34	30074.00	0.84
32620.24	32895.00	0.84
27041.30	27255.00	0.78
26128.36	26348.00	0.83
20490.62	20704.00	1.03
17693.27	17883.00	1.06
15448.87	15615.00	1.06
5638.32	5753.00	1.99
129.90	113.00	14.65

Table A.3 Back wall weighing system calibration

Cumulative Measured Mass (g)	Cumulative Actual Mass (g)	Relative Error (%)
2365.00	2365	0.00
2774.18	2817	1.52
3254.61	3273	0.56
5353.89	5539	3.34
5585.50	5766	3.13
7877.42	8070	2.39
10168.18	10338	1.64
10379.46	10565	1.76
8107.03	8297	2.29
5829.52	5993	2.73
5356.30	5541	3.33
5142.12	5314	3.23
2977.44	3048	2.32
2766.87	2821	1.92
2353.52	2365	0.49

A.2 Specimen Construction

The following section describes the materials and construction of a wall assembly used to test the experimental setup in the laboratory.

The construction first involved the erection of the brick wall within a steel frame. The second component, insulating back wall, is the second component of the wall assembly. The two components, when separated by a 20 mm air space, form the test wall assembly.

Component One - Brick

The bricks used to construct the brick wall were I-XL red fired clay. They were 0.19 m x 0.09 m x 0.06 m high with a density of 2150 kg/m^3 and a w_{sat} of 175 kg/m^3. A 1.25x10^{-4} m^3 of mortar weighs 0.2 kg giving a density of about 1680 kg/m^3 and a w_{sat} of 160 kg/m^3. Half an inch of mortar was used to space the joints between the bricks, about 0.08 m^3 in total.

228 bricks were permanently set within a steel frame. Thermocouples (TC_1 through TC_6) were glued along the central vertical axis to both the interior and exterior façades of the brick. The glue spots were made as small as possible as to reduce any experimental influences. Both the front and back surfaces of the brick were equipped with three thermocouples each to monitor the 2 dimensional heat distribution across the construction.

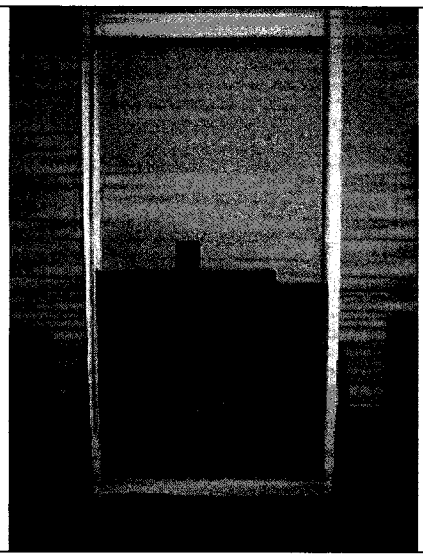

Figure A.9 Erection of brick wall in steel frame

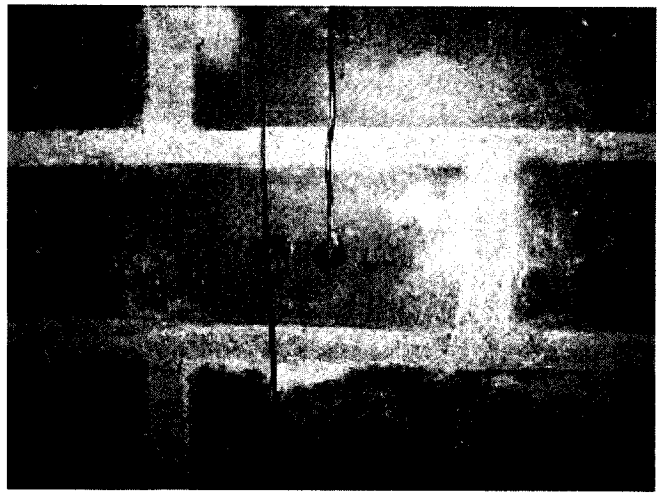

Figure A.10 Thermocouple T_2 placed at centre of exterior brick surface

Component Two – Insulating Back Wall

The frame of the insulating back wall is constructed of 2" x 4" S-P-F lumber. The 2 x 4 studs used to frame the back wall are spaced 400 mm o/c seen in Figure A.11. OSB sheathing is sized, cut and screwed to the exterior side of the frame. Glass fiber insulation is used to insulate the cavities within the frame. Prior to insulating, the sheathing was outfitted with six thermocouples (TC_7 through TC_{12}); three on the exterior surface and three on the interior surface at the sheathing/insulation interface. After the thermocouples were fixed to the sheathing, mineral wool was placed between the studs.

Spun bonded polyolefin is stapled to the exterior of the sheathing which covers the thermocouples, shown in Figure A.16.

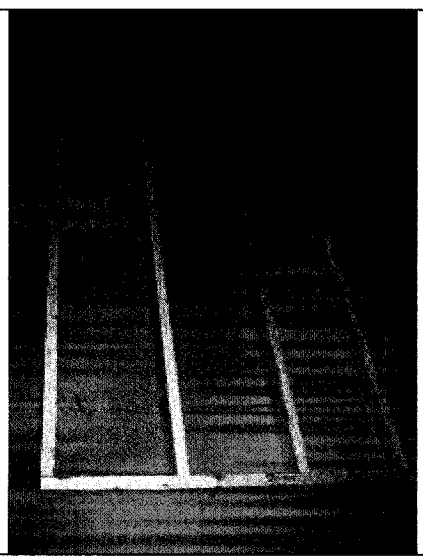

Figure A.11 Light weight wood stud frame

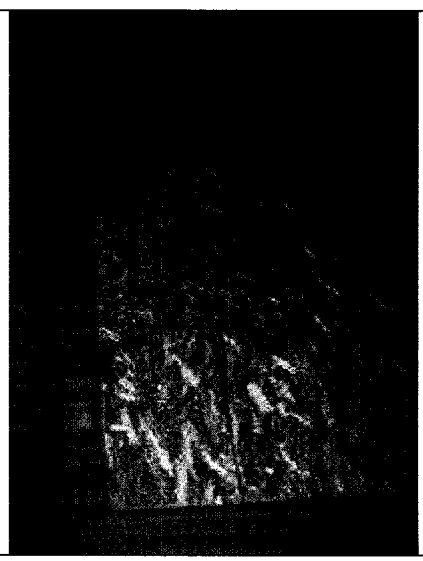

Figure A.12 OSB sheathing affixed to stud frame

Figure A.13 Sheathing thermocouple

Figure A.14 Thermocouple TC_{12} added to sheathing

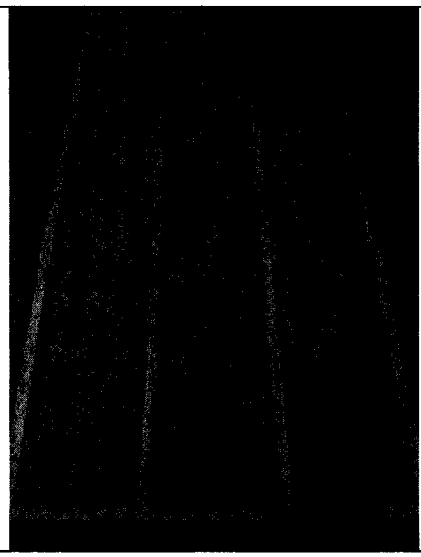

Figure A.15 Glass fiber placed between studs

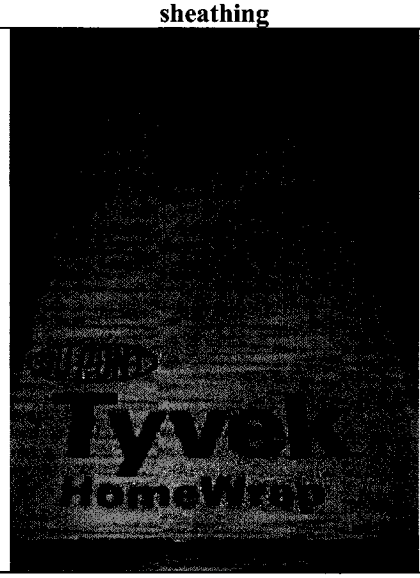

Figure A.16 SBPO stapled to exterior sheathing

The gypsum sheathing was secured to the interior side of the wood frame and finished with a sheet of vinyl wall covering. Once again, six thermocouples (TC_{13} through TC_{18}) were fixed to the exterior and interior of the gypsum. A relative humidity probe was secured to the exterior surface of the gypsum panel between the gypsum and mineral wool insulation. All sensors measuring the temperature and relative humidity within the insulating cavity are fed though a one centimeter hole at the top of the stud frame wall. The hole is sealed with silicone sealant to prevent the flow of air and moisture.

The exterior sheathing was outfitted with three sets of moisture pins to measure the moisture content of the OSB. In addition, a relative humidity probe was attached to the exterior sheathing at a distance of 10 mm, to record the humidity levels within the air cavity. The humidity probe was anchored using a pair of modified steel angles and tie wraps. A set of moisture pins and relative humidity probe are seen in Figure A.18.

The interior of the test hut is outfitted with a relative humidity probe to measure the interior conditions of the hut, shown in Figure A.18. The probe is placed 3 cm from the interior gypsum surface.

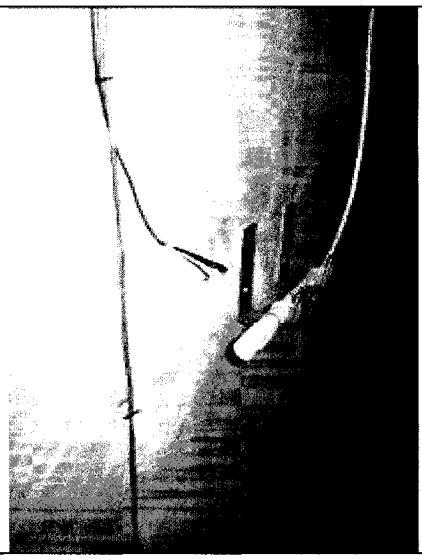

Figure A.17 Moisture pins and RH probe on OSB

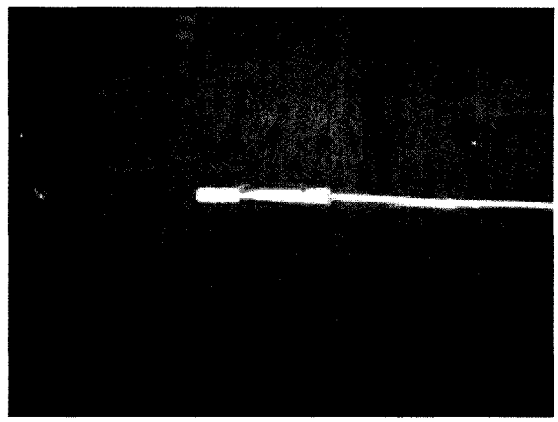

Figure A.18 RH probe at hut interior

A.3 Description of Test Hut Construction

A test hut of overall dimension 8' 6 5/8" x 4' 9" x 8' 10" high is constructed to maintain indoor conditions during solar driven moisture transfer tests.

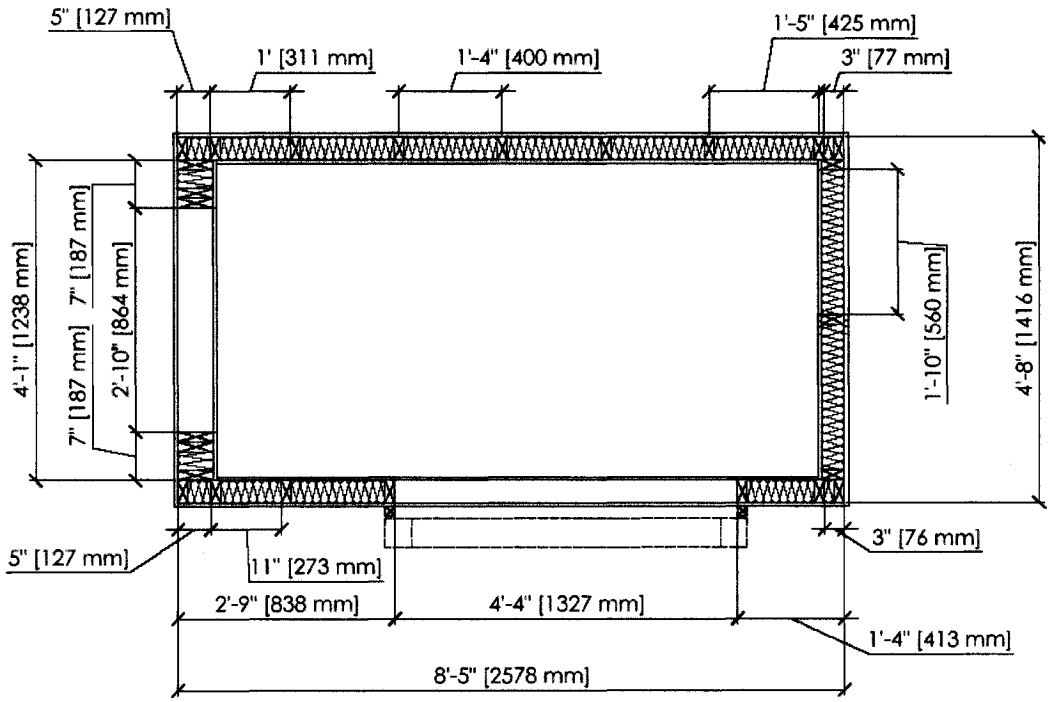

Figure A.19 Test Hut Plan

Wood Framing

The frame of the structure is made primarily of 2'x'4 lumber. 2'x6' lumber is used to frame the structure in a few locations. All the lumber used is kiln dried SPF.

Floor:

The floor of the hut is a sandwich panel. The joists used to frame the floor are 2x6's. The floor joists are spaced at 16" (400 mm) c/c. Along the perimeter of the floor, double rim joists are used for added strength and stability. 5/8" plywood sheathing is used above and below the floor framing to create the sandwich panel system.

Roof:

The roof, like the floor system, is constructed as a sandwich panel system. The ceiling joists are spaced at 16" (400 mm) c/c. The perimeter of the roof uses double ceiling joists for added strength and stability along with 5/8" sheathing above and below the joists. However, the lumber used for the ceiling joists are 2x4's compared to 2x6's used for the floor.

Figure A.20 below shows the layout and spacing for both the floor and ceiling joists.

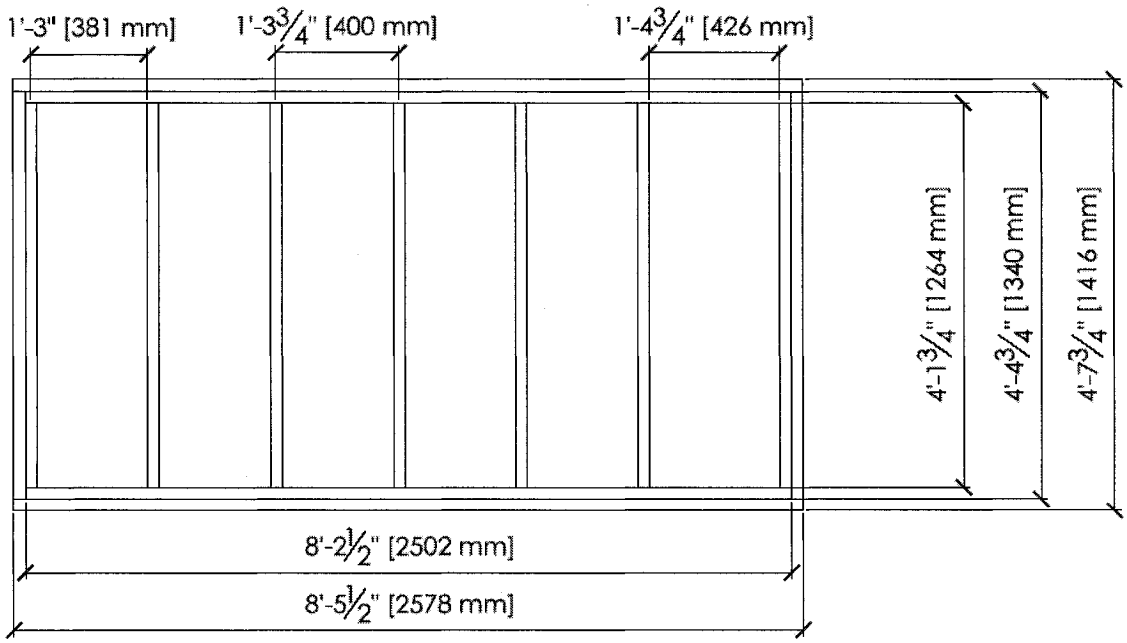

Figure A.20 Floor/ceiling joists plan

Walls:

The walls of the structure are framed using 2x4 lumber, except for the wall with the door which is made with 2 x 6.The studs of the walls are spaced at a distance of 16" (400 mm) center on center.

Plywood is the chosen sheathing for the exterior and interior. In the case of the exterior sheathing, 5/8" thick plywood is used while the interior sheathing is ½" thick. A section of the test hut is provided in Figure A.21.

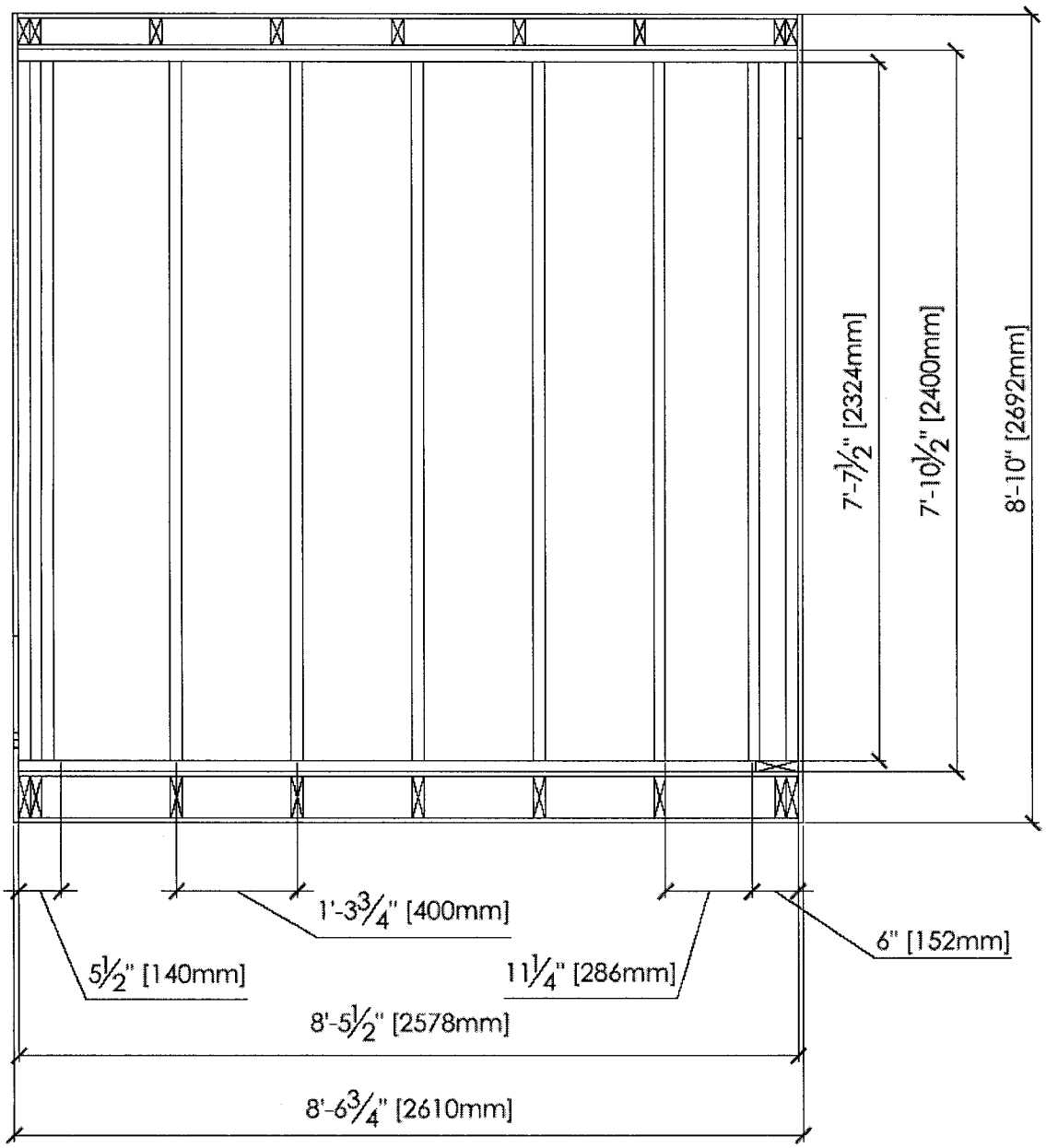

Figure A.21 Rear wall elevation

The dimensions of the test hut are shown in Table A.4.

Table A.4 Dimensions of test hut

	Exterior	Interior
Length	8' 6 5/8"	7' 7 1/2"
Width/Depth	4' 9"	3' 11 5/8"
Height	8' 10"	7' 10 1/4"

Openings between the Interior and Exterior

Several openings are made in the walls of the hut. These openings and holes are placed to allow for wiring to pass from the interior to the exterior of the hut. Two other openings are made; one to house the air conditioning unit which is to cool the interior, and the second for the test wall specimens can be installed.

The opening in the wall for the A/C unit is dimensioned to receive the air conditioner with a one inch gasket above and below to prevent the passage of heat and air. The size of the opening is about 22" (560 mm) x 16" (400 mm).

A large opening, slightly larger than the desired test panels, is made in one of the walls. The test panels to be studied are placed within the opening where they are exposed to both the interior and exterior conditions of the hut. The opening is 4' 4 1/4" long and 7' 7 1/2" high.

A 2" diameter conduit is installed to allow measurement wires (thermocouples, RH sensors, etc...) to pass through to a data acquisitioner which is placed to the exterior of the hut. Extension cords can also be passed through the conduit if need be.

Insulating and Weather Proofing

One of the major factors influencing solar driven moisture is the difference between the interior and exterior environmental conditions. To maintain specific conditions acting on the interior and exterior of the wall assemblies, both heat and air flow through the hut envelope must be minimized.

Insulation:

Mineral wool is used to insulate the hut. In the case of 2x4 studs and joists, R13.5 [RSI 2.4] is used. R21.5 [RSI 3.8] is used for the wall and floor which are built using 2x6 studs/joists.

Sealants:

The use of silicone sealant prevents the passage of air through joints between the interior and exterior of the test hut. The silicone caulking is applied:

- between the joints of the exterior plywood sheathing
- between the exterior sheathings and the top/bottom plates of the wall frames
- around all conduit openings that are installed to allow the passage of wiring from the interior to the exterior

In addition to the silicone caulking, one-part polyurethane foam is used to seal the gaps between the door frame and the 2x6 studs.

Test Hut Accessories

Access Door:

The door used to access the interior of the hut is 32" wide and 79" high. The door is of galvanized steel panels and the interior is injected with bonded polyurethane foam giving the door an R16 factor. The door is installed to swing outwards.

Air Conditioning Unit:

An A/C unit is installed to condition the interior environment of the hut as required. The Panasonic CW-XC120VK is the make and model of the A/C unit which is placed in the upper part of the wall opposite to the door. The dimensions of the unit are 22.1" (560 mm) x 14.9" (375 mm). The minimum rated temperature capacity, as per the manufacturer, is 60.8 F (16°C). The cooling capacity is 11,500 Btu/h.

Casters:

The test hut sits on four swivel locking casters. The overall height of the casters is 5 5/8" and each caster has a maximum capacity of 650 lbs.

Electrical Outlets and Lighting:

The interior of the hut is outfitted with a 60W fluorescent light bulb, which provides light without any heat generation. In addition, four outlets are installed within the hut to power the A/C unit and any other devices that may need to be powered from within the hut.

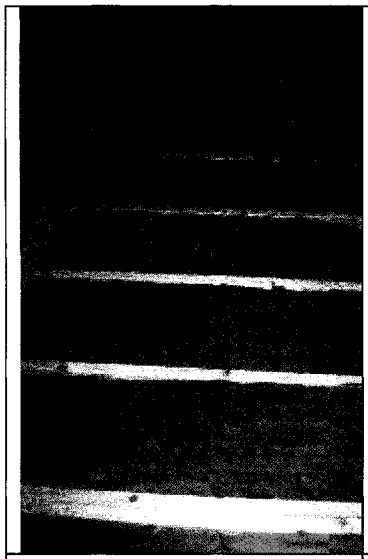

Figure A.22 Floor Joists with Mineral Wool Insulation

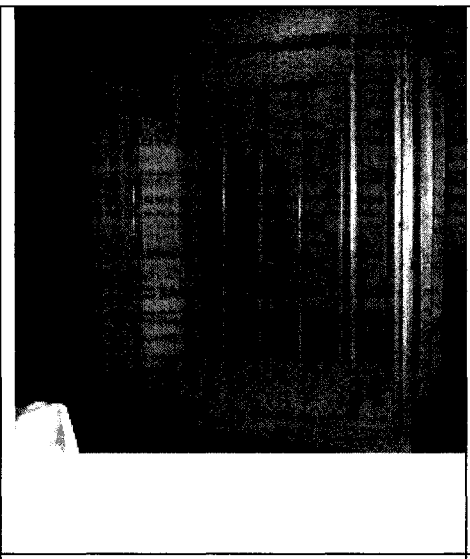

Figure A.23 Placement of Test Hut Studs

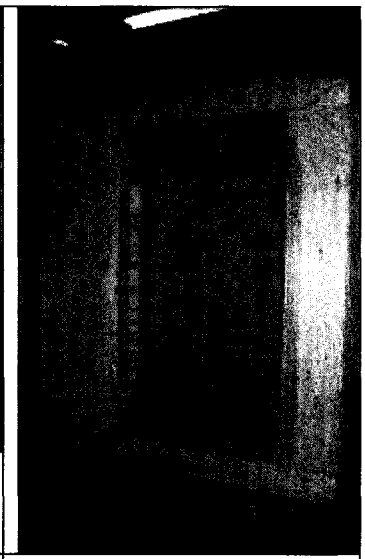

Figure A.24 Test Hut Opening for Testing Specimens

A.4 Rain Simulation

ASTM E 547: Standard Test Method for Water Penetration of Exterior Windows, Skylights, Doors, and Curtain Walls by Cyclic Static Air Pressure Difference, section 9 was followed, which describes a method to calibrate uniform wetting on vertical surface. According to the standard, a water-spray system is required to deliver water uniformly against a vertical exterior surface. Furthermore, the standard states that the system should be comprised of spray nozzles mounted to a rack and the nozzles must be at a uniform distance form the wetting surface.

Standard residential gardening spray nozzles which have an on/off switch, seen in Figure A.25, are selected for their multiple spray settings. These nozzles can eject a relatively homogeneous cone mist with a varying flow rate. At a distance of 0.5 m, they produce a spray radius of about 0.4 m. Eight nozzles are used to supply the flow and spray area required for the experiment.

Calibration

To calibrate the system, a catch box is used. The catch box is comprised of a series of squares of equal size on a vertical surface. The smaller each square, the more precise the wetting system can be calibrated. According to the standard, each catch box must be 30 cm x 30 cm. A large plastic bag is fixed to each square which enable the amount of water entering that particular box to be accumulated and measured for analysis. For the purposes of this research, a curtain wall of water is desired to be acting across the entire area of a vertical surface.

The results of the calibration test performed led to several observations. Firstly, the water supply in the lab is not constant and therefore the water pressure cannot be predicted. Furthermore, since the pressure is not constant, the nozzles must be placed in an orientation that can wet the wall evenly, where no parts of the vertical specimen remain dry following wetting. The results of the testing performed with one nozzle in ml/m^2.s are shown below in Figure A.28.

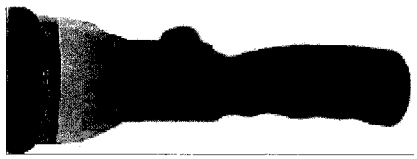

Figure A.25 Spray nozzle

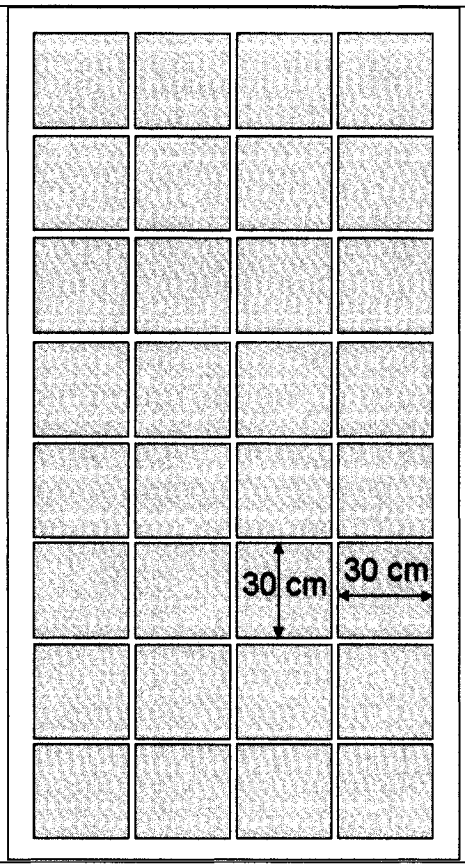

Figure A.26 Front elevation of catch box

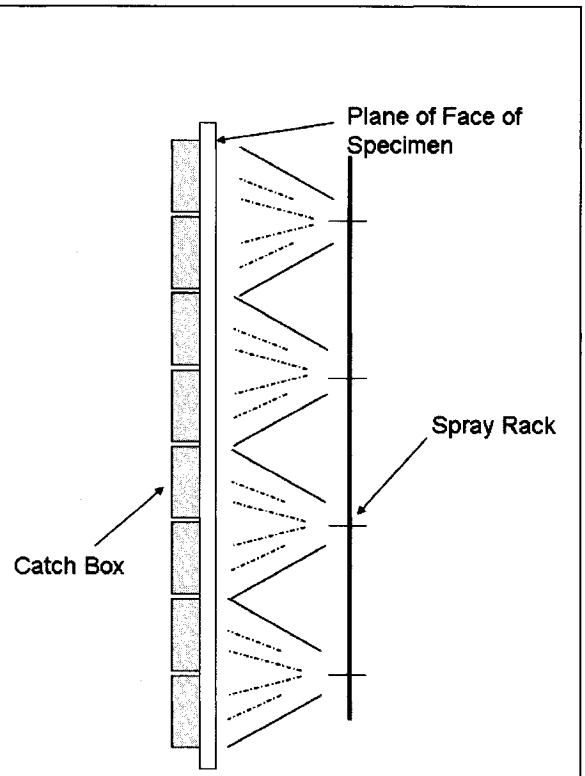

Figure A.27 Side section of catch box during wetting calibration

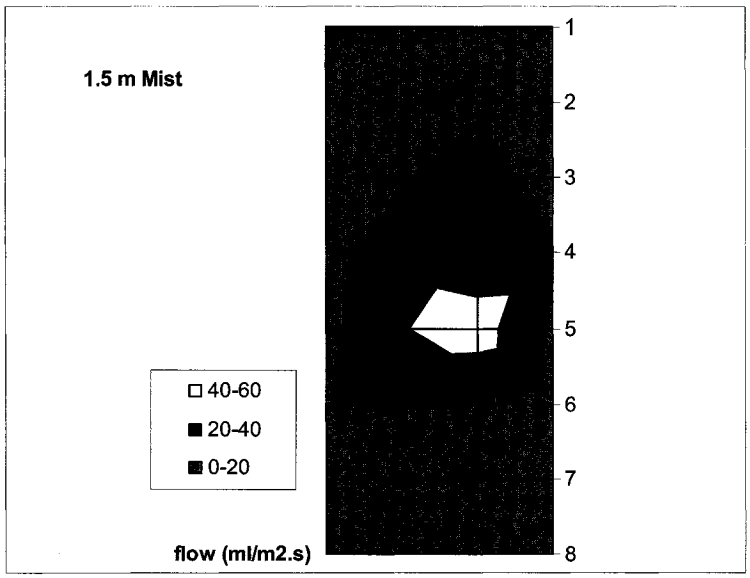

Figure A.28 Single spray nozzle distribution

Spray Rack

The spray nozzles were mounted to a moveable rack which holds them level at a given distance from the wall and at a calibrated height. The frame supporting the nozzles is constructed of lumber and sits on 4 swiveling castors with a wheel diameter of 120 mm.

The nozzles are mounted to the frame with metal straps screwed into the frame. The hoses feeding the nozzles are coupled to a manifold which supplies enough pressure to operate all nozzles. The manifold is connected to the supply main located within the laboratory.

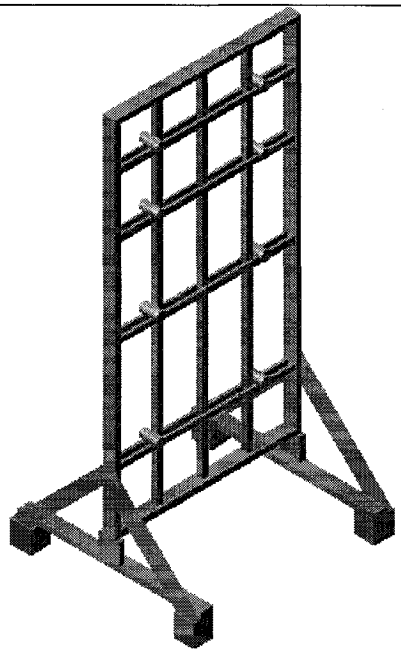

Figure A.29 Spray rack system design

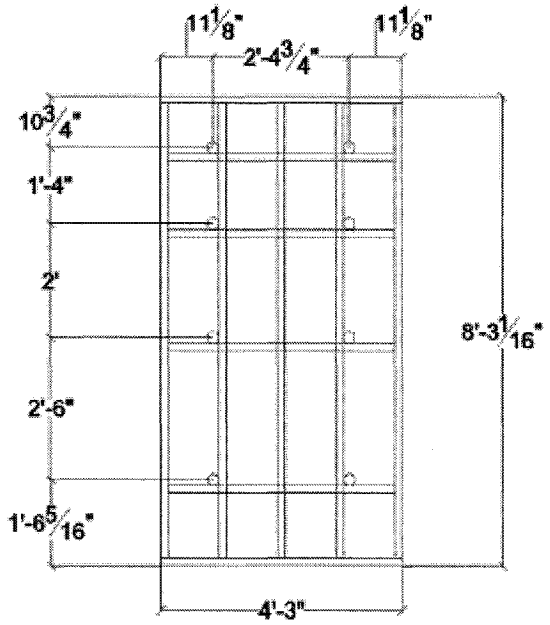

Figure A.30 Nozzle Placements

Full Scale Testing

Based on the spray pattern obtained through calibration, the layout of the nozzles was designed. A pressure difference between the top and bottom nozzles was also accounted for in the design. Since the higher nozzles have less water pressure than the lower ones, the nozzle distribution varies depending on height. The nozzle distribution is better explained in Figure A.30.

A preliminary test was performed on the brick façade to further calibrate the system. The purpose of the second calibration is to ensure an even distribution of moisture on the wall surface when the above described design is implemented. The spray rack was positioned so that the nozzles were at a distance of 1.5 m from the brick surface.

Due to pressure differences and gravity, the bottom two nozzles were set to 25% of their flow capacity while the second to bottom row are set to 50%. The top two nozzles are set to 100% flow capacity and the second to top row at 75%. Adjusting the flow rates allow for a more uniform curtain wall of water to run down the brick façade resulting in even moisture uptake by the wall.

Testing of the spray rack began by wetting the large-scale brick wall. Attention was made on the wetting pattern made on the brick wall. Using an initial nozzle layout, where each nozzle was equidistant from one another, it was observed that some dry spots were present on the upper portion of the wall surface, as demonstrated in Figure A.32.

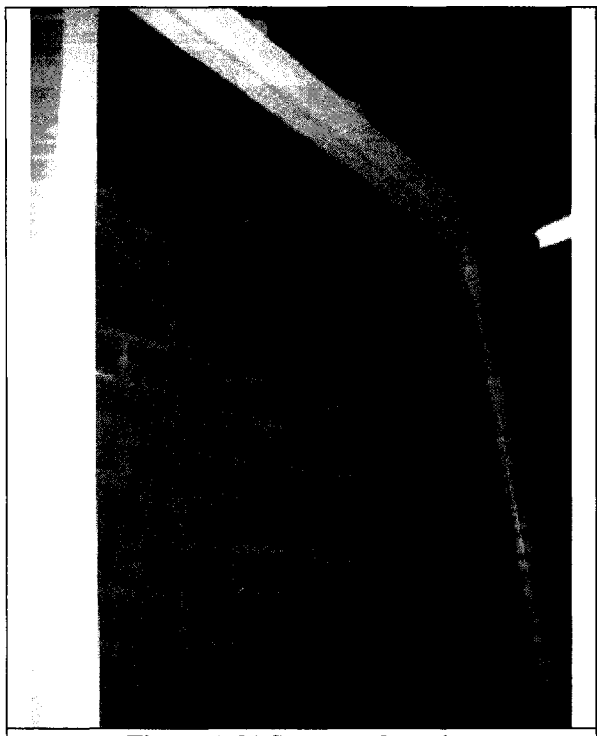

Figure A.31 Spray rack testing

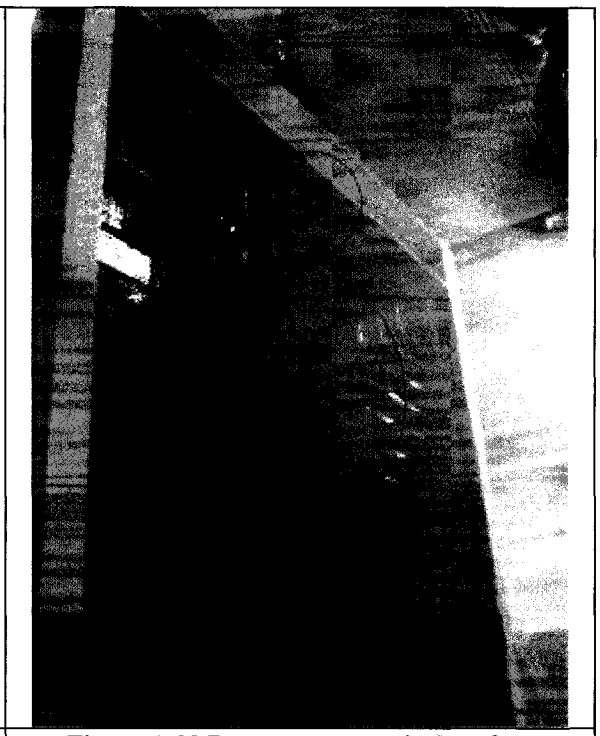

Figure A.32 Dry spots on vertical surface

Since the nozzles are supplied by the same water source, the upper nozzles receive less pressure than the lower nozzles. Obtaining an even film of water across the brick surface required a redistribution of the nozzles along the spray rack. By concentrating the nozzles towards the top of the grid, a more uniform spraying pattern is achieved. In addition, each pair of nozzles had their water supply flow modified where the bottom nozzles saw the least amount of flow and the top nozzles supplied maximum flow. As a result, an even film of water was passed over the entire brick surface.

A.5 Solar Radiation Simulation System

A radiation system was developed to uniformly heat a 1.2 m x 2.4 m vertical wall surface to 50°C. Implementing the Hottel model in MathCAD resulted in eight hours of radiation exposure for a south facing wall situated in Charleston, South Carolina. Ecotect was used to simulate the light distribution acting on a wall with different lamp arrays. Based on the Ecotect outputs, preliminary radiation tests acting on a one meter square brick wall were carried out using 12 lamps in different arrays. The lamp properties are as follows:

Table A.5 Light Bulb Properties

Watts	175
Base	E26 Medium Skirted
Avg. Rated Life (hrs)	5000
Volts	120

Lamp Type	(A) Maximum Overall Length (in.)	(B) Diameter (in.)
PAR38 Heat	5 5/16	4 3/4

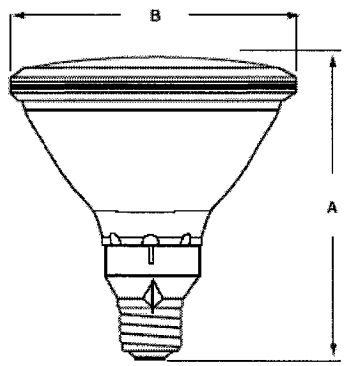

Figure A.33 Light Bulb Dimensions

The lamps were at full capacity during all preliminary testing at a distance of 1.2 meters from the brick surface. This distance was selected due to laboratory constraints while a sufficient distance was required to prevent hot spots from occurring on the brick surface. It was understood that a concentration of lamps towards the perimeter of the array is optimal for creating a uniform heat distribution on said vertical surface.

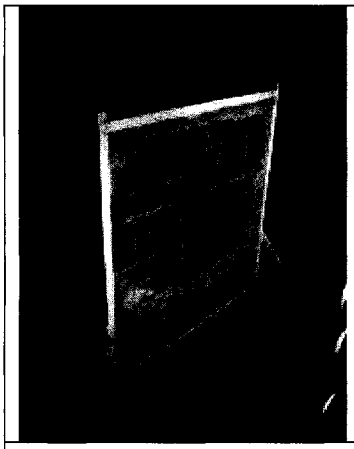

Figure A.34 Brick wall

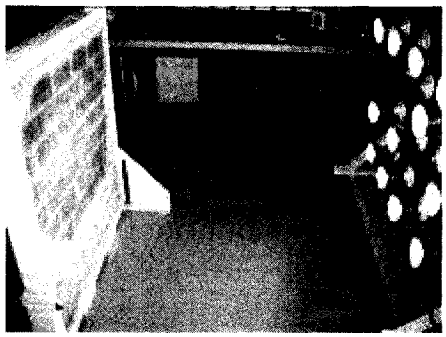

Figure A.35 1.2 m distance between lamps and brick surface

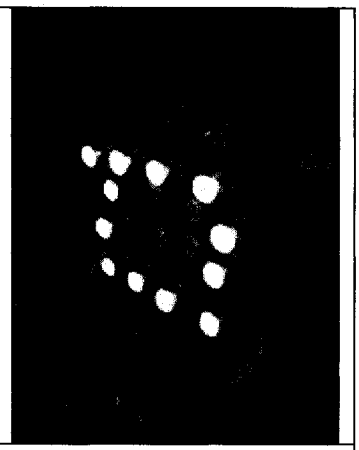

Figure A.36 One of many lamp arrangements used during preliminary testing

The results of the above configuration return a maximum temperature of 58.1°C after 3 hours and 58.3°C after 4 hours as seen in Figure A.37 and Figure A.38 respectively. This shows that the temperature does not vary much after prolonged periods of exposure. However, a reflective box will be needed to limit the heat acting on the wall from escaping to the environment as an alternative to over designing the system. The reflective box is also believed to induce a uniform heat distribution.

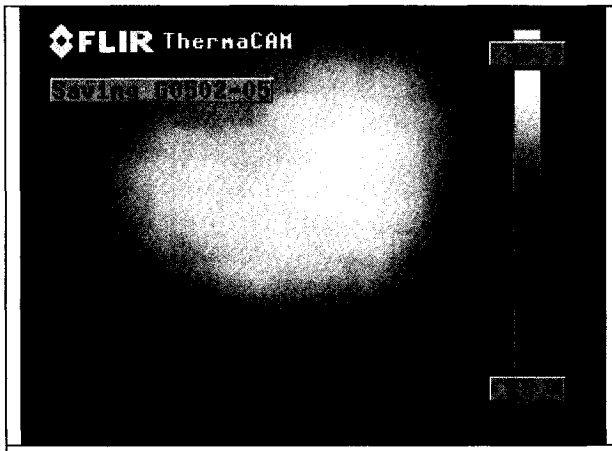

Figure A.37 Brick surface temperature after 3 hours

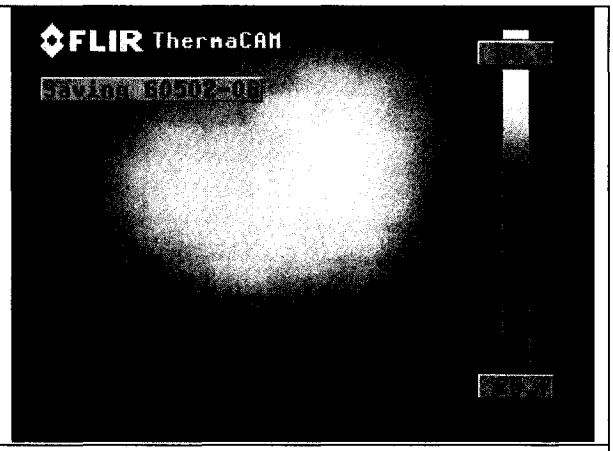

Figure A.38 Brick surface temperature after 4 hours

Full Scale Testing

It was then decided that a total of 40 x 175-Watt heat lamps would be sufficient in heating a 1.2 m by 2.4 m brick wall evenly to a minimum of 50°C placed within a 48" x 50" x 8' high reflective box. Once the full scale brick wall was erected, along with the completion of the reflective box, testing continued. Based on the information gathered through modeling and small scale testing, a preliminary array was implemented.

Initially, the 40 lamps were evenly placed within the reflective box and the heat absorbed by the brick wall was measured. The lamps were arranged in 10 rows with four lamps per row. It was observed, that although the aluminum which reflects the heat and optimizes the heat distribution on the wall, heat concentrated at the centre of the specimen. Further modifications to the lamp array lead to an increase in spacing between the two middle lamps in each row, placing them closer to their respective reflective box edges. This modification placed the lamps an ovular shape.

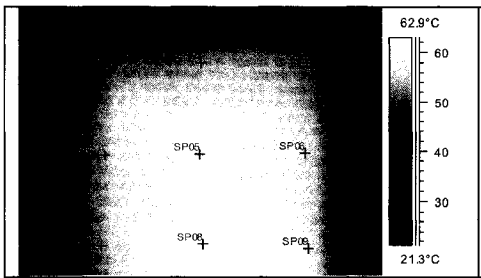

Figure A.39 Top brick surface temperature after 5.5 hours

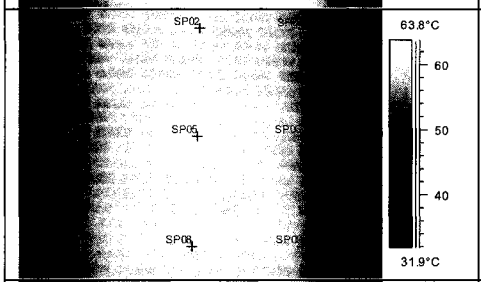

Figure A.40 Mid brick surface temperature after 5.5 hours

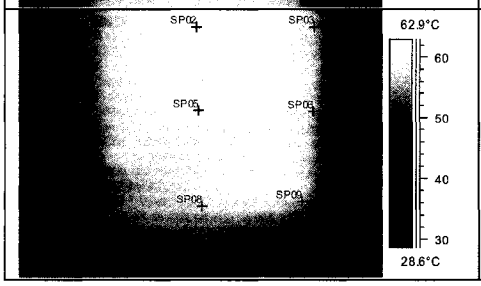

Figure A.41 Bottom brick surface temperature after 5.5 hours

The temperature across the brick surface observed in Figure A.39 thru Figure A.41 varies by 10°C from the centre and the edges, ranging between 50° to 60°C. To counter the unevenness of heat across the wall, the lamps were divided into six different circuits, where each circuit could be controlled with a rotary dimmer. The circuits were designed in such a way that the lamps could be strategically dimmed where the intensity at the center of the array can be decreased while increasing the intensity along the perimeter.

Seven circuits power the lamps and each series of lamps is controlled with a 1500W capacity, commercial rotary dimmer. Each circuit is strategically designed in specific zones to allow the lamps to be controlled in a manner that can optimize the uniformity of heat acting on the test specimens. For instance, it was observed that to create a uniform heat distribution on a given specimen, the inner lamp circuits (zones #2 and #6) need to be at 75% of the full capacity, top and bottom circuits (zones #1 and #5) must be at 85% capacity, while the side circuits (zones #3 and #4) must be at full capacity. The circuit zone layouts are depicted in Figure A.44.

The following figures represent the results of the heat lamps acting on the brick surface with controlled intensities after 5 hours. The temperatures across the wall range from about 47° to 51°C, a difference of roughly 4°C. Table A.6 lists all the spot temperatures across the brick wall surface. This uniformity is seen to be substantial for the purposes of the testing with an average surface temperature of 49.9°C.

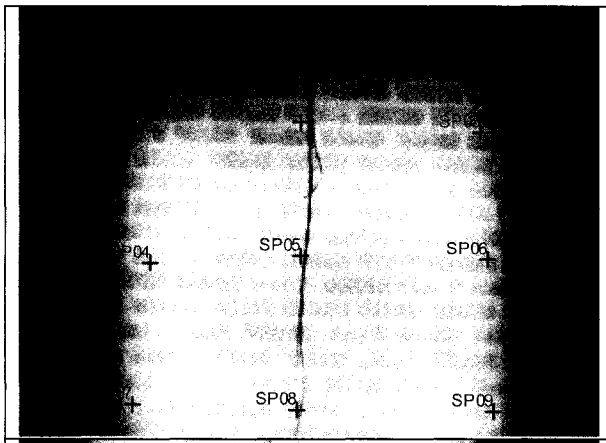

Figure A.42 Top brick surface temperature after 5 hours

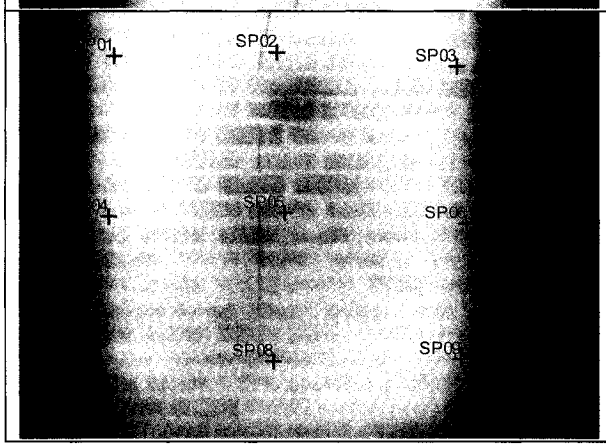

Figure A.43 Bottom brick surface temperature after 5 hours

Table A.6 Surface spot temperature of brick

48.9°C	49.9°C	49.9°C
51.1°C	50.5°C	50.0°C
49.9°C	51.0°C	50.2°C
51.3°C	51.2°C	50.3°C
50.2°C	49.3°C	49.0°C
47.1°C	49.8°C	48.5°C

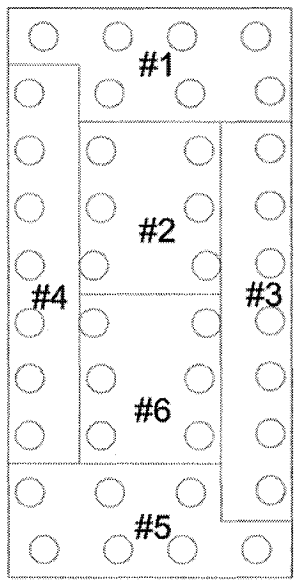

Figure A.44 Circuit zone layout

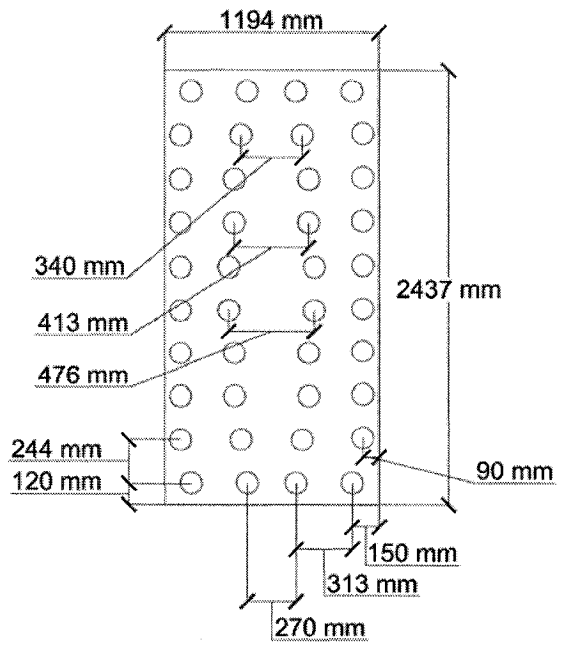

Figure A.45 Lamp spacing

A.6 Test Wall System Construction

The back wall and respective counter weight were secured to a lever arm. Steel strips are bolted the back wall and connected to the lever arm with a chain. Water was used to fill a 20L jug until the wall was suspended in equilibrium. The perimeter of the back wall was then insulated with expanded polystyrene to prevent the loss of heat through the frame to the environment.

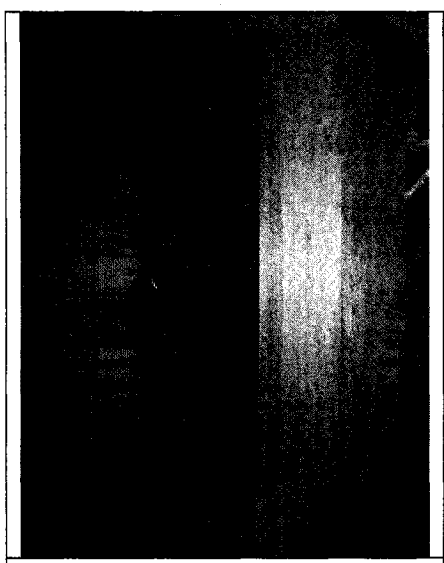

Figure A.46 Test hut opening

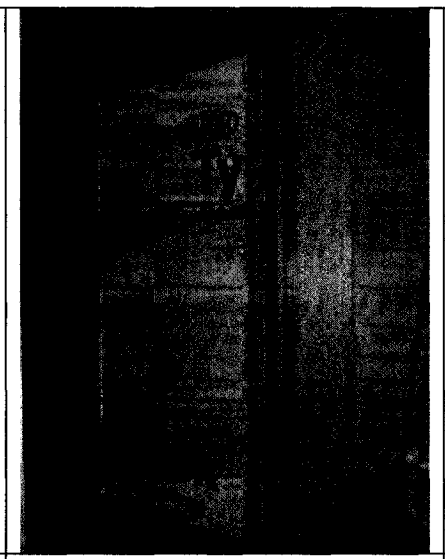

Figure A.47 Back wall placed before hut opening

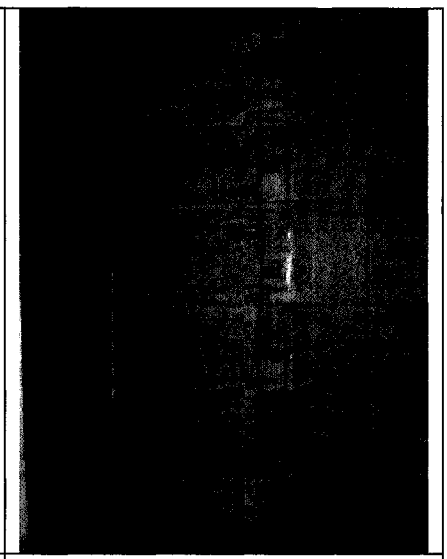

Figure A.48 Sides of back wall insulated

The perimeter of the insulated back wall was sealed to the test hut using a light polyethylene sheet. The polyethylene sheet was secured using a double sided tape. Attention was made to prevent any tension in the polyethylene sheet as it may cause experimental errors in the weighing of the individual wall components.

The same procedure was followed for the brick wall and its respective counter weight. The 200 gallon tank was filled with water until the brick wall was lifted off the ground. Once the brick component was suspended in equilibrium, it was placed in front of the insulating back wall. A 20 mm air cavity was formed between the two wall components. The polyethylene sheet was used to seal the perimeters of the two components, seen in Figure A.49. Once again, attention is made to assure no tension was created in the polyethylene sheet.

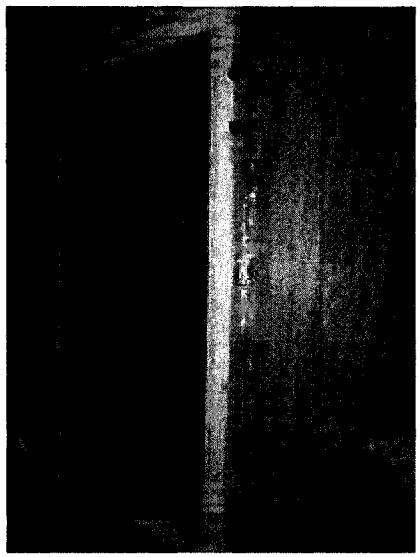

Figure A.49 Brick component placed before back wall component

All sensor wiring used to monitor the conditions of the test assembly were passed from the top of the walls and braced on the roof of the hut to prevent any disturbance to the system.

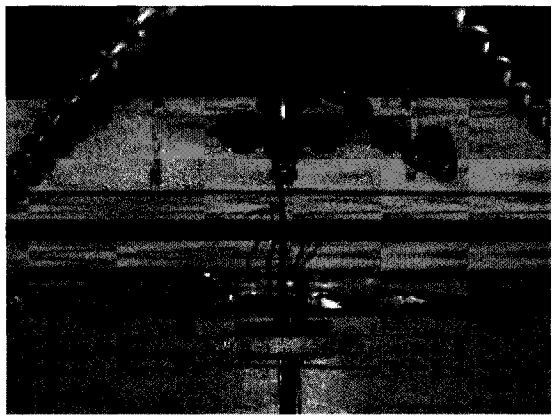

Figure A.50 Securing of sensor wiring

The counter weights were connected to the respective load cells, which were subjected to slight tensions. Subjecting the load cells to tension, prevent measurement error since the devices have greatest error in the 10% loading range.

Appendix B: Small-Scale Experimental Results

This section presents the experimental results of eight wall specimens. The measuring of the experiment includes temperature, relative humidity and moisture content throughout the samples as well as moisture accumulation in the gravimetric samples and individual materials as described in the experimental protocol.

The following table indicates which wall assemblies the different trends being represented are associated with. The label B. Paper represents building paper, SBPO represents spun bonded polyolefin, Vinyl represents vinyl wall covering, Acrylic represents acrylic paint and Stud denotes the inclusion of a wooden stud in the construction.

Table B.1 Assembly legend and construction variables

		Sheathing Paper			Interior Finishing		
Symbol	Wall #	Bldg P.	SBPO	Stud	Vinyl W.P.	Acrylic Paint	Comments
———	1	x			x		Non-hygroscopic, with inner vapor barrier, high outside permeance
———	2		x		x		Non-hygroscopic, with inner vapor barrier, low outside permeance
———	3	x				x	Non-hygroscopic, without inner vapor barrier, high outside permeance
———	4		x			x	Non-hygroscopic, without inner vapor barrier, low outside permeance
•••••	5	x		x	x		Hygroscopic, with inner vapor barrier, high outside permeance
•••••	6		x	x	x		Hygroscopic, with inner vapor barrier, low outside permeance
•••••	7	x		x		x	Hygroscopic, without inner vapor barrier, high outside permeance
•••••	8		x	x		x	Hygroscopic, without inner vapor barrier, low outside permeance

B.1 Experimental Conditions

The temperature, relative humidity and moisture content are collected throughout the experiment and examined to assure that the test was performed under the correct conditions. The following figures present the environmental conditions all of the tests which illustrate the variations between the tests.

The exterior and interior temperature and relative humidity profiles are shown below.

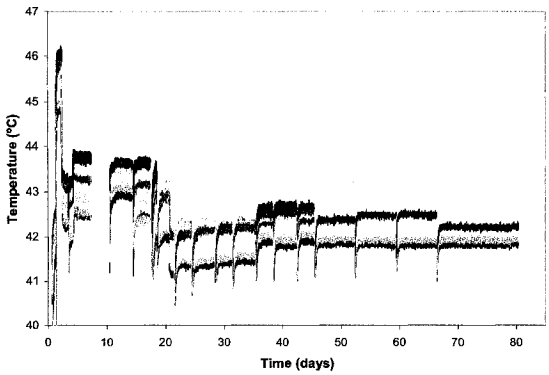

Figure B.1 Exterior temperature 3 cm from brick

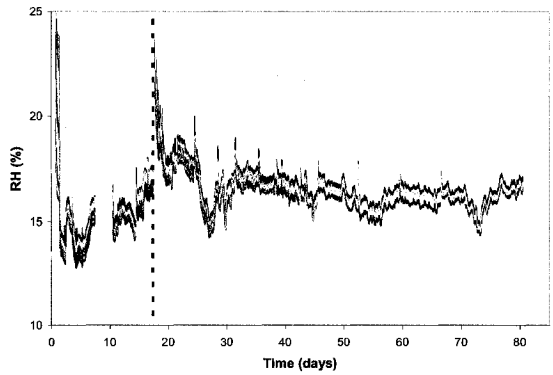

Figure B.2 Exterior relative humidity 3 cm from brick

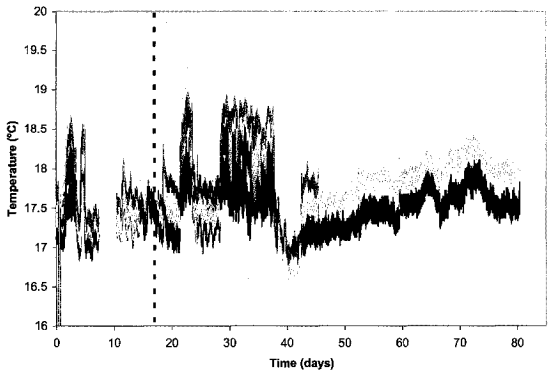

Figure B.3 Interior temperature 3 cm from interior finishing

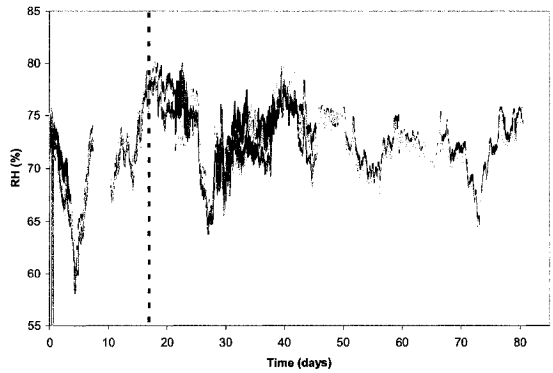

Figure B.4 Interior relative humidity 3 cm from interior finishing

Figure B.1 and Figure B.2 show exterior temperature and relative humidity recorded throughout the experiment.

The interior temperature and relative humidity are depicted in Figure B.3 and Figure B.4 respectively.

Some of the readings taken at the beginning of the experiment for the exterior conditions have been disregarded. This has been done since it took a few days for the system to stabilize during experimentation. This can be seen in the above graphs for the first few days of the experiment where temperatures and relative humidities can be seen to increase and decrease rapidly over a short period of time. This is not the case for the interior conditions since these are controlled by the laboratory environment. However, once the exterior conditions stabilized, the exterior of the test specimens are better controlled than the interior, leading to a greater variation in the readings for the interior values versus those recorded on the exterior.

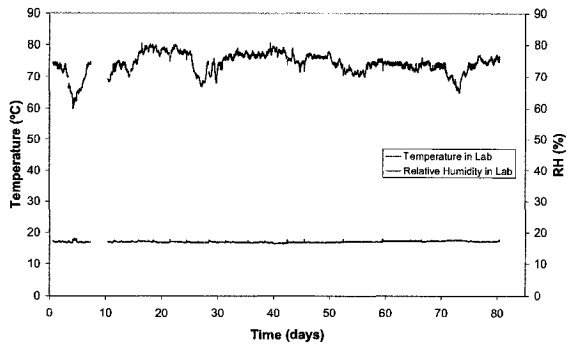

Figure B.5 Laboratory Conditions

Some technical errors occurred during data acquisitioning resulting in some temperature and relative humidity data being omitted.

B.2 Surface Temperatures of the Materials

Throughout each specimen, thermocouples are placed to record the temperatures of the material surfaces. The following figures show the conditions of each specimen from outside to inside.

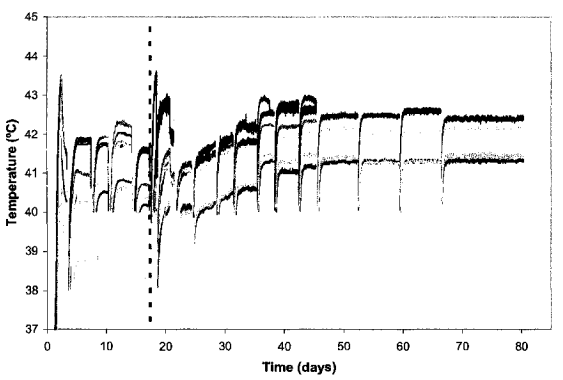

Figure B.6 Exterior surface temperature of brick

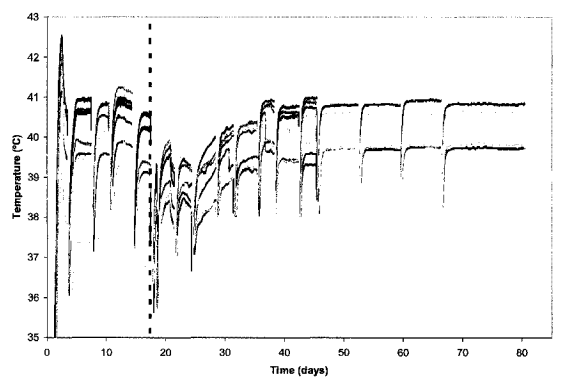

Figure B.7 Interior surface temperature of brick

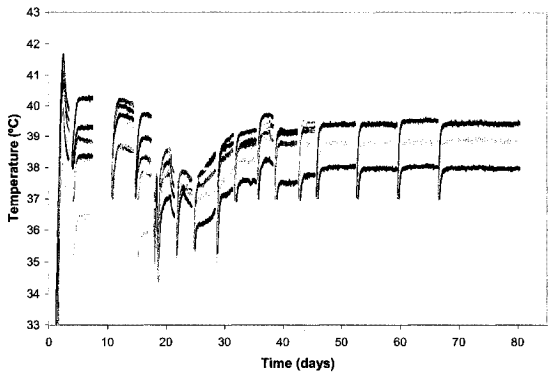

Figure B.8 Air cavity temperature

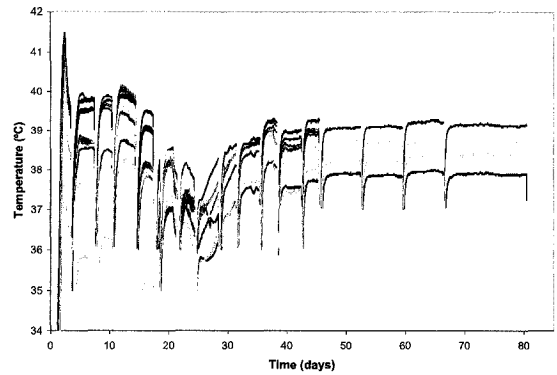

Figure B.9 Exterior temperature of sheathing

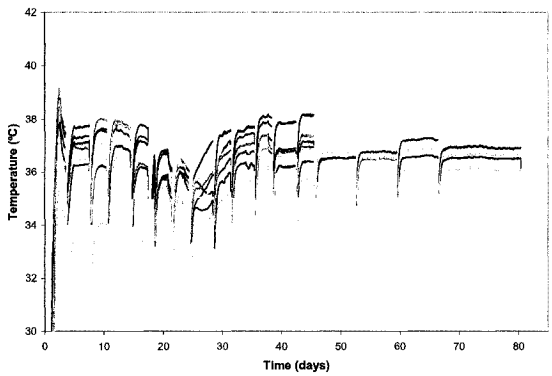

Figure B.10 Exterior temperature of insulation

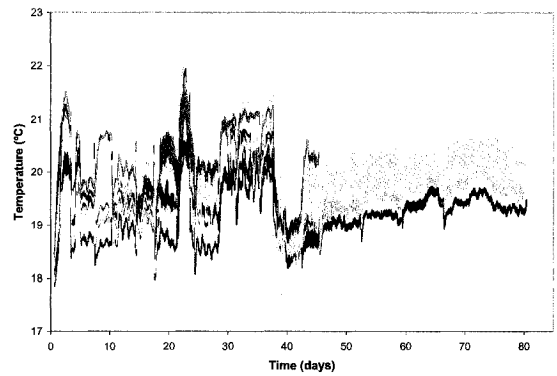

Figure B.11 Temperature between insulation and gypsum

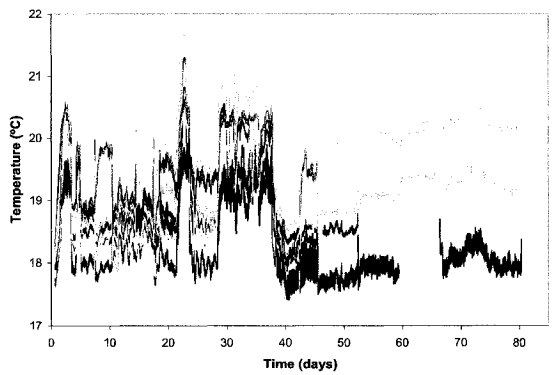

Figure B.12 Interior temperature of gypsum

B.3 Relative Humidity of the Specimens

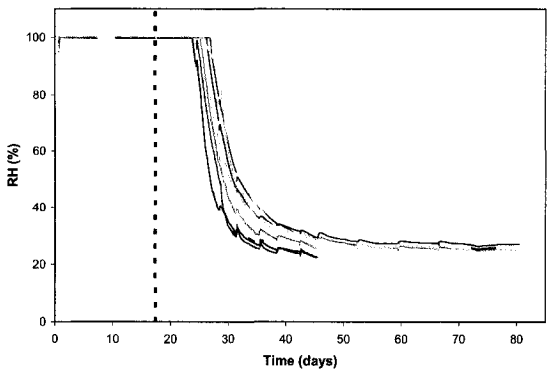

Figure B.13 Relative humidity of cavity spaces

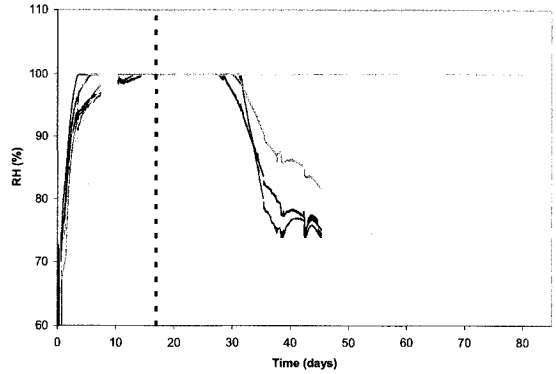

Figure B.14 Relative humidity between insulation and gypsum

B.4 Moisture Accumulation in the Gravimetric Samples

Mass of Walls by Components

The follow set of tables and figures represent the change in moisture in each wall assembly as a system as well as in the three components of the assemblies: Component 1, Bricks; Component 2, Sheathing; Component 3, Insulation & Gypsum.

Table B.2 Mass of Wall Assemblies – Wetting Period (g)

Days	0	0	3	7	10	14	17
Wall #							
B. Paper - Vinyl	38899.7	40320.7	40248.5	40120.2	40039.4	39970.5	39919.5
SBPO - Vinyl	39005.7	40438.5	40387.6	40268.8	40207.7	40156.7	40095.1
B. Paper - Acrylic	38970.6	40385.6	40320.4	40165.2	40059.2	39923.7	39827.6
SBPO - Acrylic	38883.8	40304.4	40253.7	40106.2	40013.6	39892.2	39795.2
B. Paper - Vinyl - Stud	39543.4	40903.2	40816.4	40722.7	40650.8	40593.1	40536.6
SBPO - Vinyl - Stud	39784.1	41216.0	41142.6	41027.8	40971.8	40914.1	40885.7
B. Paper - Acrylic - Stud	39743.3	41160.3	41078.9	40953.1	40844.5	40727.6	40637.0
SBPO - Acrylic - Stud	39930.6	41328.8	41273.8	41132.8	41037.2	40900.1	40811.6

Table B.3 Mass of Wall Assemblies - Drying Period (g)

21	24	28	31	35	38	42	45	52	59	66	80
36861.1	36780.4	36780.4	36774.1	36750.4	36735.6	36725.8	36717.8	36701.8	36684.5	36668.0	36630.9
36948.9	36853.1	36826.5	36818.3	36799.6	36787.4	36775.8	36768.7	36753.1	36738.4	36726.0	36698.8
36673.0	36530.1	36427.4	36359.4	36325.4	36316.8	36313.0	36310.2				
36578.7	36423.4	36314.2	36271.7	36249.7	36242.1	36237.4	36234.6				
37398.0	37327.4	37333.0	37322.0	37291.7	37274.6	37265.9	37257.1	37237.6	37216.6	37195.4	37149.6
37728.2	37626.0	37611.5	37600.6	37576.6	37562.3	37552.1	37542.1	37520.8	37500.3	37481.7	37440.8
37485.8	37332.5	37254.0	37209.2	37160.8	37142.5	37128.6	37121.1				
37637.6	37495.1	37407.9	37362.9	37326.5	37312.7	37301.8	37294.0				

Table B.4 Mass of Part 1 – Wetting Period (g)

Days	0	0	3	7	10	14	17
Wall #							
B. Paper - Vinyl	27214.6	28705.8	28615.9	28449.5	28332.7	28190.6	28082.4
SBPO - Vinyl	27316.1	28819.1	28748.3	28588.6	28488.8	28369.0	28252.5
B. Paper - Acrylic	27341.2	28826.4	28739.6	28569.8	28451.0	28295.1	28194.1
SBPO - Acrylic	27229.8	28720.6	28655.5	28492.5	28389.3	28251.4	28157.9
B. Paper - Vinyl - Stud	27081.5	28511.5	28419.6	28286.8	28185.8	28064.8	27965.6
SBPO - Vinyl - Stud	27338.1	28840.2	28746.4	28614.8	28509.6	28380.5	28302.5
B. Paper - Acrylic - Stud	27325.8	28813.0	28713.8	28566.5	28446.0	28306.0	28206.8
SBPO - Acrylic - Stud	27483.2	28951.6	28879.8	28714.5	28607.8	28450.8	28355.8

Table B.5 Mass of Part 1 – Drying Period (g)

21	24	28	31	35	38	42	45	52	59	66	80
27541.3	27383.8	27301.8	27278.7	27258.3	27248.7	27242.6	27239.8	27235.5	27233.8	27233.3	27231.8
27645.4	27496.8	27413	27389.8	27367.8	27356.8	27347.5	27343.4	27336.5	27333.3	27332.7	27330.7
27634.6	27485.5	27415.9	27389	27370.3	27363.5	27359.6	27357.3				
27512.8	27354.4	27290.3	27273.4	27261.1	27255.4	27251.1	27248.6				
27370.4	27221.1	27156.8	27135.7	27115.7	27107.5	27102.4	27100.3	27096.9	27095.7	27095.1	27094
27671.3	27507.2	27425.5	27401.8	27380.1	27369.8	27361.4	27357.4	27351.2	27348.4	27347	27344.5
27646.7	27486	27414.1	27391.3	27365.8	27354.3	27345.2	27341.6				
27787.8	27640.9	27566.2	27541	27519.9	27510.3	27502.3	27497.9				

Table B.6 Mass of Part 2 - Wetting Period (g)

Days	0	3	7	10	14	17
Wall #						
B. Paper - Vinyl	1162.6	1220.6	1282.5	1310.1	1336	1337.9
SBPO - Vinyl	1125.8	1177.5	1231.6	1255.7	1276.5	1282.5
B. Paper - Acrylic	1168.2	1223.8	1287.9	1317.6	1343.7	1343.3
SBPO - Acrylic	1094.1	1136.1	1197.0	1217	1235.3	1230.5
B. Paper - Vinyl - Stud	1162.5	1218.0	1277.0	1311.7	1338.4	1353.2
SBPO - Vinyl - Stud	1100.2	1153.6	1215.8	1241.1	1265.6	1273.2
B. Paper - Acrylic - Stud	1190.4	1249.5	1327.4	1372.7	1400.8	1412.6
SBPO - Acrylic - Stud	1143.3	1191.0	1257.9	1284.9	1311	1328.9

Table B.7 Mass of Part 2 - Drying Period (g)

21	24	28	31	35	38	42	45	52	59	66	80
1318.4	1284.4	1193.7	1161.6	1147.2	1142.8	1140.9	1139.1	1136.6	1135.2	1135.1	1134.0
1249.3	1225.5	1159.7	1130.4	1116.1	1110.7	1106.2	1104.8	1102.0	1100.8	1100.3	1099.7
1313.0	1257.9	1171.2	1146.8	1136.2	1132.9	1132.0	1130.0				
1187.4	1146.6	1090.1	1078.7	1071.9	1069.2	1067.8	1066.2				
1340.3	1292.3	1192.4	1158.3	1141.1	1136.7	1134.5	1132.2	1130.1	1128.9	1128.4	1127.3
1241.8	1218.1	1137.4	1107.9	1093.8	1088.9	1085.8	1084.2	1081.5	1080.4	1079.8	1078.9
1404.2	1364.9	1249.6	1195.1	1169.2	1161.3	1155.8	1152.6				
1289.8	1253.7	1166.6	1137.0	1122.9	1118.3	1115.7	1113.2				

Table B.8 Mass of Part 3 - Wetting Phase (g)

Days	0	3	7	10	14	17
Wall #						
B. Paper - Vinyl	7839.3	7857.0	7895.1	7931.1	8004.3	8061.5
SBPO - Vinyl	7844.7	7864.6	7905.5	7944.2	8013.0	8067.9
B. Paper - Acrylic	7773.7	7795.3	7809.9	7822.7	7843.1	7848.0
SBPO - Acrylic	7815.0	7829.4	7844.9	7855.5	7872.0	7868.5
B. Paper - Vinyl - Stud	8599.9	8605.0	8644.1	8673.2	8736.5	8779.2
SBPO - Vinyl - Stud	8609.2	8629.6	8646.4	8695.6	8767.0	8816.6
B. Paper - Acrylic - Stud	8573.5	8591.3	8612.8	8624.7	8647.8	8656.4
SBPO - Acrylic - Stud	8591.4	8608.2	8632.5	8643.6	8663.5	8670.0

Table B.9 Mass of Part 3 - Drying Phase (g)

21	24	28	31	35	38	42	45	52	59	66	80
8157.2	8234.0	8316.0	8332.8	8329.5	8324.3	8320.6	8315.4	8303.7	8288.1	8272.1	8236.5
8140.9	8193.7	8250.9	8265.9	8269.2	8268.0	8265.7	8262.7	8254.0	8242.5	8230.7	8205.5
7875.8	7882.0	7848.9	7807.8	7792.5	7790.7	7790.8	7790.3				
7903.3	7906.4	7861.3	7835.7	7826.0	7824.1	7823.7	7823.4				
8865.0	8943.7	9013.6	9023.7	9013.4	9004.5	9000.9	8994.2	8978.1	8958.3	8937.7	8893.0
8894.3	8956.2	9023.4	9036.2	9033.9	9029.9	9028.1	9022.1	9007.0	8989.3	8972.1	8933.7
8676.5	8683.9	8677.3	8655.3	8632.4	8625.6	8620.8	8616.9				
8687.2	8691.6	8679.1	8659.3	8644.0	8639.8	8636.9	8633.5				

Table B.10 Moisture Removed from Sheathing Paper Surface (g)

Days	0	3	7	10	14	17	21	24	Total
Wall #									
B. Paper - Vinyl	0.0	12.2	16.4	17.3	12.1	13.2	11.9	1.7	84.8
SBPO - Vinyl	0.0	8.4	11.4	13.7	12.6	13.6	11.1	2	72.8
B. Paper - Acrylic	0.0	9.0	17.2	15	15.5	12.1	6	2.7	77.5
SBPO - Acrylic	0.0	8.4	10.0	10.7	10.8	11.7	5.6	0.5	57.7
B. Paper - Vinyl - Stud	0.0	9.0	14.8	11.5	12.1	7.7	6.5	0.4	62.0
SBPO - Vinyl - Stud	0.0	6.8	15.6	12.6	12.7	9.5	9.2	1.6	68.0
B. Paper - Acrylic - Stud	0.0	9.8	17.8	15.3	16.3	14.6	12.3	2.3	88.4
SBPO - Acrylic - Stud	0.0	9.8	10.6	12.8	10.6	8.7	5.3	1.2	59.0

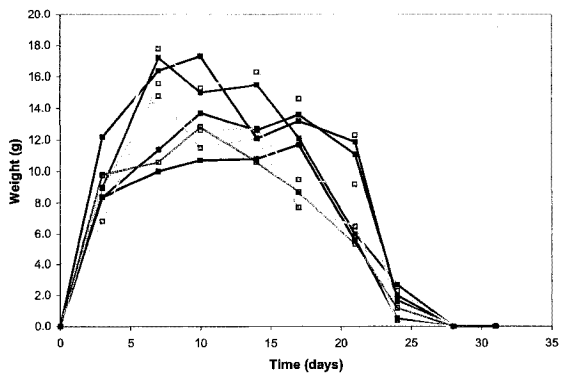

Figure B.15 Moisture Removed from Sheathing Paper Surface

Mass and Moisture Content of Individual Wall Materials

The following tables list the masses and calculated moisture contents of the individual assembly materials throughout the experiment.

Table B.11 Mass of Weather Resistive Barrier (g)

Wall #	Start	Day 17	Finish	Dry
B. Paper - Vinyl	51.50	58.5	46.8	45.7
SBPO - Vinyl	9.85	12.1	9.9	9.8
B. Paper - Acrylic	51.80	56.9	46.6	46.3
SBPO - Acrylic	10.00	14.1	10.1	10.1
B. Paper - Vinyl - Stud	50.30	58.3	46.3	45.8
SBPO - Vinyl - Stud	10.00	13.4	10.1	9.9
B. Paper - Acrylic - Stud	52.70	59.4	46.8	46.5
SBPO - Acrylic - Stud	9.95	14.3	10	9.9

Table B.12 Calculated moisture content of WRB (%)

Wall #	Start	Day 17	Finish	Dry
B. Paper - Vinyl	12.7%	28.0%	2.4%	0.0%
SBPO - Vinyl	0.5%	23.5%	1.0%	0.0%
B. Paper - Acrylic	11.9%	22.9%	0.6%	0.0%
SBPO - Acrylic	0.0%	39.6%	0.0%	0.0%
B. Paper - Vinyl - Stud	9.8%	27.3%	1.1%	0.0%
SBPO - Vinyl - Stud	1.0%	35.4%	2.0%	0.0%
B. Paper - Acrylic - Stud	13.3%	27.7%	0.6%	0.0%
SBPO - Acrylic - Stud	0.5%	44.4%	1.0%	0.0%

Table B.13 Mass of OSB (g)

Wall #	Start	Day 17	Finish	Dry
B. Paper - Vinyl	919.3	1081.8	898.3	880
SBPO - Vinyl	922.6	1049.3	900.9	887.9
B. Paper - Acrylic	920.80	1088.6	894.6	882.2
SBPO - Acrylic	892.70	996.3	867.8	855.5
B. Paper - Vinyl - Stud	949.90	1133.1	927.9	912.5
SBPO - Vinyl - Stud	941.70	1073.1	916.8	904
B. Paper - Acrylic - Stud	979.00	1183.5	945.2	928.1
SBPO - Acrylic - Stud	977.00	1127.8	951.1	934.1

Table B.14 Calculated moisture content of OSB (%)

Wall #	Start	Day 17	Finish	Dry
B. Paper - Vinyl	4.5%	22.9%	2.1%	0.0%
SBPO - Vinyl	3.9%	18.2%	1.5%	0.0%
B. Paper - Acrylic	4.4%	23.4%	1.4%	0.0%
SBPO - Acrylic	4.3%	16.5%	1.4%	0.0%
B. Paper - Vinyl - Stud	4.1%	24.2%	1.7%	0.0%
SBPO - Vinyl - Stud	4.2%	18.7%	1.4%	0.0%
B. Paper - Acrylic - Stud	5.5%	27.5%	1.8%	0.0%
SBPO - Acrylic - Stud	4.6%	20.7%	1.8%	0.0%

Table B.15 Mass of Insulation (g)

Wall #	Start	Day 17	Finish	Dry
B. Paper - Vinyl	196.7	198.3	197.4	194.9
SBPO - Vinyl	196.3	197.8	197	194.8
B. Paper - Acrylic	197.1	198.5	197.5	196.5
SBPO - Acrylic	203.3	205	204	202.7
B. Paper - Vinyl - Stud	189.40	190.6	188.4	187.2
SBPO - Vinyl - Stud	186.10	189.6	192	185.5
B. Paper - Acrylic - Stud	199.60	201	203.0	201.6
SBPO - Acrylic - Stud	192.10	193.1	196.2	195.2

Table B.16 Calculated moisture content of insulation (%)

Wall #	Start	Day 17	Finish	Dry
B. Paper - Vinyl	0.92%	1.74%	1.28%	0.00%
SBPO - Vinyl	0.77%	1.54%	1.13%	0.00%
B. Paper - Acrylic	0.31%	1.02%	0.51%	0.00%
SBPO - Acrylic	0.30%	1.13%	0.64%	0.00%
B. Paper - Vinyl - Stud	1.18%	1.82%	0.64%	0.00%
SBPO - Vinyl - Stud	0.32%	2.21%	3.50%	0.00%
B. Paper - Acrylic - Stud	0.00%	1.34%	0.69%	0.00%
SBPO - Acrylic - Stud	0.00%	1.08%	0.51%	0.00%

Table B.17 Mass of Wooden Studs (g)

Wall #	Start	Day 17	Finish	Dry
B. Paper - Vinyl - Stud	754.8	786.7	802.6	756.9
SBPO - Vinyl - Stud	756.9	787.5	797.4	753.7
B. Paper - Acrylic - Stud	751.3	780.5	783.4	749
SBPO - Acrylic - Stud	759.4	787.8	790.1	757.4

Table B.18 Calculated moisture content of studs (%)

Wall #	Start	Day 17	Finish	Dry
B. Paper - Vinyl - Stud	0.00%	3.94%	6.04%	0.00%
SBPO - Vinyl - Stud	0.42%	4.48%	5.80%	0.00%
B. Paper - Acrylic - Stud	0.31%	4.21%	4.59%	0.00%
SBPO - Acrylic - Stud	0.26%	4.01%	4.32%	0.00%

Table B.19 Mass of Gypsum (g)

Wall #	Start	Day 17	Finish	Dry
B. Paper - Vinyl	1487.5	1705.9	2000.9	1598.7
SBPO - Vinyl	1517.5	1738.8	1995.3	1626.8
B. Paper - Acrylic	1454.1	1520.4	1582.8	1572.9
SBPO - Acrylic	1470.4	1523.1	1600.4	1590
B. Paper - Vinyl - Stud	1501.6	1648	1862	1604.4
SBPO - Vinyl - Stud	1508.3	1686.5	1909.7	1621.1
B. Paper - Acrylic - Stud	1446.2	1499.1	1579.3	1566.7
SBPO - Acrylic - Stud	1475.7	1521.7	1605.4	1593.9

Table B.20 Calculated moisture content of gypsum (%)

Wall #	Start	Day 17	Finish	Dry
B. Paper - Vinyl	0.0%	14.7%	34.5%	0.0%
SBPO - Vinyl	0.0%	14.6%	31.5%	0.0%
B. Paper - Acrylic	0.0%	4.6%	8.9%	0.0%
SBPO - Acrylic	0.0%	3.6%	8.8%	0.0%
B. Paper - Vinyl - Stud	0.0%	9.7%	24.0%	0.0%
SBPO - Vinyl - Stud	0.0%	11.8%	26.6%	0.0%
B. Paper - Acrylic - Stud	0.0%	3.7%	9.2%	0.0%
SBPO - Acrylic - Stud	0.0%	3.1%	8.8%	0.0%

Moisture Accumulation Relations within Wall Assemblies

Figure 3.17 to Figure 3.18 exhibit the moisture accumulation relations between the brick, sheathing and gypsum specimens of the experimental wall assemblies.

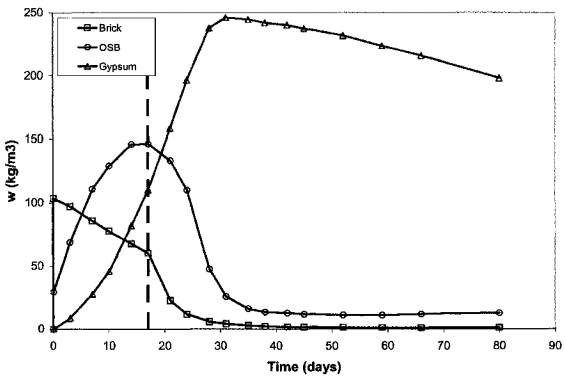

Figure B.16 Moisture in B. Paper - Vinyl components

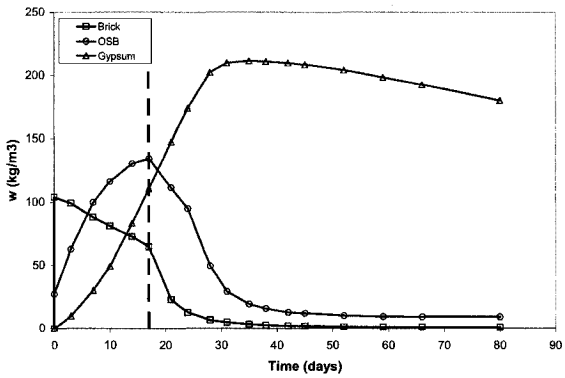

Figure B.17 Moisture in SBPO - Vinyl components

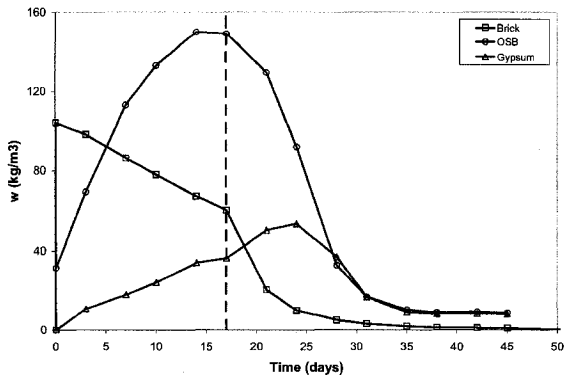

Figure B.18 Moisture in B. Paper - Acrylic components

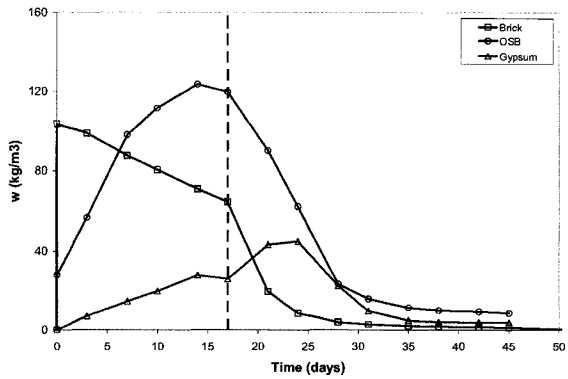

Figure B.19 Moisture in SBPO - Acrylic components

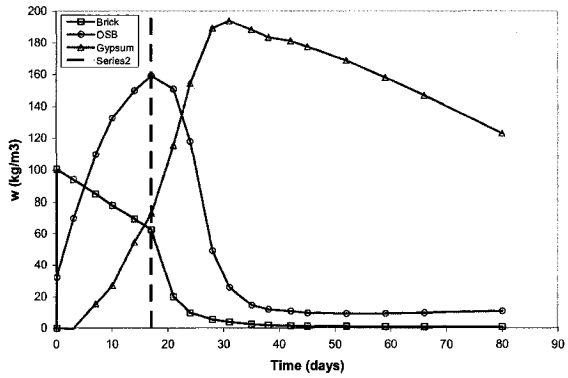

Figure B.20 Moisture in B. Paper - Vinyl - Stud components

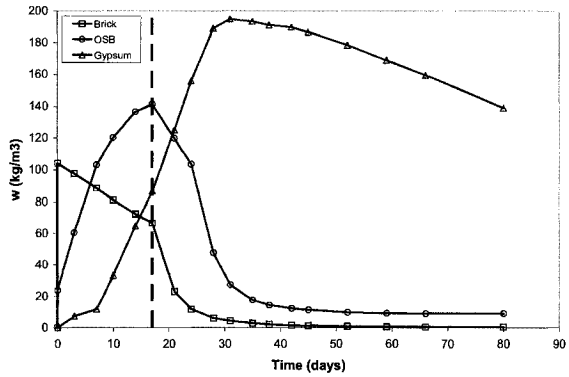

Figure B.21 Moisture in SBPO - Vinyl - Stud components

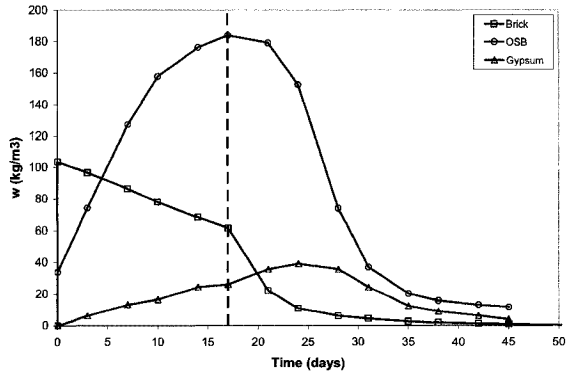

Figure B.22 Moisture in B. Paper - Acrylic - Stud components

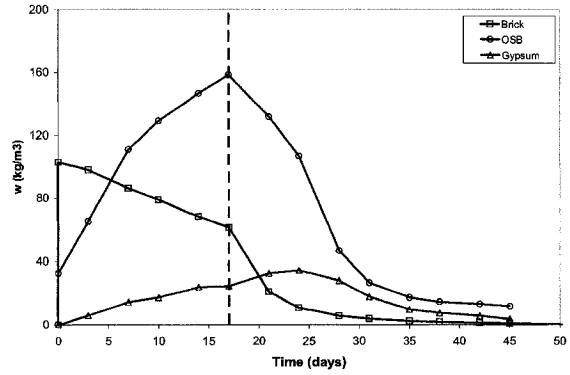

Figure B.23 Moisture in SBPO - Acrylic - Stud components

Effect of Hygric Buffering of Wooden Stud

Figure B.24 to Figure B.27 exhibit the moisture accumulation in the gypsum panels related to the hygric buffering effect of the inclusion / absence of a wood stud.

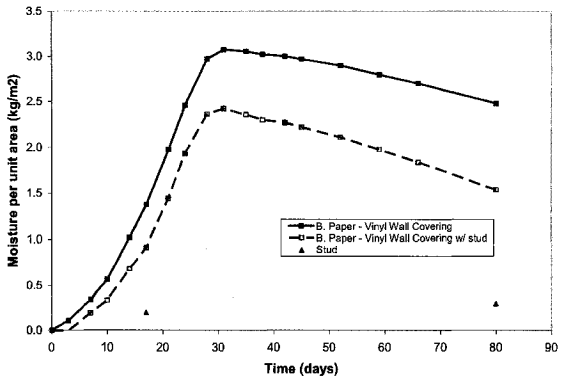

Figure B.24 Moisture in gypsum in B. Paper – Vinyl - (Stud)

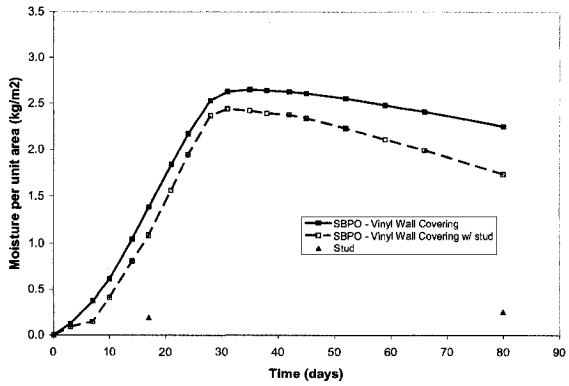

Figure B.25 Moisture in gypsum in SBPO – Vinyl - (Stud)

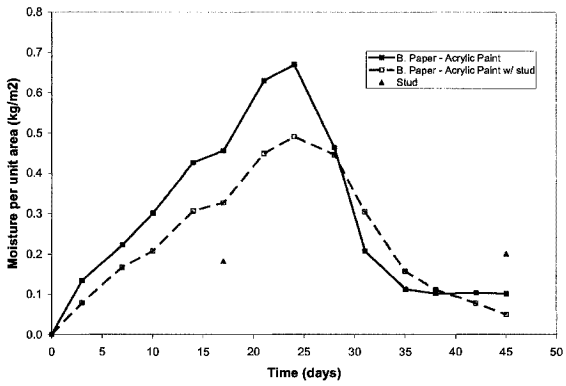

Figure B.26 Moisture in gypsum in B. Paper – Acrylic - (Stud)

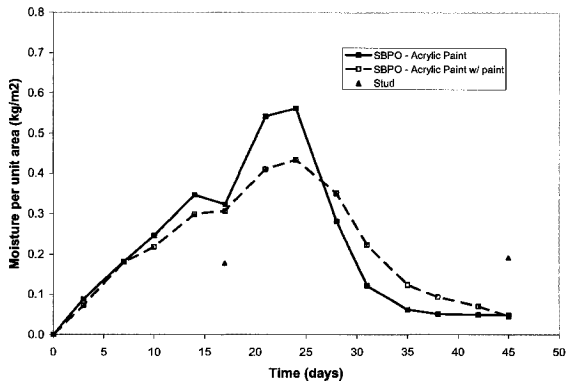

Figure B.27 Moisture in gypsum in SBPO – Acrylic - (Stud)

Appendix C: Large-Scale Experimental Results

This section presents the experimental results of the tested wall specimen. The measuring of the experiment includes temperature, relative humidity and moisture content throughout the sample as well as moisture accumulation in the gravimetric samples as described in the experimental protocol.

C.1 Experimental Conditions

The temperature, relative humidity and moisture content are collected throughout the experiment and examined to assure that the test was performed under the correct conditions. The following figures present the environmental conditions all of the tests which illustrate the variations between the tests.

The exterior and interior temperature and relative humidity profiles are shown below.

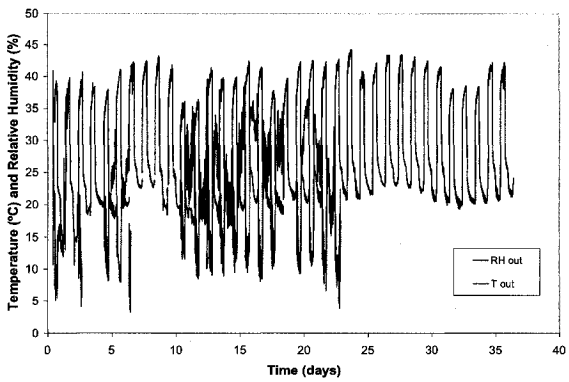

Figure C.1 Exterior conditions 3 cm from brick surface

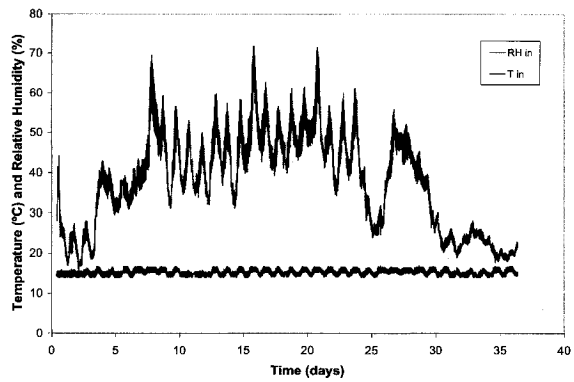

Figure C.2 Interior conditions 3 cm from gypsum surface

Figure C.1 and Figure C.2 show the exterior and interior conditions acting on the test specimen. As seen, the exterior temperatures oscillate between 20° and about 40°C due to the cyclic radiation conditions which simulate solar gains. The relative humidity is also seen to vary. During the time where no radiation is induced, the relative humidity recorded is that of the laboratory, while when radiative heat is promoted, the humidity measured is not representative since it is influenced to decrease due to the radiation. It must be noted that the exterior relative humidity probe ceased to record data midway through the experiment since it may have become damaged by the simulated radiation.

The interior temperature of the test hut is seen to be relatively constant while only fluctuating by about 2°C which is influenced by the exterior temperatures acting on the brick cladding. The relative humidity however follows not pattern and is believed to be a result of the environmental conditions taking place outside the laboratory. Studying weather history files of the outside environment, it is noted that in the cases where the humidity within the hut peaks, the exterior relative humidity recorded in Montreal is seen

to be as high as 95%RH. This influence may only be noticed in the test hut and not the laboratory since the test hut is better conditioned than the laboratory.

The laboratory conditions are presented below in Figure C.3. The temperature remains quite constant during the day, when the measurement readings were taken. However, the relative humidity decreases to about 11% over the weekends and increases to upwards of 35% during the week when the laboratory is occupied.

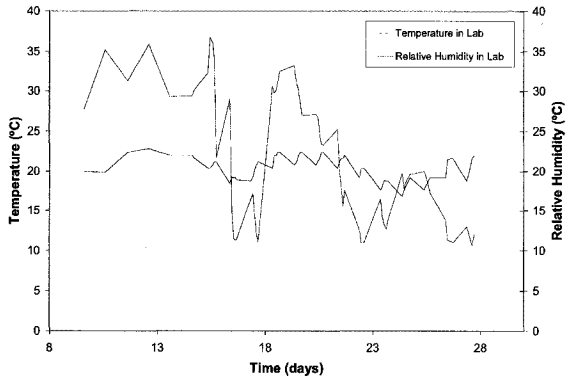

Figure C.3 Laboratory conditions

C.2 Surface Temperatures of the Materials

Throughout each specimen, thermocouples are placed to record the temperatures of the material surfaces. The following figures show the conditions of each specimen from outside to inside.

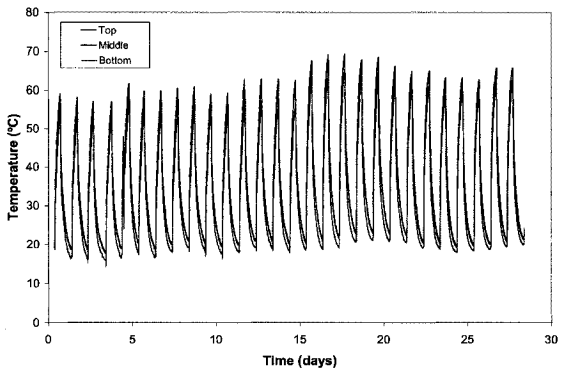

Figure C.4 Exterior surface temperature of brick

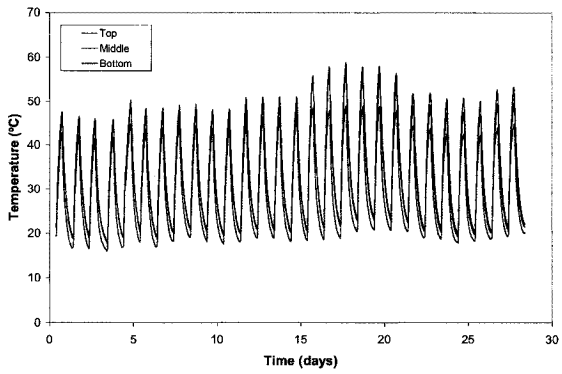

Figure C.5 Interior surface temperature of brick

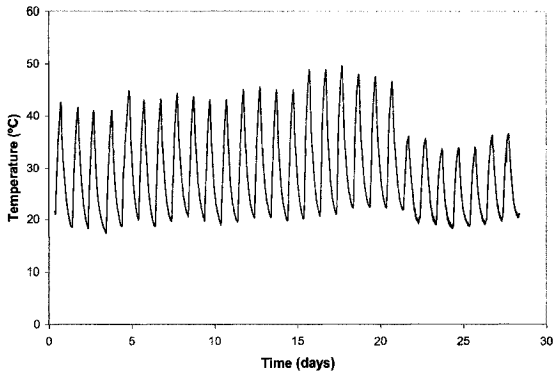

Figure C.6 Air cavity temperature

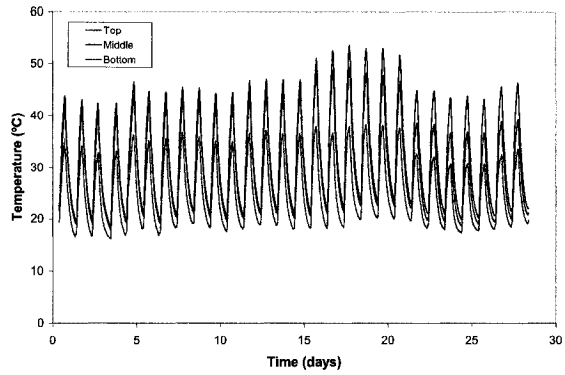

Figure C.7 Exterior surface temperature of OSB

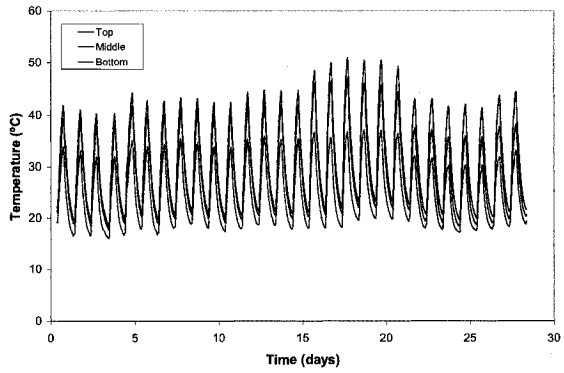

Figure C.8 Interior surface temperature of OSB

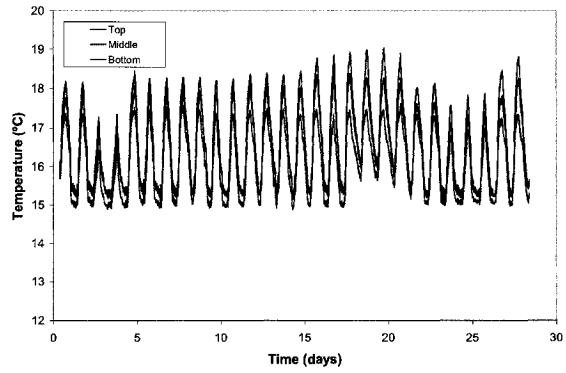

Figure C.9 Exterior surface temperature of gypsum

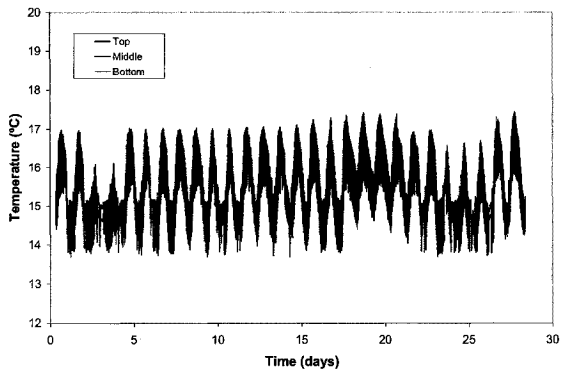

Figure C.10 Interior surface temperature of gypsum

C.3 Relative Humidity of the Specimens

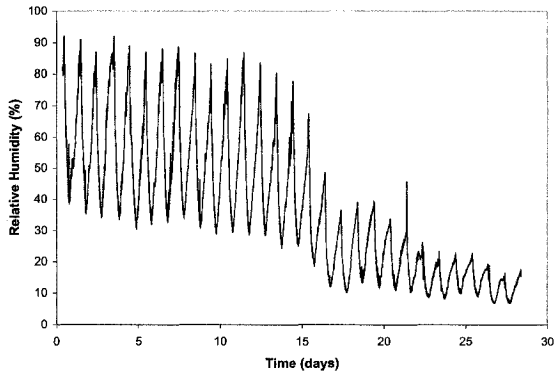

Figure C.11 Air cavity relative humidity

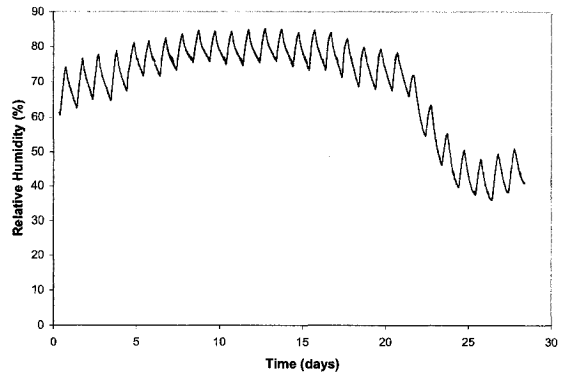

Figure C.12 Relative humidity between insulation and gypsum

C.4 Moisture Accumulation in the Gravimetric Samples

Table C.1 Mass of gravimetric samples

Day	Time	Top Gypsum (g)	Bottom Gypsum (g)	Top Stud (g)	Bottom Stud (g)
0	9:30	204.47	204.76	2.88	2.62
	11:00	204.54	204.79	2.92	2.71
	12:00	204.55	204.81	2.92	2.71
	13:30	204.66	204.86	2.91	2.68
	15:00	204.7	204.89	2.92	2.69
	17:30	204.77	204.9	2.93	2.69
1	9:15	204.75	204.88	2.93	2.69
	10:30	204.75	204.87	2.93	2.7
	11:45	204.84	204.89	2.93	2.69
	13:00	204.85	204.94	2.93	2.69
	14:45	204.86	204.98	2.93	2.69
	16:30	204.86	205.09	2.93	2.69
	18:00	205.01	205.09	2.93	2.69
2	9:15	204.88	204.89	2.94	2.69
	11:15	204.88	204.91	2.94	2.69
	12:30	204.91	205.11	2.93	2.69
	14:00	204.87	204.89	2.93	2.68
	15:15	204.91	204.92	2.93	2.69
	17:00	204.95	204.89	2.94	2.68
	18:00	204.99	204.9	2.94	2.69
3	8:00	204.97	204.89	2.94	2.69
	10:00	204.96	204.91	2.94	2.69
	12:00	205.01	204.92	2.94	2.69

	13:30	205.01	204.92	2.94	2.69
	15:00	205.05	204.94	2.95	2.69
	16:30	205.09	204.98	2.95	2.69
4	10:00	205.06	204.97	2.96	2.7
	12:00	205.06	204.96	2.96	2.7
	14:00	205.07	204.98	2.96	2.7
	15:30	205.15	205.05	2.96	2.7
	17:15	205.21	205.05	2.96	2.7
	18:30	205.24	205.04	2.96	2.7
5	9:30	205.22	205.02	2.96	2.7
	11:45	205.22	205.02	2.96	2.7
	15:30	205.32	205.08	2.96	2.7
	18:00	205.46	205.14	2.96	2.7
6	9:15	205.45	205.09	2.97	2.7
	12:00	205.42	205.1	2.97	2.7
	14:45	205.48	205.18	2.98	2.7
	17:30	205.62	205.21	2.98	2.71
7	9:00	205.62	205.16	2.99	2.71
	11:45	205.56	205.12	2.99	2.71
	14:30	205.67	205.21	2.99	2.72
	19:00	206.31	205.32	3	2.72
8	8:45	206.59	205.3	3.02	2.73
	11:30	206.59	205.31	3.01	2.72
	14:30	206.72	205.38	3.02	2.72
	17:30	206.99	205.38	3.02	2.72
9	9:15	207.56	205.49	3.04	2.71
	11:30	207.48	205.48	3.04	2.72
	14:00	207.5	205.45	3.04	2.72
	17:30	207.94	205.55	3.04	2.72
10	8:00	208.46	205.45	3.05	2.72
	12:00	208.48	205.46	3.05	2.72
	15:45	208.95	205.5	3.05	2.72
11	10:15	209.41	205.39	3.06	2.73
	12:00	209.31	205.39	3.07	2.74
	14:15	209.25	205.46	3.06	2.73
	19:00	209.69	205.56	3.07	2.73
12	9:00	209.89	205.45	3.07	2.73
	13:45	209.91	205.44	3.08	2.73
	16:00	210.04	205.47	3.08	2.73
	18:15	210.3	205.54	3.08	2.74
13	9:00	211.17	205.53	3.08	2.74
	11:30	211.05	205.51	3.08	2.74
	14:15	211.22	205.52	3.08	2.74
	18:00	211.97	205.58	3.08	2.74

14	9:15	211.97	205.47	3.09	2.74
	12:00	211.84	205.47	3.1	2.75
	15:00	212.04	205.5	3.1	2.75
	18:00	212.52	205.59	3.1	2.75
15	9:00	212.97	205.53	3.1	2.76
	11:30	212.85	205.51	3.1	2.75
	14:45	213.08	205.58	3.1	2.75
	17:30	213.41	205.66	3.1	2.75
16	9:00	213.87	205.62	3.1	2.75
	11:30	213.76	205.62	3.1	2.75
	14:45	213.91	205.65	3.1	2.75
	17:30	214.21	205.68	3.1	2.76
17	8:45	214.49	205.58	3.1	2.76
	12:00	214.4	205.58	3.1	2.76
	15:00	214.6	205.63	3.1	2.76
	17:15	214.81	205.66	3.1	2.76
18	8:30	214.85	205.56	3.1	2.76
	11:00	214.71	205.58	3.1	2.76
	14:30	214.86	205.61	3.11	2.76
	17:15	215.19	205.69	3.11	2.76
19	9:00	215.24	205.61	3.11	2.76
	12:00	215.13	205.57	3.11	2.76
	15:30	215.39	205.67	3.11	2.76
	17:30	215.64	205.73	3.11	2.76
20	9:00	215.68	205.66	3.11	2.77
	11:00	215.55	205.6	3.11	2.77
	15:00	215.79	205.7	3.11	2.77
	18:15	216.31	205.82	3.12	2.77
21	9:00	216.2	205.66	3.11	2.76
	11:30	216.05	205.66	3.12	2.76
	14:15	216.16	205.68	3.12	2.76
	17:30	216.53	205.74	3.12	2.76
22	9:15	216.32	205.58	3.11	2.76
	11:00	216.17	205.55	3.11	2.76
	15:00	216.32	205.59	3.11	2.76
	17:30	216.71	205.67	3.12	2.77
23	8:45	216.67	205.48	3.11	2.77
	11:00	216.53	205.48	3.11	2.76
	14:00	216.78	205.54	3.11	2.77
	15:30	216.98	205.58	3.11	2.77
	17:45	217.23	205.61	3.11	2.76
24	8:45	217.22	205.43	3.11	2.76
	11:30	217.07	205.41	3.11	2.76
	13:30	217.21	205.43	3.11	2.76

	15:00	217.39	205.44	3.11	2.76
	16:30	217.46	205.45	3.11	2.76
25	8:30	217.33	205.24	3.11	2.76
	10:30	217.18	205.24	3.11	2.76
	12:30	217.22	205.31	3.11	2.76
	14:30	217.46	205.31	3.11	2.76
	16:30	217.63	205.33	3.11	2.76
26	8:30	217.41	205.27	3.11	2.76
	10:30	217.22	205.2	3.11	2.76
	12:30	217.17	205.31	3.11	2.76
	14:30	217.23	205.34	3.11	2.76
	16:30	217.34	205.36	3.11	2.76
27	8:45	217.21	205.34	3.11	2.76
	11:30	217.06	205.33	3.11	2.76
	13:30	217.11	205.39	3.11	2.76
	15:30	217.06	205.35	3.11	2.75
	17:00	217.04	205.41	3.1	2.76
28	8:45	216.8	205.33	3.11	2.75
	11:00	216.55	205.27	3.1	2.75
	13:00	216.27	205.29	3.1	2.75
	14:45	216.22	205.29	3.1	2.76
	16:45	216.35	205.35	3.1	2.75
29	8:45	216.05	205.33	3.11	2.76
	11:00	215.76	205.29	3.11	2.76
	12:45	215.6	205.3	3.1	2.75
	15:00	215.34	205.29	3.1	2.76
	16:45	215.3	205.32	3.1	2.75
30	9:15	214.82	205.24	3.1	2.75
	11:15	214.64	205.23	3.1	2.75
	14:15	214.66	205.26	3.1	2.74
31	8:45	214.36	205.17	3.1	2.74
	10:45	214.21	205.14	3.09	2.74
	12:45	214.17	205.16	3.09	2.74
	15:15	214.19	205.17	3.1	2.73
	16:45	214.06	205.19	3.1	2.74
32	8:45	213.52	205.11	3.09	2.74
	11:00	213.4	205.13	3.1	2.72
	12:45	213.31	205.08	3.1	2.73
	17:30	213.53	205.11	3.1	2.73
33	9:15	212.99	205.03	3.09	2.73
	11:45	212.8	205.01	3.09	2.72
	16:00	212.95	205.04	3.09	2.73
34	9:15	212.4	204.9	3.08	2.73
	11:15	212.15	204.91	3.09	2.72

	15:15	212.13	204.98	3.08	2.73
	17:30	212.09	204.98	3.08	2.72
35	8:45	211.7	204.9	3.08	2.72
	11:30	211.34	204.9	3.08	2.72
	14:30	211.3	204.98	3.07	2.72
	17:15	211.29	205	3.07	2.72
36	8:45	210.93	204.96	3.09	2.72
	12:00	210.72	204.92	3.07	2.72
	15:00	210.69	204.94	3.08	2.72
	17:30	210.7	204.92	3.08	2.71
37	8:45	210.33	204.9	3.08	2.72
	12:00	210.25	204.89	3.08	2.72
	15:00	210.16	204.91	3.07	2.72
	16:30	210.21	204.92	3.07	2.72
Dry Mass		203.8	203.69	2.76	2.55

Appendix D: Numerical Simulation of Wall Assemblies Using HAMFEM

A series of simulations were performed using HAMFEM to give insight into the different parameters, as well as the loading protocol and design of the experimental set-up. Based on realistic climatic data, desired loads were defined for the interior and exterior sides of the assemblies. The software allowed the analyses of several wetting and drying periods until one was selected. Once the desired parameters were inputted, the experiment as it would be was simulated. The results of the experimental testing were compared to those of the numerical modeling. The selection of this hygrothermal tool was based on its availability and the capability of inputting directly into the source code all boundary conditions as well as material properties. Even though the program has 3D capabilities, only a 1D simulation is investigated.

D.1 Description of the Assemblies

Only four of the eight specimens were simulated since only a 1D model was studied. This is due to the fact that four of the eight specimens included a wooden stud within the insulating space. Simulating the assemblies that included the stud would have required a 2D simulation, which is beyond the scope of this report.

The four specimens modeled are identical in size, configuration and material types as described in the experimental protocol. Their characteristics and properties are described below in the text and in Table D.5.

The composition of the walls remained mainly constant:

- rain screen – brick veneer
- air space
- sheathing paper* - weather resistive barrier (WRB)
- sheathing – oriented strand board
- insulation – mineral wool
- interior sheathing – gypsum board
- interior finishing*

  - '*' denotes variable element of the modeled assemblies.

Of the construction materials, two parameters were variable, as discussed in the small-scale experimental setup.

To successfully model the assembly, an adequate mesh had to be developed. Since only the uninterrupted specimens (without studs) are simulated, the model can be 1-dimentional. The development of the mesh was done through trial and error. Each element of the assembly had a mesh created separately. Using the individual meshes, the

program was run until the outputted temperatures and pressures between the nodes were transitioning fluidly. Once each mesh was adequately sized, being neither too fine nor coarse, they were combined into one.

The mesh designed for these simulations consists of 68 quadratic elements and 137 nodes. Each component of the assembly was assigned a specific number of elements of the mesh depending on the thickness of the assembly material: 23 (brick), 2 (WRB), 12 (OSB), 17 (insulation), 12 (gypsum) and 2 (interior finishing). Since material interfaces may lead to significant gradients in temperature and capillary pressure, a denser grid is required. The width of the elements in the mesh taper off towards each material's edges. This is done to ensure better simulation between the different mediums. An image of the mesh is shown below in Figure D.1.

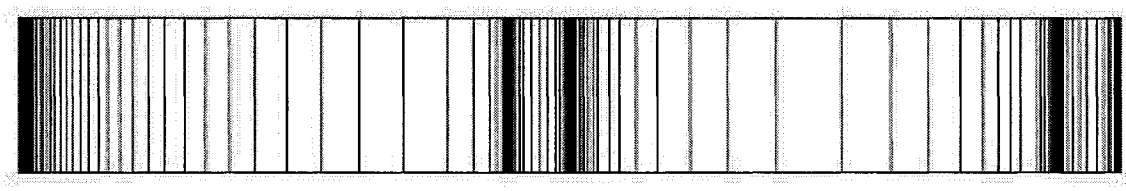

Figure D.1 Applied Mesh

D.2 Material Properties

Many of the materials used in the simulation were not previously inputted into the software. These properties were either taken from the manufacturer websites or from published literature. The following briefly describes the procedures taken to determine the material properties used in HAMFEM:

By using published data from Kumaran et al (2002), Roels et al (2006), and Kumaran et al (2006), simple material properties are plotted and graphed. The preceding demonstrated either measured material properties such as sorption/desoprtion curves or tables which included material properties such as permeabilities. One of the published documents included analytical functions to model the permeability and sorption curves of certain materials. By taking the measured material properties, plotting them in a spreadsheet allowed for functions of the properties to be modeled. These function properties were then inputted into the modeling software for simulation. Among the properties modeled were the permeability (both liquid and vapor) and sorption curves to capillary saturation.

To describe the permeability and sorption, the following two models were used:

i. $\delta(s) = a + b\exp^{c\phi}$
ii. $w\ (kg/m^3) = w_{sat}(1 + (a * \ln(\phi))^n)^m$ van Genuchten model

Nevertheless, the published data was modified since the materials used in the experiment are not the same as those tested which reflect the published properties. Below is the description of the available hygrothermal data followed by the results of the two above models.

Building Paper:

Two series of data are available for 60 minute building paper (Kumaran et al 2006), which is the type of building paper used in the experiment. Their properties are listed below.

Table D.1 Building paper properties

	60 min I	60 min II
Density (kg/m^3)	925.8	823.5
Thickness (mm)	0.31	0.34
RH (%)	$kg/m^2.s.Pa$	$kg/m^2.s.Pa$
10	2.87E-09	1.51E-09
20	2.87E-09	1.70E-09
30	2.87E-09	1.91E-09
40	2.87E-09	2.16E-09
50	2.87E-09	2.44E-09
60	2.87E-09	2.78E-09
70	2.87E-09	3.18E-09
80	2.87E-09	3.66E-09
90	2.87E-09	4.24E-09
100	2.87E-09	4.95E-09

It can be seen that one of the permeabilities is constant while the second is a function of relative humidity. Since building paper is an absorptive material, the varying permeability is chosen for the simulations. However, through preliminary simulations a variation of the 60 min II paper, 0.38 times the permeability, gives best trends. The permeabilities of the papers are displayed in Figure D.2, where the building paper used is highlighted in red.

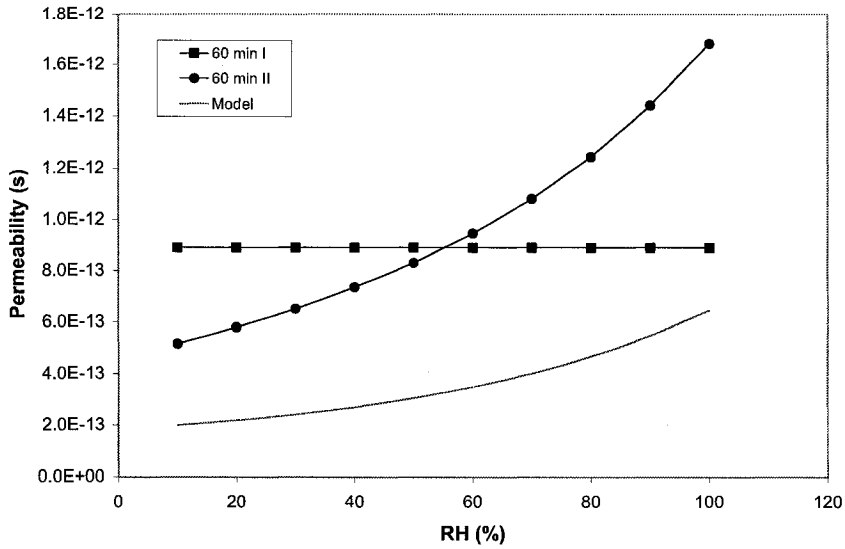

Figure D.2 Building Paper Permeability

Spun Bonded Polyolefin

Spun Bonded Polyolefin has the most available published data including the manufacturer's specified permeability. Kumaran et al (2006) tested five papers and their permeances are as follows:

Table D.2 SBPO permeance

	SBPO I	SBPO II	SBPO III	SBPO IV	SBPO V
RH (%)	kg/m^2.s.Pa	kg/m^2.s.Pa	kg/m^2.s.Pa	kg/m^2.s.Pa	kg/m^2.s.Pa
10	1.06E-09	2.37E-09	8.35E-10	4.37E-09	3.17E-09
20	1.06E-09	2.37E-09	8.35E-10	4.37E-09	3.17E-09
30	1.06E-09	2.37E-09	8.35E-10	4.37E-09	3.17E-09
40	1.06E-09	2.37E-09	8.35E-10	4.37E-09	3.17E-09
50	1.06E-09	2.37E-09	8.35E-10	4.37E-09	3.17E-09
60	1.06E-09	2.37E-09	8.35E-10	4.37E-09	3.17E-09
70	1.06E-09	2.37E-09	8.35E-10	4.37E-09	3.17E-09
80	1.06E-09	2.37E-09	8.35E-10	4.37E-09	3.17E-09
90	1.06E-09	2.37E-09	8.35E-10	4.37E-09	3.17E-09
100	1.06E-09	2.37E-09	8.35E-10	4.37E-09	3.17E-09
Perms	18.5	41.3	14.5	76.2	55.3

It is found through testing that the manufacturer's published permeability of 58 gives the best trend.

A graphical output of the permeabilities is below in Figure D.3.

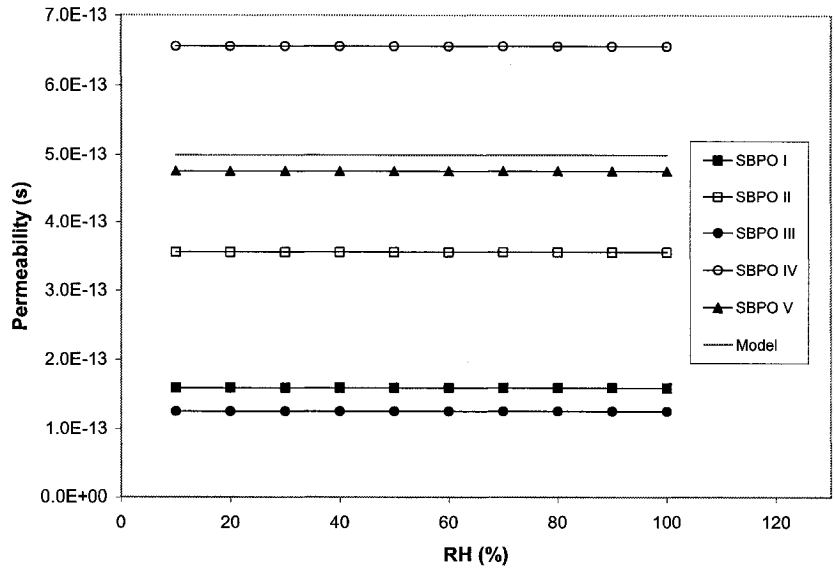

Figure D.3 SBPO Permeabilities

Oriented Strand Board:

A total of five OSB sheathing board data are available. Three of the sheathings have detailed material properties such as their respective densities (Kumaran et al 2002), one of which is an average of seven different OSB properties. The fourth OSB reflects the results of testing completed by Ojanen and Ahonen (2005).

Each sheathing board has a different density, sorption/desoprtion curve and permeability. The permeabilities of the OSB sheathing boards are displayed below in Table D.3 and are also graphically represented in Figure D.4. A vapor permeability test is carried out with the OSB used in the experiment and the permeability of it is listed as OSB 5.

Table D.3 OSB Permeability

	OSB 1	OSB 2	OSB 3	OSB 4	OSB 5
Density (kg/m^3)	650	660	650	650	580
RH	kg/m.s.Pa	kg/m.s.Pa	Kg/m.s.Pa	kg/m.s.Pa	kg/m.s.Pa
10	4.39E-14	6.42E-14	2.56E-13		5.00751E-13
20	1.61E-13	1.06E-13	4.01E-13	1.905E-13	5.02256E-13
30	3.44E-13	1.77E-13	6.02E-13	4.295E-13	5.06778E-13
40	5.91E-13	2.93E-13	8.73E-13	7.635E-13	5.20363E-13
50	9.00E-13	4.87E-13	1.23E-12	1.2E-12	5.61173E-13
60	1.27E-12	8.11E-13	1.70E-12	1.735E-12	6.83774E-13
70	1.70E-12	1.35E-12	2.30E-12	2.375E-12	1.05209E-12
80	2.19E-12	2.27E-12	3.08E-12	3.125E-12	2.15856E-12
90	2.75E-12	3.83E-12	4.08E-12	3.97E-12	5.48259E-12
100	3.37E-12	6.54E-12	5.35E-12	4.945E-12	

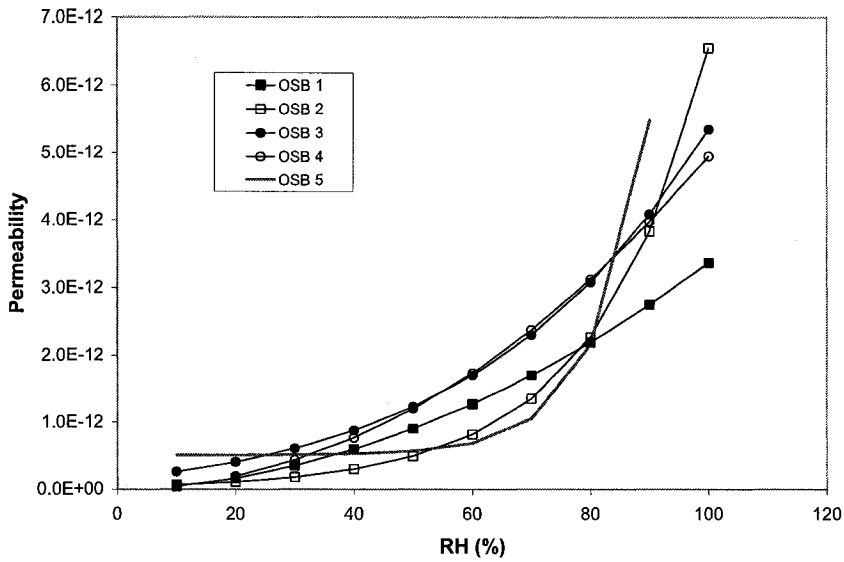

Figure D.4 OSB Permeability

Acrylic Paint:

Using the model described above by Roels et al (2006), a permeability for acrylic paint is developed.

$\delta = a + b * \exp^{c\phi}$

where $a = 2.5x10^{-4}$

$b = 1.35x10^{-5}$

$c = 5.65$

A variation of the above model is used to model the wall assemblies tested. The result of the model's permeability is graphed below in Figure D.5:

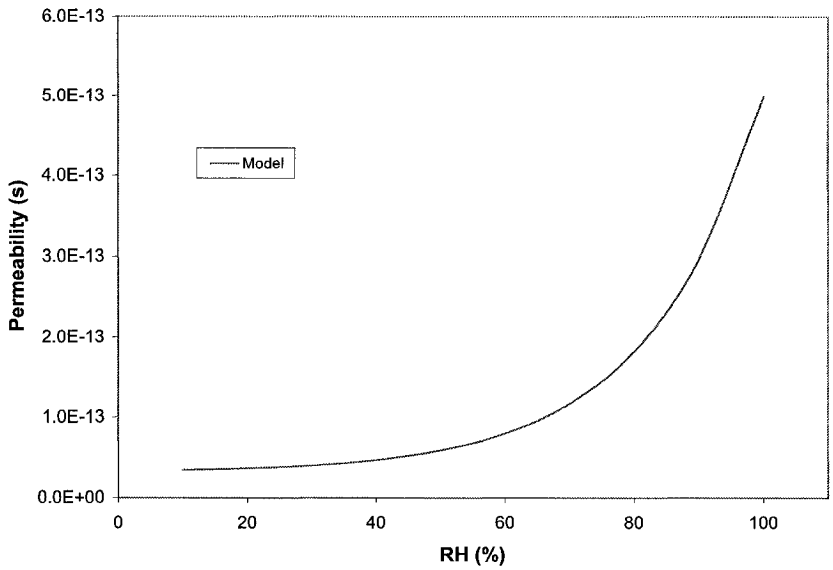

Figure D.5 Paint permeability

Vinyl Wall Paper:

The permeability of one vinyl wall paper is published by Kumaran et al (2006) which is described below.

Table D.4 Vinyl wall paper permeance

RH	kg/m2.s.Pa
10	8.50E-11
20	1.06E-10
30	1.35E-10
40	1.69E-10
50	2.10E-10
60	2.59E-10
70	3.16E-10
80	3.82E-10
90	4.60E-10
100	5.51E-10

A vapor permeability test was carried out to determine the permeability of the vinyl wall paper used in the experiment. Through preliminary simulations, a variation of the vinyl wall covering, 15 times the permeability, gives best trends. The results are plotted below.

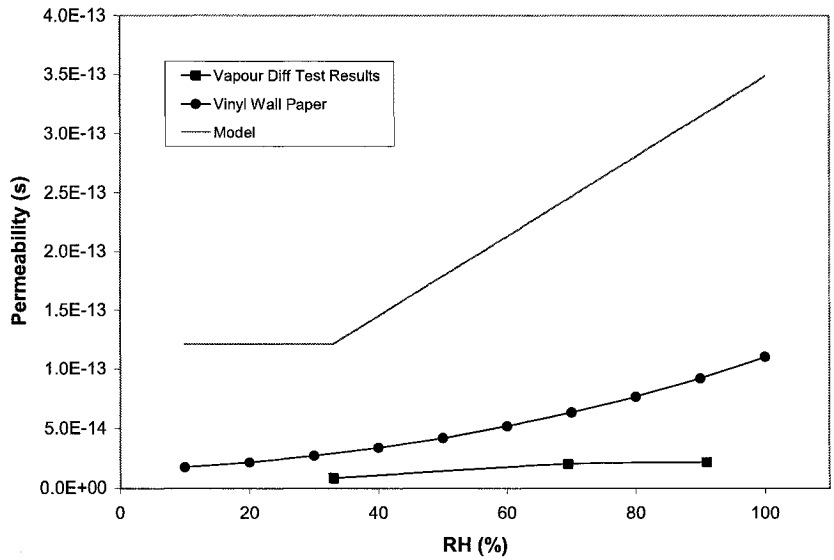

Figure D.6 Vinyl wall paper permeability

D.3 Moisture Input Properties

- **Brick**

δ (s) = 2.61×10^{-5} * (1-S) / (Rv * T * 30 * (0.503 * $(1-S)^2$ + 0.497))

where $S = w/w_{cap}$

w (kg/m^3) = 220 *[0.3 *$((1-1.25 \times 10^{-5} * pc)^{1.65})^{-0.3939}$ + 0.7 *$((1-1.8 \times 10^{-5} * pc)^6)^{-0.8333}$]

- **Building Paper** - no liquid permeability assumed

δ (s) = 0.38 * [3×10^{-13} + 1.8×10^{-13} * $\exp^{(2.05 * \phi)}$]

w (kg/m^3) = 0

- **Spun Bonded Polyolefin** - no liquid permeability assumed

δ (s) = 4.9935×10^{-13}

w (kg/m^3) = 0

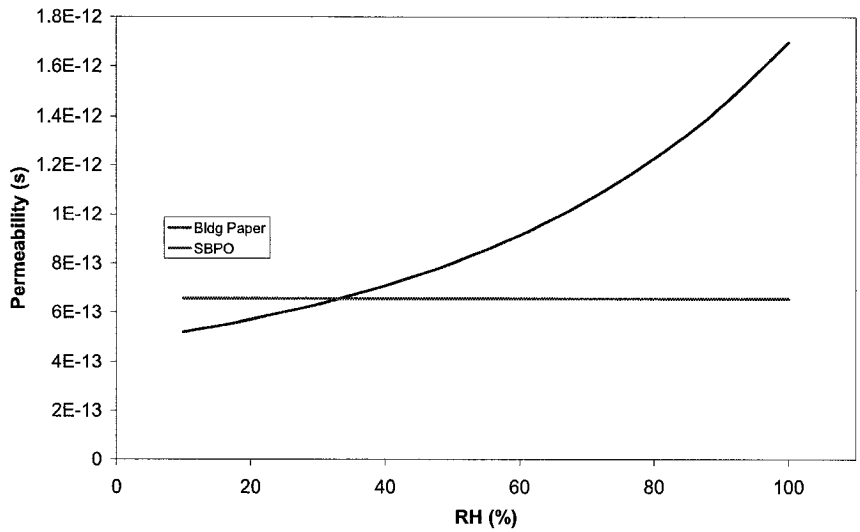

Figure D.7 Permeability of sheathing papers

- **Oriented Strand Board**

δ (s) = $2.385 \times 10^{-13} * \exp^{(3.125*\phi)}$

w (kg/m^3) = $830 * (1 + (5.1 \times 10^{-5} * pc)^{1.28})^{-0.28}$

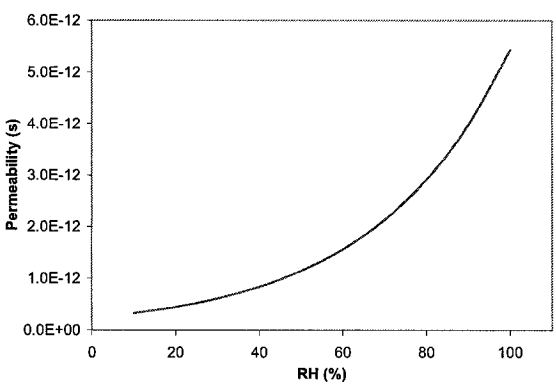

Figure D.8 Permeability of OSB

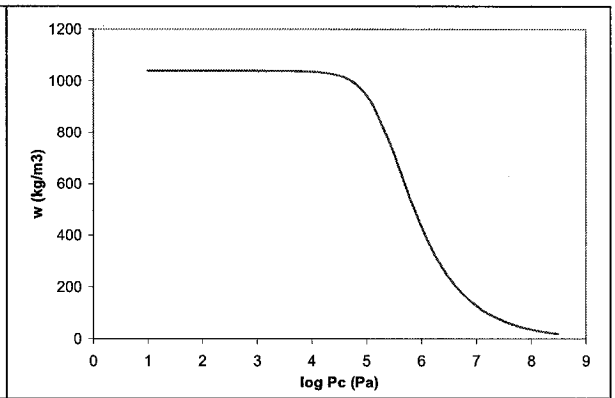

Figure D.9 Moisture absorption of OSB

- **Mineral Wool** - no liquid permeability assumed

δ (s) = $6.9 \times 10^{-11} + 1.9 \times 10^{-14} * \exp^{(10 * \exp (pc / (Rv * \rho * T)))}$

w (kg/m^3) = $0.83 * (1 + (5.1 \times 10^{-5} * pc)^{1.28})^{-0.28}$

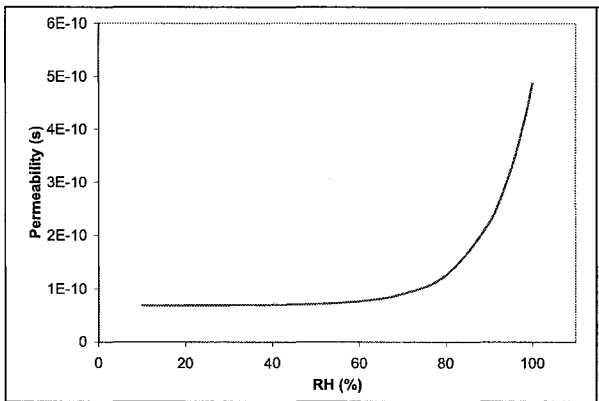

Figure D.10 Permeability of mineral wool

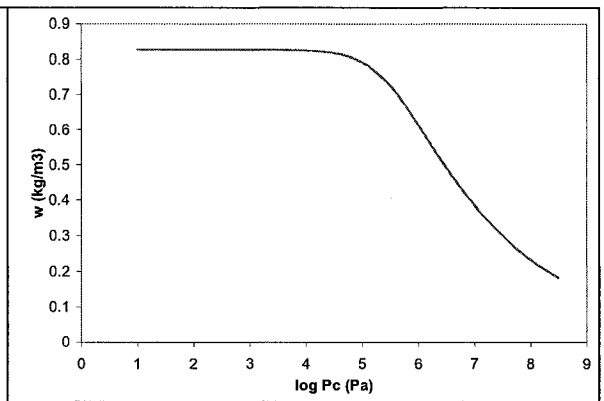

Figure D.11 Moisture absorption of mineral wool

- **Gypsum Board**

δ (s) = 2.61×10^{-5} * (1-S) / (Rv * T * 5.6 * (0.503 * $(1-S)^2$ + 0.497))

w (kg/m^3) = 810 * $(1 + (3.4 \times 10^{-6} * pc)^{1.62})^{-0.62}$

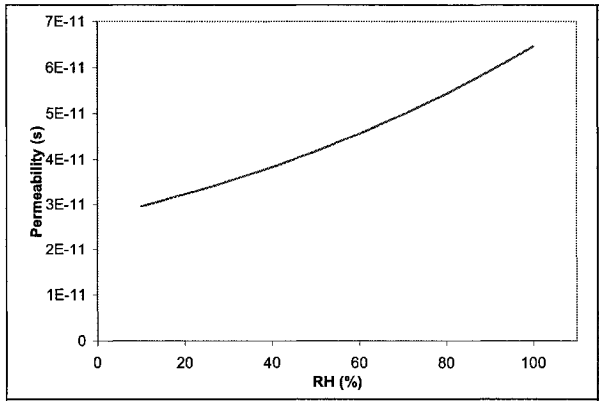

Figure D.12 Permeability of gypsum

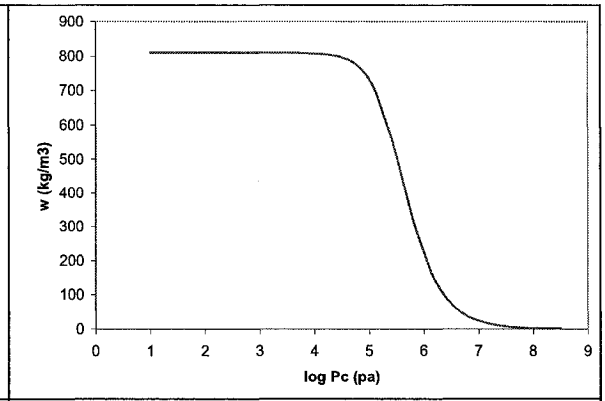

Figure D.13 Moisture absorption of gypsum

- **Acrylic Paint** - no liquid permeability assumed

δ (s) = 1.22×10^{-10} * (2.5×10^{-4} + 1.35×10^{-5} * $\exp^{(5.65 * \phi)}$

w (kg/m^3) = 200 * $(1 + (3.0 \times 10^{-7} * pc / (Rv * \rho * T))^{1.55})^{-0.35}$

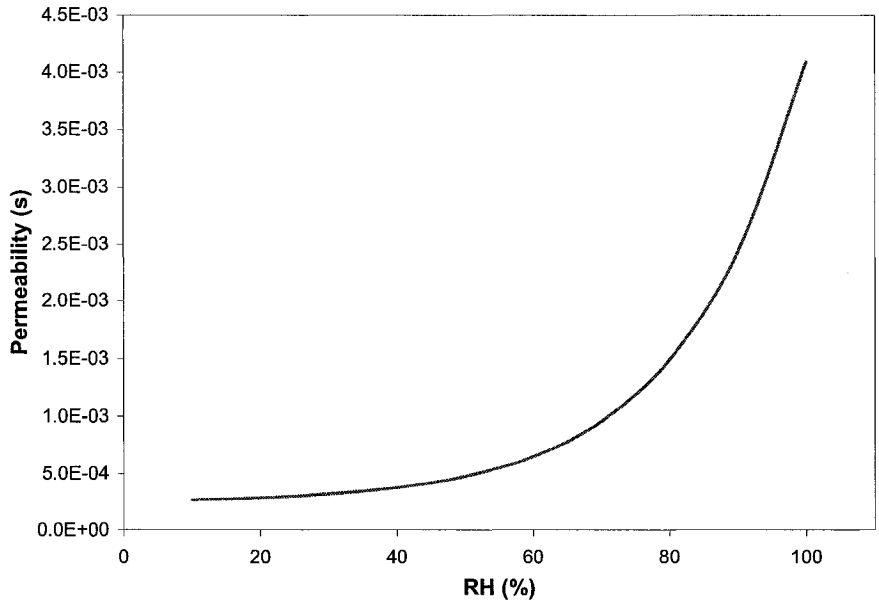

Figure D.14 Permeability of acrylic paint

- **Vinyl Wall Paper** - no liquid permeability assumed

δ (s) = 1.21×10^{-13} (RH<33%)

= $(3.39 \times 10^{-15} * \phi) + 9.3 \times 10^{-15}$ (RH >=33%)

w (kg/m^3) = 0

In addition to deriving the above properties, the air cavity properties were altered to be combined with those of the sheathing papers. This was performed since the air space is not considered as an element of the software, but still needs to be incorporated into the program for proper analyses. By adjusting the thicknesses and vapor permeabilities of the weather resistive barriers, the air space was incorporated.

- air space $\mu d = 0.03m$ ($\mu = 1$, $d = 0.03m$)
- building paper $\mu d = 0.7m$ ($\mu = 3500$, $d = 2 \times 10^{-4}m$)
- SBPO $\mu d = 0.0825m$ ($\mu = 825$, $d = 1 \times 10^{-4}m$)

μd (air space + building paper) = 0.1125

$d = \mu d/\mu = 0.1125/825 = 0.136mm$

μd (air space + SBPO) = 0.73

$d = \mu d/\mu = 0.73/3500 = 0.209mm$

Using the new thicknesses calculated by combining the air space with the sheathing papers allowed for the new thermal conductivities of the weather resistive barriers to be determined. By using an R-value of 0.17 W/m^2K for the air space, the following was determined:

$$\Rightarrow \lambda_{building\ paper} = d/R = 0.136/0.17 = 8x10^{-4}\ W/mK$$
$$\Rightarrow \lambda_{SBPO} = d/R = 0.209/0.17 = 1.23x10^{-3}\ W/mK$$

Using the table below, all material properties were inputted into HAMFEM and used to simulate the thermal and hygric capabilities of the experimental specimens.

Table D.5 Simulation material properties

Material	Thickness m	Density kg/m3	Heat Capacity J/kgK	Heat Conductivity W/mK	Capillary Saturation kg/m3
Brick	0.09	2005	840	0.5 + 0.0045w	220
Air Space	0.03	1.3	1000	0.047	0
Bldg Paper	0.00034	850	0	0.0008	1.00E-07
SBPO	0.00015	316	0	0.00123	1.00E-07
OSB	0.009	615	1880	0.09	260
Mineral Wool	0.089	42	840	0.035	0.83
Gypsum	0.125	625	870	0.16	810
Acrylic Paint	0.0001	1500	0	1	200
Vinyl Paper	0.0002	850	0	1	1.00E-07

* w - moisture content [kg/m3]

The main factors which influence the difference in performance between the different assemblies are the use of either spun bound polyolefin or building paper and finishing the interior of the gypsum with acrylic paint versus vinyl wall paper.

D.4 Boundary Conditions

The simulations are performed under specific loading conditions. The conditions under which the modeling was conducted reflect the conditions observed in the laboratory. The indoor conditions of the experiment are as follows:

The relative humidity and temperature of the interior side of the assemblies is kept constant at 70% RH and 17°C and at 35% RH and 16°C for the small-scale and large-scale experiments respectively.

The exterior conditions of the small-scale assemblies are as follows:
The relative humidity acting on the cladding is 15% RH while the temperature is 40°C throughout the entire experiment.
The exterior conditions of the large-scale assembly are as follows:

The relative humidity acting on the cladding is 15% RH while the temperature is 50°C during the eight hours of sunlight and 20°C throughout the 16 hours of night.

The thermal loading acting on the assemblies varies between the wetting and drying phases. The thermal loads for the wetting and drying phases are respectively:

Thermal load = H_c * (T-Ts)
Thermal load = B * (T-Ts) + I_b * B * (p-p_s)
where H_{ce} = surface coefficient = 13.4 ($W/m^2.K$)
B_e = surface coefficient = $10.318x10^{-8}$ (s/m)
Hci = 9.5 ($W/m^2.K$)
B_i = $7.315x10^{-8}$ (s/m)
T = temp away from wall (K)
T_s = unknown surface temp (K)
I_b = latent heat of vaporization = $2.5x10^6$ (kJ/kg)
P = vapor pressure away from wall (Pa)
P_s = unknown vapor pressure at surface (Pa)

The initial conditions of the brick contain 1.5 L of water which translates to roughly -65892.56 Pa in capillary pressure. The rest of the materials are believed to be at standard room conditions which amount to $-8x10^7$ Pa in capillary pressure.

Appendix E: Sensor Equipment

E.1 Thermocouple

The thermocouples used to determine the temperatures within the specimens were type P-26-TT-IEC. This thermocouple model has an accuracy of 0.1°C. Since it is of type T, it is best suited for measurements in the -200 to 350°C range.

E.2 Relative Humidity Probe

To measure both relative humidity and temperature across the assemblies, E+E Elektronic type EE06-FT1 A6-K300 relative humidity probes were used in all experiments. The RH probes have an accuracy within 3% relative humidity at 20°C. The accuracy of the temperature output is within 0.3°C and 0.4°C at 20°C and 40°C respectively. The accuracy between 20°C and 40°C is linear, while below 20°C, the accuracy begins to rise above 0.3°C. These probes were factory calibrated, and with a dew point hygrometer, a random verification was performed using saturated salt solutions of 35% and 80% RH.

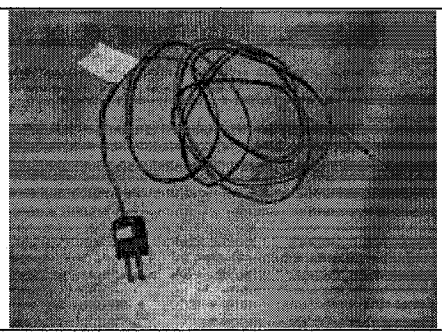

Figure E.1 Thermocouple

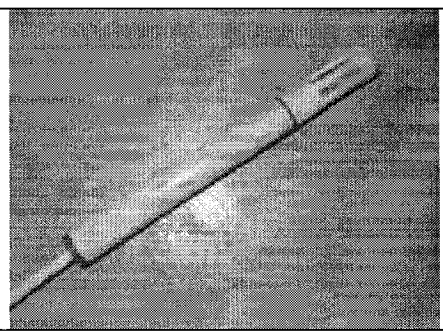

Figure E.2 Relative Humidity Probe

E.3 Moisture Pins

The moisture content of the wooden studs and the sheathing boards in the small-scale experiment were measured with the use of moisture pins (or transmitters). These pins were calibrated with an electronic resistance as a function of moisture content. A conversion table allowed for the voltage outputs to be converted into moisture content. The function used to convert the outputs to moisture content is $f(v) = a + b \exp(c * v)$, where a, b and c are constant and v is the voltage output from the moisture pins. The actual modeled function is:

$$f(v) = -27.84 + 113.70 \exp (0.258 * v)^{-1}$$

The pins are comprised of nails connected to a positive and negative end of a data logger which are driven into the wooden materials at predetermined depths and locations. The

pins used in the sheathing were placed at the center, while two pin-set depths were applied to the SPF studs, 4mm and 19mm. Depending on the type of finishing material, the pins were also placed at two different distances from the edge of the stud: 5mm for vinyl paper and 13mm for acrylic paint.

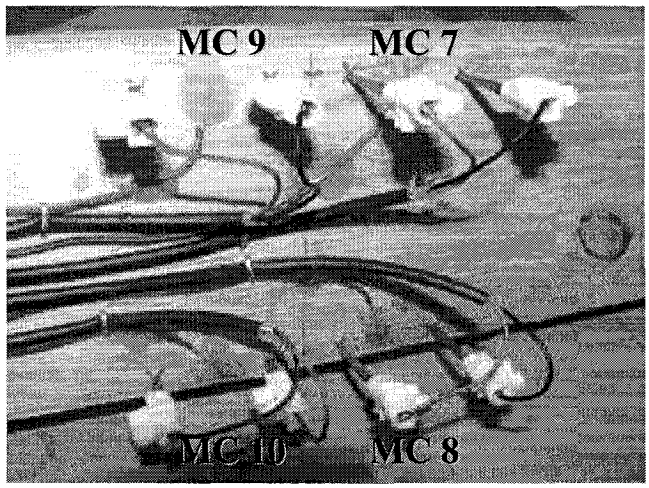

Figure E.3 Moisture pins in wood stud

Each stud was equipped with four moisture pin-sets, seen above: MC 7, MC 8, MC 9 and MC 10. These four moisture content measurement locations were at the various depths and distances which can be seen in Table E.1.

Table E.1 Moisture pin locations in S-P-F studs

	Acrylic Paint Finish		Vinyl Wall Paper Finish	
Label	Distance from Edge (mm)	Depth (mm)	Distance from Edge (mm)	Depth (mm)
MC 7	5	4	5	4
MC 8	5	4	13	4
MC 9	5	19	5	19
MC 10	5	19	13	19

The moisture content of the sheathing board in the large-scale experiment were also measured with moisture pins. The pins comprised of gold plated nails which were driven into the sheathing at a depth of 1 cm. The pins were connected to a DELMHORST moisture content meter which outputted the results.

E.4 Calibration

Small Scale

The thermocouples and relative humidity probes used in the small-scale experiment were calibrated by De Meulenaer (2006) to assure that the measurement recordings were accurate.

The thermocouples were calibrated using a calibrator which is to both 20° and 40°C and the thermocouples were used to measure the temperatures. The temperatures output by the thermocouples were then recorded and their differences from the calibrator were noted.

The RH probes were factory calibrated. Nevertheless, three probes at random were selected to be tested at both 35% and 80% RH. The testing of the probes was carried out at a temperature of 20°C giving the sensors an accuracy of ± 3%RH, according to the manufacturer.

Table E.2 RH probe calibration results

RH	35%		80%		
Exposure time	50 min	60 min	60 min	150 min	24 hrs
Sensor					
RH 5	35.6 % 20.8 °C	35.4 % 20.8 °C	75 % 20.8 °C	76.3 % 20.6 °C	78 %
RH 16	35.2 % 20.7 °C	35.1 % 20.6 °C	75.4 % 20.6 °C	76.1 % 20.3 °C	77.6 %
RH 19	36.1 % 20.9 °C	35.9 % 20.7 °C	75.5 % 20.6 °C	76.4 % 20.4 °C	78.2 %

In the 35%RH environment, the probes reacted quickly and outputted measurements within expected limits. This observation is seen above in Table E.2. However, the results of the 80%RH calibration were not as precise. Although all the probes had similar responses, it took them longer to reach a more accurate reading than when exposed to 35%RH. Conducting this test shows that the higher the relative humidity, the slower the probes react.

Large Scale

The thermocouples and relative humidity probes were all calibrated to assure that the measurement recordings are accurate but were not implemented in the results.

The thermocouples were calibrated after testing by placing the thermocouples in a 22.3° and 37.4 °C baths. The bath temperatures were measured with an analogue thermometer. The average temperatures outputted by the thermocouples over a minute were recorded and their differences from the thermometer were noted. TC_{13} deviates by about 0.75°C at 22.3°C while TC_3 deviates by over 1°C at 37.4°C. Refer to Figure E.4 and Figure E.5 for the respective deviations. Note that thermocouples TC_5, TC_8, TC_9 and TC_{12} were damaged during disassembly and were not calibrated.

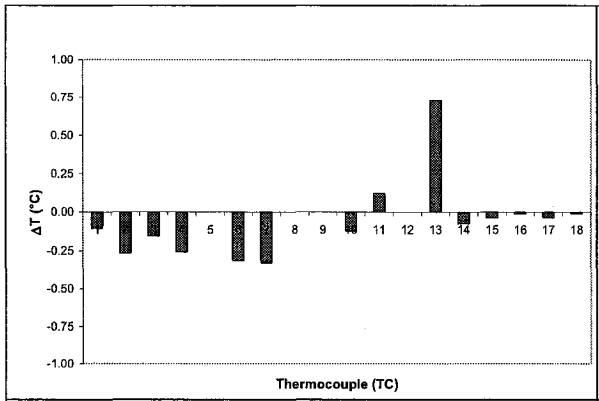

Figure E.4 Thermocouple deviations at 22.3°C

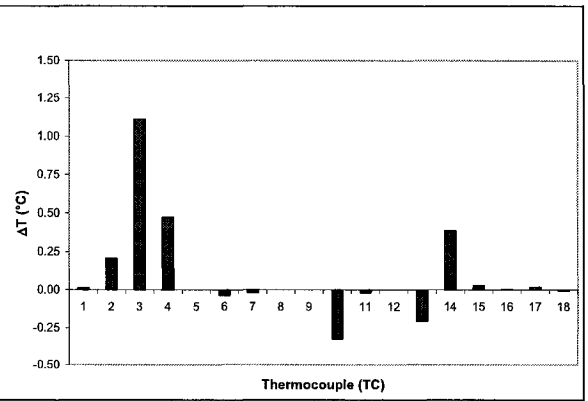

Figure E.5 Thermocouple deviations at 37.4°C

The RH probes were factory calibrated. Nevertheless, all four probes were tested at various RH levels to assure their 3% accuracy before and after testing. The testing of the probes was carried out at a temperature of 23.5°C, before the experiment, which should result in RH outputs having an accuracy of ± 3%RH, according to the manufacturer.

Table E.3 RH probe calibration results before experimentation

RH	35%				80%					
Exposure time	30 min		45 min		20 min		60 min		90 min	
Sensor										
RH 1	32.8	%	33.0	%	77.1	%	77.6	%	77.8	%
	23.3	°C	23.4	°C	23.6	°C	23.7	°C	23.7	°C
RH 2	33.1	%	33.3	%	76.9	%	78.2	%	78.2	%
	23.1	°C	23.3	°C	23.6	°C	23.6	°C	23.7	°C
RH 3	32.6	%	32.8	%	76.0	%	76.5	%	76.6	%
	23.4	°C	23.6	°C	23.8	°C	23.8	°C	23.9	°C
RH 4	33.3	%	33.4	%	77.0	%	77.3	%	77.5	%
	23.3	°C	23.3	°C	23.6	°C	23.7	°C	23.7	°C

In the 35%RH environment, the probes react quite quickly and output measurements are within expected limits. This observation can be seen above in Table E.3. The relative humidity nears the 35% mark by 0.2% RH in 15 minutes between 30 and 45 minutes. However, the results of the 80%RH calibration are not as precise. Although all the probes have similar responses, it takes them longer to reach equilibrium than when exposed to 35%RH. Monitoring the RH sensors exposed to 80%RH between 20 and 90 minutes, the output differs by as much as 1%RH. Increasing the exposure time beyond 90 minutes will be sufficient for the probes to be within 3% RH as per the manufacturer. Conducting this test illustrates the slow reaction time the probes have as the relative humidity increases.

In the case of this experiment, high relative humidity is expected in the air cavity, making the response time of the probes questionable. However, since the probes will be continuously measuring over a long period of time, the sensors should be able to rise to the expected RH.

Following experimentation, the relative humidity probes were re-calibrated to determine if they were damaged during experimentation. The temperature was 24.7°C, 1.2° more than the initial calibration. The probes returned fairly good outputs. RH 3 is the only probe to return an output out of the 3% range initially specified by the manufacturer.

Table E.5 shows the drift of the probes from the beginning to the end of the experiment.

Table E.4 RH probe calibration results after experimentation

RH	35%				80%			
Exposure time	30 min		45 min		20 min		60 min	
Sensor								
RH 1	32.6	%	33.0	%	78.3	%	78.7	%
	24.2	°C	24.5	°C	24.7	°C	25.0	°C
RH 2	33.8	%	34.9	%	78.3	%	78.5	%
	24.1	°C	24.3	°C	24.6	°C	24.9	°C
RH 3	38.6	%	39.0	%	83.3	%	83.8	%
	24.2	°C	24.3	°C	24.5	°C	24.9	°C
RH 4	34.0	%	34.4	%	77.6	%	78.1	%
	24.2	°C	24.4	°C	24.8	°C	25.0	°C

Table E.5 RH probe drift

RH	35%				80%			
Exposure time	30 min		45 min		20 min		60 min	
Sensor								
RH1	0.2	%	0.0	%	1.2	%	1.1	%
RH2	0.7	%	1.6	%	1.4	%	0.3	%
RH3	6.0	%	6.2	%	7.3	%	7.3	%
RH4	0.7	%	1.0	%	0.6	%	0.8	%

Appendix F: Step-By-Step Running of a Test Procedure

The following is a step-by step procedure to conduct an experiment on a large-scale test specimen with the above said setup. The step-by-step procedure assumes that wall components have already been constructed and all experimental sensors have been installed within the different component elements.

F.1 Installation of Test Wall Assembly

Back Wall

1. Fasten steel strips at top of exterior side studs.
2. Connect lever arm to steel strips with chain and shackles.
   2.1. Assure that when suspended, the back wall will hang exactly vertical to ensure an even air cavity throughout the entire height of the assembly.
3. Match counter weight to back wall mass to suspend both objects in equilibrium.
4. Align back wall with test hut opening.
   4.1. Raise back wall to required height.
5. Counter weight must be placed beside hut with enough room for reflective box to be passed through without creating any disturbance.
6. Insulate sides of back wall with 3 inches polystyrene.
7. Organize all sensor wires to either be passed inside or over hut.
   7.1. Interior sensors to be passed through pipe in wall, which must then be sealed with insulation.
   7.2. Exterior sensors must be braced on roof of hut to prevent any measurement disturbances during experiment.
8. Connect 11 kg weight to load cell with slight tension acting on the load cell.
9. Special attention must be made to assure counter weight does not rest on ground at any time once the load cell has been connected.
10. Seal perimeter of back wall to hut with double sided fabric tape and polyethylene sheet.
    10.1. Use staples to give double sided tape extra security to prevent the seal from breaking.
    10.2. Assure no tension in polyethylene sheet.

Brick Wall

11. Connect lever arm to steel frame with hook, chain and shackle.
12. Match counter weight to brick wall mass to suspend both objects in equilibrium.
13. Align brick wall with back wall.
    13.1. Raise brick wall to required height.
14. Counter weight must be suspended at an angle from the brick wall orientation as to not come in contact with the test hut.
15. Assure air gap is minimal with even thickness along length and height of wall.

15.1. RH sensor between wall components cannot contact brick wall.
16. Organize all sensor wires to be placed over the hut and braced on roof with other sensor wires.
17. Connect 45 kg weight to load cell with slight tension acting on the load cell.
18. Special attention must be made to assure counter weight does not rest on ground at any time once the load cell has been connected.
19. Seal perimeter of steel frame to back wall with double sided fabric tape and polyethylene sheet
    19.1. Use staples to give double sided tape extra strength to prevent seal from breaking in stud frame.
    19.2. Assure no tension in polyethylene sheet.
20. Begin cooling interior of test hut with A/C unit and fan.
21. Verify all sensors are connected and output realistic results with preliminary Agilent VEE run.

F.2 Wetting Regimen of Test Wall Assembly

1. All hose connections (supply main, manifold, and nozzles) must be securely fastened.
2. Manifold flow for nozzle pairs must be set at 25%, 50%, 75% and 100% from bottom to top respectively.
3. PVC basin must be placed under specimens and have hose drain to gutter.
4. Expose brick wall component to spray rack system.
    4.1. Arrange SBPO sheet to drain excess water from nozzles into PVC basin.
5. Seal sides of spray rack system to hut with polyethylene sheets and staples to prevent the spraying of water onto surroundings and counter weights.
    5.1. Ends of polyethylene sheets should drain all excess water into basin.
6. Run Agilent VEE and set recording time to 60 second time steps to monitor and measure the "initial" masses of the wall components.
7. Turn spray rack system on when ready while monitoring the mass increase of the brick component through Agilent VEE.
8. Turn off spraying when desired moisture gain is achieved.
9. Remove spray rack system from brick component without disturbing the system.
    9.1. Remove seal between spray rack and test hut.
    9.2. Remove SBPO drain from basin.
10. Remove excess moisture from bottom of brick wall at the steel beam interface with paper towel.

F.3 Drying Cycle of Test Wall Assembly

1. Expose brick wall to reflective box.
    1.1. Assure reflective box does not come in contact with wall system during installation.
2. Set dimmers #3 and #4 to 100% capacity, #1 and #5 to 85% capacity and #2 and #6 to 75% capacity.
3. Set timers for eight hours on, 16 hours off, in a 24 hour cycle.

4. Connect lamp circuits to timers which are plugged into extension cords.
5. Connect outside RH sensor, placed within reflective box, to data acquisitioner.
6. Monitor brick surface to guarantee even temperature across wall.
7. After eight hours of radiation is delivered to brick veneer and timers begin to turn off, unplug circuits to prevent unexpected radiation.
8. Change Agilent VEE recording time step from 60 to 600 seconds.
9. 24 hours since exposing cladding to radiation, removing reflective box from brick wall without disturbing the system.
   9.1. Disconnect exterior RH sensor.
10. Repeat wetting and drying cycles as needed.

F.4 Periodic Manual Measurement Readings

1. Before the wetting regimen, after simulated solar radiation exposure and several times in between, gravimetric measurement readings of the back wall are to be taken.
2. Stop or pause Agilent VEE.
3. Open door to test hut carefully to minimize a pressure differential between the exterior and interior of the hut.
4. Enter test hut and turn on light.
5. Carefully remove gypsum and stud samples to minimize the amount of condensation running off the exterior sheathing.
6. Set scale to zero and place samples on balance.
7. Note the day, time and sample mass in the correct space on data sheet. Repeat for all samples.
8. Return samples quickly to back wall from within the test hut.
9. Turn off light and exit test hut.
10. Close door to test hut carefully to minimize the pressure differential between the exterior and interior of the hut.
11. Using a moisture meter, read the moisture content within the exterior sheathing and note it in the correct space on data sheet.
12. Using a hygro-thermometer, read the temperature and relative humidity within the laboratory and note them in the correct spaces on the data sheet.
13. Set recording time step to either 60 or 600 seconds.
14. Play or run Agilent VEE.